The development of an oscillating steerable bone drill

Msc. Thesis

R.A. Blok

Technische Universiteit Delft

TU Delft

The development of an oscillating steerable bone drill

Msc. Thesis

by

R.A. Blok

to obtain the degree of Master of Science
at the Delft University of Technology,
to be defended publicly on Friday September 23, 2022 at 10:00.

Student number: 4218841

Thesis committee:	Prof.Dr.Ir. P. Breedveld	TU Delft, Supervisor
	Ir. E.P. de Kater	TU Delft, Daily supervisor
	Dr. Jovana Jovanova	TU Delft, External member

TU Delft

Preface

This Thesis presents the design and experimentation of a steerable oscillating drill prototype. This project is part of of the graduation requirements in attaining the title Master of Science from the Master Mechanical Engineering at the Delft University of Technology. The project was undertaken at the Bio-Inspired Technology research group.

Firstly, I want to thank Paul Breedveld for providing feedback and creative ideas during different stages of the project. I want to thank my daily supervisor Esther de Kater for her help and support during the project. Her dedication towards guiding students during their Master Thesis is truly appreciated, as well as her efforts to creating a group for Mater students for sharing their Thesis project and experiences. Furthermore, I want to thank David Jager for his help in designing and manufacturing the prototype drill and I want to thank Remi van Starkenburg and Mario van der Wel for rebuilding the drill prototype during the summer vacation period.

I would like to express my deepest appreciation to my girlfriend Annebregt who stood by me throughout the whole project and was always ready to help, inspire and motivate me. Lastly I want to thank my parents and sister for their unconditional support.

R.A. Blok
Delft, September 2022

Abstract

The goal of spinal fixation is to provide immediate stability through rigid immobilization of the spine. This is done by placing an implant that increases the stiffness in a section of the spine by attaching a structure of stiff metal rods. Pedicle screws connect these rods to the vertebrae. The straight pedicle screw needs to distribute its forces to strong cortical bone elsewhere in the vertebra and poorly accounts for the inhomogeneous properties of the bone. An improvement would be if the implanted device can then directly transfer its forces to the strongest parts of the bone. The first hurdle to overcome, would be the creation of a curved trajectory through the bone that follows the strong cortical bone. The problem is: there is currently no device commercially available that can drill through cancellous bone and actively steer to form such a curve.

A prior project by R. Müller produced a design and working prototype of an oscillating flexible bone drill. This drill consists of a cylindrical body that oscillates rotary around its centre axis and receives this motion by two bendable parallel leaf springs that counter-oscillate in longitudinal direction. This drill design forms the basis of the design presented in this thesis. The goal of this project is to adapt the flexible oscillating drill design of Müller to a steerable drill that can create a curved hole in artificial cancellous bone.

The oscillating drill constantly produces a sideways force since the cutters produce a friction force tangential to the cylindrical wall. The friction force induced by the drilling action on the forward stroke is currently cancelled out by an equal and opposite force during the reversed stroke. Introducing a difference between the two oscillating inputs to the drill head can create a force difference between the forward and reverse stroke, which provides a net sideways force over many repetitions. This net sideways force is expected to occur with a difference in phase or amplitude between the two oscillations.

A prototype drill and accompanying oscillator have been designed and built to further research the effects of the amplitude and phase difference on the drill motion and drilling performance. The drill consists of a drill head and a motion transfer module. The drill head is based on a cylinder that oscillates over a 30° angle around its centre axis. A 210° section of the circumference contains cutter teeth that are specifically designed for cutting cancellous bone. The drill should produce a rectangular drill hole of approximately 5 by 6 mm. The 'motion transfer module' transfers the motion from the oscillator to the drill head and consists of two parallel leaf springs that can only slide longitudinally along each other. At the front end the leaf springs split apart into a Y-shape to attach to the drill. The flexibility of the leaf springs is used as a hinge to convert the sliding motion to a rotation of the drill head. At the rear end, each leaf spring receives a translating oscillation from the oscillator. A single DC-motor generates the motion for the oscillator. The motor output is split into two cranks, of which the second is attached with a spline-coupling. The spline provides 20 setpoints for adjusting phase of the second output relative to the first at 18° increments. Both of the cranks provide amplitude setpoints at 1.5 mm, 3.0 mm and 4.5 mm radius. With the total drill rotation of 30° and the attachment points separated by 3.0 mm, the maximum supplied stroke length of the oscillation is approximately 0.75 mm. The 4.5 mm crank radius supplies a stroke length of 9.0 mm which is reduced (12:1) to 0.75 mm by a cantilever beam.

The preliminary results showed that the drill got embedded in the drilled hole, only reaching a maximum depth of 5.6 mm. This depth is insufficient for measuring a steering effect. Therefore, two alternative drill designs were proposed and evaluated in an effort to increase the drilling depth. The design adaptation that provides the most promising result, is to drastically lower the stiffness of the connection between the drill head and the leaf springs. The experiments showed that this solution significantly increased the rotation angle of the drill head by 28%, increasing the travel distance of the cutters. Furthermore, it was observed that the adapted drill did not get itself embedded as easily as the original design, allowing it to reach greater drilling depths.

An amplitude or phase difference applied by the oscillator causes the drill head to produce a different motion pattern. The pattern from the amplitude difference (stroke distance: left: 0.75 mm, right 0.25 mm) shows a decrease in the deviation distance which is expected to have diminishing effect on the effectiveness of the drill. A phase difference of 144° between the two oscillations, causes the drill to produce an oval motion pattern which is expected to be the most effective in generating a steering effect.

This project provides a great basis for the future development of a drill that can steer without a steering actuator. The next step forward with this design should be to incorporate hinges between the leaf springs and the drill head, to maximise the rotational motion of the drill head.

Contents

1
Introduction

1.1. Background on spinal fixation

1.1.1. What is spinal fixation

The goal of spinal fixation is to provide immediate stability through rigid immobilization of the spine [1]. This is done by placing an implant that increases the stiffness in a section of the spine and thereby reduces the mobility of the spine. Figure 1.1 provides an example of a section of a fixated spine. A common procedure is posterior spinal fixation where the spine is braced by using a structure of stiff metal rods along the spine. Pedicle screws are used for attaching these rods to the vertebrae. The procedure is often performed in combination with bone grafting, meaning that bone growth in the treated region is stimulated to fuse the vertebrae together over time. This procedure is then called spinal fusion.

The procedure for inserting pedicle screws in the vertebra as explained in [3] and [4] starts with determining the insertion point. With an awl, burr or rongeur, a portion of cortical bone will be removed for better access. Then, the correct angulation for the hole is determined. A pedicle probe is used to create a cavity through the centre of the pedicle into the vertebral body. Imaging techniques are used to confirm a correct placement and insertion angle. A pedicle sounder is then used to test if the cortical wall is still intact. Modern methods involve robotic assistance to accurately determine the correct hole angulation and screw placement. These methods are regarded as superior compared to the free-hand technique according to McKenzie *et al.* [5]. A fitting screw length and diameter are chosen for the created hole. Optionally, the hole can be tapped before screw insertion. Finally, the screw is inserted and secured in the hole, after which the bracing rods can be attached.

1.1.2. Vertebral anatomy

Figure 1.2 shows the general structure of a vertebra. The anterior (front side of the body) side of the vertebra is formed by a cylindrical-shaped structure, called the vertebral body. This is built to resist the high stresses induced by the body's mass in the vertical direction. Between each two vertebral bodies lies an intervertebral disk. This disk is made of soft tissue and allows for movement between the vertebrae, allowing the spine to bend and twist. On the posterior side of the vertebra, two pedicles stick out that connect to the lamina and the facets. The laminae connect forming an enclosed open space between the vertebral body, the laminae and the pedicles. Through this space lies the spinal cord. Each facet connects to a facet on the vertebra above or below. This connection provides a limit on the freedom of movement between the vertebrae and thereby

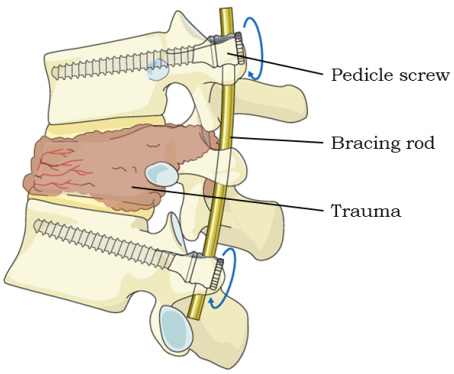

Figure 1.1: A side view sketch of a short posterior spinal fixation. On the left of the image is the front side of the spine (anterior) and the right is the back side of the spine (posterior). Image adapted from [2].

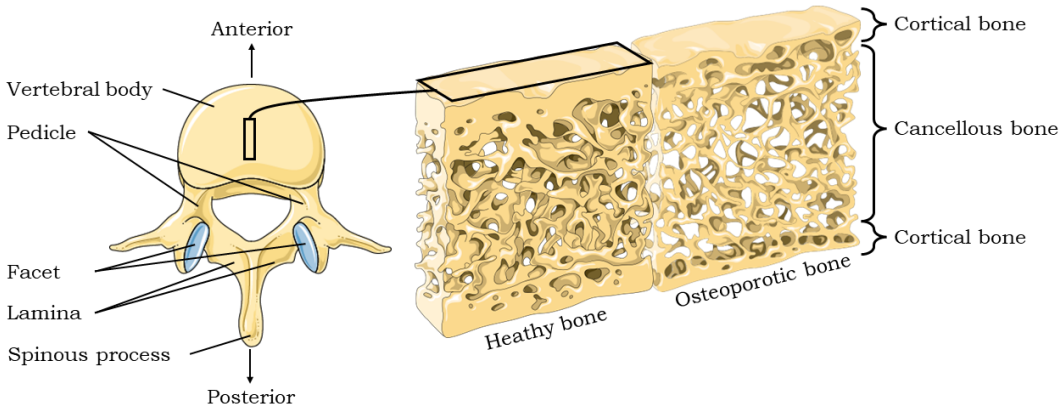

Figure 1.2: On the left side, a vertebra in top view perspective is displayed. A cutout section of the inner bone structure of the vertebra is shown on the right. The outer cortical bone layers and inner cancellous bone are shown for both healthy bone and osteoporotic bone. The images are adapted from `smart.servier.com`.

forms a guidance structure for the motion allowed by the intervertebral disk [1]. The outside of the vertebra is made of a thin layer of strong and dense cortical bone. This encapsulates the inside of the bone which is made of porous and lightweight cancellous bone, also called trabecular bone or spongy bone. The pores of the cancellous bone are filled with marrow, nerve tissue and interstitial fluid and is continuously supplied with blood through the cylindrical wall of the vertebral body.

1.1.3. Pedicle screw failures and risks

For pedicle screw insertion, multiple risk zones are located along the spine and near the vertebrae as indicated by Paul Anderson [6] and Galbusera and Wilke [1]. Figure 1.3 provides reference to these risk zones. Perforation of the cortical wall by the screw can lead to different complications depending on the location of the perforation. In the thoracic and lumbar spine, the abdominal aorta lies on the anterior side of the spine. A screw or drill that accidentally protrudes through the cortical wall may perforate the aorta. Perforation of the aorta is potentially lethal but can be treated with an emergency procedure [7]. Smaller damage to the cortical wall may lead to pain complaints, but this is usually treatable with a revision surgery [8]. Smaller arteries surround the vertebrae for the blood supply to the spinal region. Perforation of one of these is less severe than with the aorta, but in any case undesired. Encapsulated in the vertebral foramen and well protected by the vertebrae lies the spinal cord. Between every two vertebrae, the spinal cord branches off laterally on both sides into the nerve roots. Damaging the smaller arteries or nerves requires a revision, where the problem area is treated and the damage is repaired. According to Du *et al.* [9] nerve damage usually emerges as pain or numbness of specific muscle groups and can in most cases be treated by revision surgery or with therapy involving medication or physical exercise. Most of the before-mentioned complications can be treated, however, this always causes additional trauma to the patient which also increased the cost of the treatment and recovery. Both effects are undesired and it is better to prevent these accidents from happening.

Besides operative risks associated with spinal fixation, the pedicle screws also account for some risks. The majority of the screw length sticks into the cancellous bone which makes it a relatively weak anchor point. In the case of healthy cancellous bone, this connection provides sufficient strength and stability, however, when the patient suffers from osteoporosis, this may not be the case. Osteoporosis is a condition that diminishes bone density and weakens bone strength as can be seen in Figure 1.2. A pedicle screw that relies on cancellous bone for its connection is particularly at risk of loosening with decreased density and strength of the bone. A loosened screw can lead to a failed immobilization of the spine which limits the bone growth and can lead to instabilities. There is also a small risk of breakout which is when the vertebral bone fails and breaks. This can lead to damage to the surrounding blood vessels and nerves.

Kazemi [11] mentions that the pedicle screws can fail in two major ways: failure of the bone and failure of the pedicle screw. In cases with lower bone density, the bone is most likely to fail. With sufficient bone density, the metal pedicle screw is more likely to fail due to cyclic load. Anderson [6] names two important failure modes of the bone. These are called "pullout", where the screw shears out of the bone in the longitudinal direction and "cantilever bending" (sometimes referred to as "toggle") caused by a moment on the screw. Cantilever bending is considered the most common failure for pedicle screws. The characteristic of cantilever

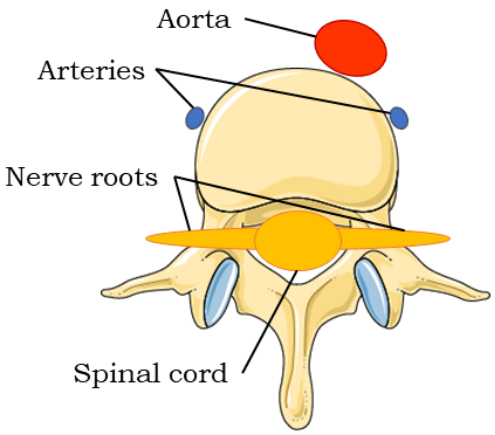

Figure 1.3: A schematic top view of a vertebra with the surrounding organs in the abdominal region shown and named. Damaging these can have severe consequences for the patient and thus should be prevented. Image adapted from `https://smart.servier.com/` based on images from [10].

bending is that the point of rotation usually lies inside the pedicle, meaning that the cancellous bone in the vertebral body has failed.

Osteoporosis is a common condition in elderly patients where bone strength diminishes. Rometsch *et al.* [12] have performed a study specifically focusing on complications with pedicle screws for patients with osteoporosis. The weaker bone diminishes the load-bearing capability of the screws for different load cases. This increases the risk of complications associated with screw loosening. Several screw augmentation methods are mentioned that can be used to decrease this risk of failure. This can be established by changing the screw geometry such as the thread, diameter, shape and roughness. Or by changing the surgical technique, such as screw trajectory, diminishing the degree of correction or the use of bone cements. According to Rometsch *et al.* the risk of screw loosening in osteoporotic bone for regular pedicle screws is 22.5%. For augmented pedicle screws, this risk lowers to 2.2%, although the report does not make a comparison between the different augmentation methods. The report mentions a reduction of re-operation risk from 5.3% for normal pedicle screws to 3.9% for augmented pedicle screws.

The pedicle screws used in spinal fixations can be placed through the pedicle into the vertebral body in two trajectories as shown in Figure 1.4. The traditional method of pedicle screw insertion is called the pedicle screw trajectory, where the pedicle screws are positioned in the horizontal plane and angled inward towards the centre of the vertebra. The second method is called the cortical trajectory, which aims to increase the contact area between the cortical screw and the cortical bone [11]. Cortical screws are currently regarded as an improvement from traditional pedicle screws according to Wang *et al.* [13]. For ease of use, pedicle screws and cortical screws will be named pedicle screws throughout the report.

A study by Singh *et al.* [15] states that the use of bone cements is the most effective in providing strength and stability for pedicle screws and also decreases the complication rate. The highest risk factor was cement leakage, but this did not lead to symptoms in most of the cases. A study from Saadeh *et al.* [16] provided a similar conclusion with the use of fenestrated pedicle screws. These are pedicle screws with internal channels for injection of bone cement through the screws, rather than pre-applied bone cement before insertion. Lorenz *et al.* [17] measured the mechanical pull-out force for regular pedicle screws, cemented pedicle screws and dual outer diameter pedicle screws. The regular screws provided an average pull-out resistance of 713 N compared to 1402 N for the cemented screws. Another test showed an average pull-out strength of 680 N for regular screws compared to 829 N for dual outer diameter screws. They concluded that cemented screws are superior for increasing screw stability. In short, these studies show a significant benefit in using bone cement to fixate pedicle screws in osteoporotic bone. Two drawbacks are that cemented pedicle screws cannot be removed and cement leakage forms a minor risk of complications.

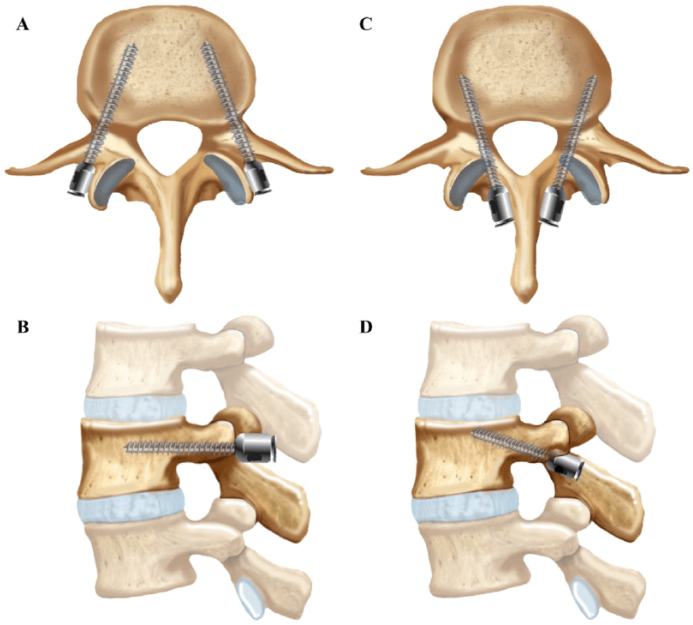

Figure 1.4: Images A and B show a traditional pedicle screw trajectory in a vertebra. Images C and D show the cortical screw trajectory. A and C are in top-view perspective, B and D are a side-view. Image source [14].

1.2. Problem description

Currently, the most effective method to mitigate the risk of pedicle screw pullout is the use of bone cement, where the surrounding of the screw is adapted to better distribute the forces of the screw. Another major improvement is the use of the cortical trajectory instead of the pedicle screw trajectory, where the trajectory is adapted to transfer the forces from the screw to stronger areas of the bone. However, both methods still use a straight screw in trying to properly distribute the forces to the strong parts of the vertebra whilst the structure of the vertebra is highly inhomogeneous and features many curved sections. Instead of adapting the bone to the screw, it would make sense to find a device that can adapt the screw to the bone. The implanted device can then directly transfer its forces to the strongest parts of the bone, providing a more stable and reliable connection. Figure 1.5 provides a sketch of what such a connection could look like. Following this approach to providing a spinal brace, the first hurdle to overcome would be the creation of a curved trajectory through the bone. The problem is that there is currently no device commercially available that can drill through cancellous bone and actively steer to form a curve that closely follows the shape of the cortical wall of a vertebra.

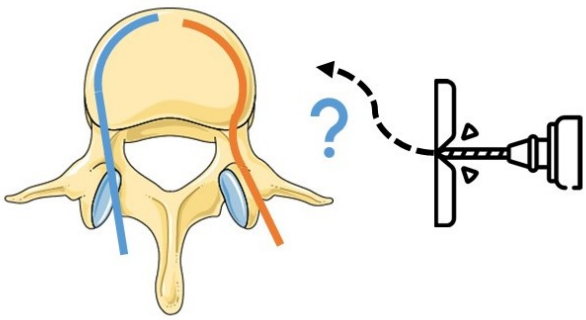

Figure 1.5: Two options for curved drill paths that can be used as opposed to a straight trajectory. A steerable drill to establish these is currently not commercially available. Vertebra image is adapted from `smart.servier.com`. Drill pictogram is adapted from `flaticon.com`

1.3. State-of-the-art bone drilling

A prior project by Rob Müller [18] produced a design and working prototype of an oscillating flexible drill based on the piercing mouthparts of a tsetse fly. Contrary to a conventional rotating drill bit, this design is flexible. The drill head consists of a cylindrical body that oscillates rotary around its centre axis. It receives its motion from a rotationally oscillating motor that can provide 10.000 to 22.000 rpm. The motion is transferred by a pair of parallel leaf springs that oscillate in the longitudinal direction which are connected with a hinge to the drill head to convert this motion back to a rotational oscillation. Figure 1.6a provides a schematic of the drill motion and Figure 1.6b provide a visual reference to the prototype. The leaf springs are flat, allowing them to bend easily in one direction, whilst resisting bending in all other directions. Flexibility is provided in the plane perpendicular to the thickness of the leaf springs. This means that the drill is capable of creating a curved trajectory however, the curvature is not controlled. The design assumes that the cortical wall of the bone is used for guiding the direction of the drill head. The leaf springs are kept parallel by rivet joints protruding through a hole in one leaf spring and a slot in the other. This connection also decreases the risk of buckling. The leaf springs are connected to the drill head with pin joints.

Due to the symmetrical design with this oscillating motion, the friction forces on the drill head counteract each other and produce a net zero friction force over many repetitions of its motion. This reduces the risk of large deviations from unequal forces generated in the drill tip. The drill provides flexibility in only a single direction, making that only this direction has to be controlled for steering whilst the other directions will always remain stiff. This drill design forms the basis of the design presented in this thesis.

1.4. Project goal

The goal of this project is to adapt the flexible oscillating drill design of Müller [18] to a steerable drill that can create a curved hole in artificial cancellous bone. The same motion system of two parallel flexible plates will be used for transferring the oscillating motion to the drill head. The aim is to keep the drill as simple as possible.

1.5. Outline

First, the method of steering for the drill had to be determined. In this regard, Chapter 2 describes the design direction of this project, provides a schematic overview of the basic design and provides the requirements for the design. Chapter 3 describes the development of the concept design and the design choices that were made for each of the modules. Chapter 4 showcases the prototype design and a series of preliminary experiments that lead to two adapted drill designs. Chapter 5 describes the evaluation of the original drill and the two adapted designs with a set of experiments. Chapter 6 provides a discussion on the outcome of the project. Chapter 8 provides a conclusion, summarizing the project results.

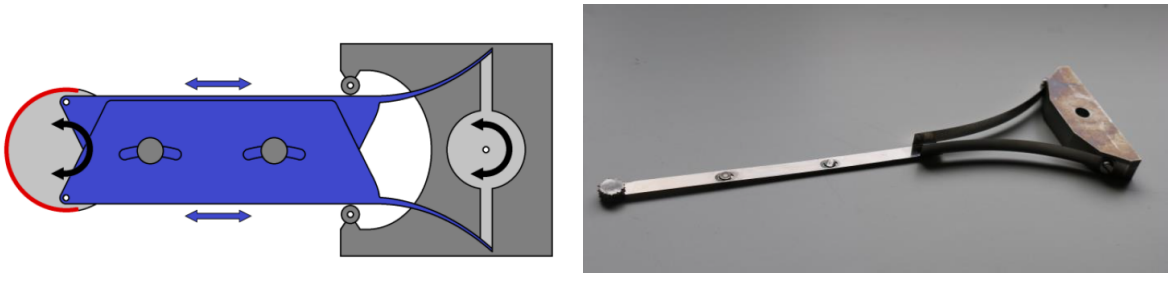

(a) (b)

Figure 1.6: (a) A schematic view of the flexible oscillating drill concept displaying the motion transmission. (b) A photograph of the flexible oscillating drill prototype. Both images are captured from Müller [18].

2
Design direction

2.1. Establishing the steering force

2.1.1. Overview of existing steering techniques for drilling devices

A literature search for steerable and bendable drilling instruments was performed to establish an overview of the available techniques to manipulate the direction of a drill tip. The overview can be found in Figure 2.1. The combined overview was created, based on a number of reviews describing steerable medical drills [19], steerable catheters [20] [21], steerable needles [22], directional drilling [23] and a self-performed patent review to steering techniques used in tunnel drilling machines.

The categorization is based on the interaction of the steering system with its environment. The first main category is free motion, meaning that the steering system uses internal forces to steer the drill tip in a new direction. The second main category is environment-based motion where the steering system relies on a force interaction with the environment to create a direction deviation force.

Within the category "free motion" a further subdivision is made based on the type of articulation and actuation. The first subdivision distinguishes between a single point articulation, where the steering system forms a hinge point and a distributed articulation, meaning that the steering system deforms a section of the drill body or multiple hinge points are distributed over its length. Within the category of distributed articulation, three sub-categories are defined based on the type of actuator. The first is a bending actuator,

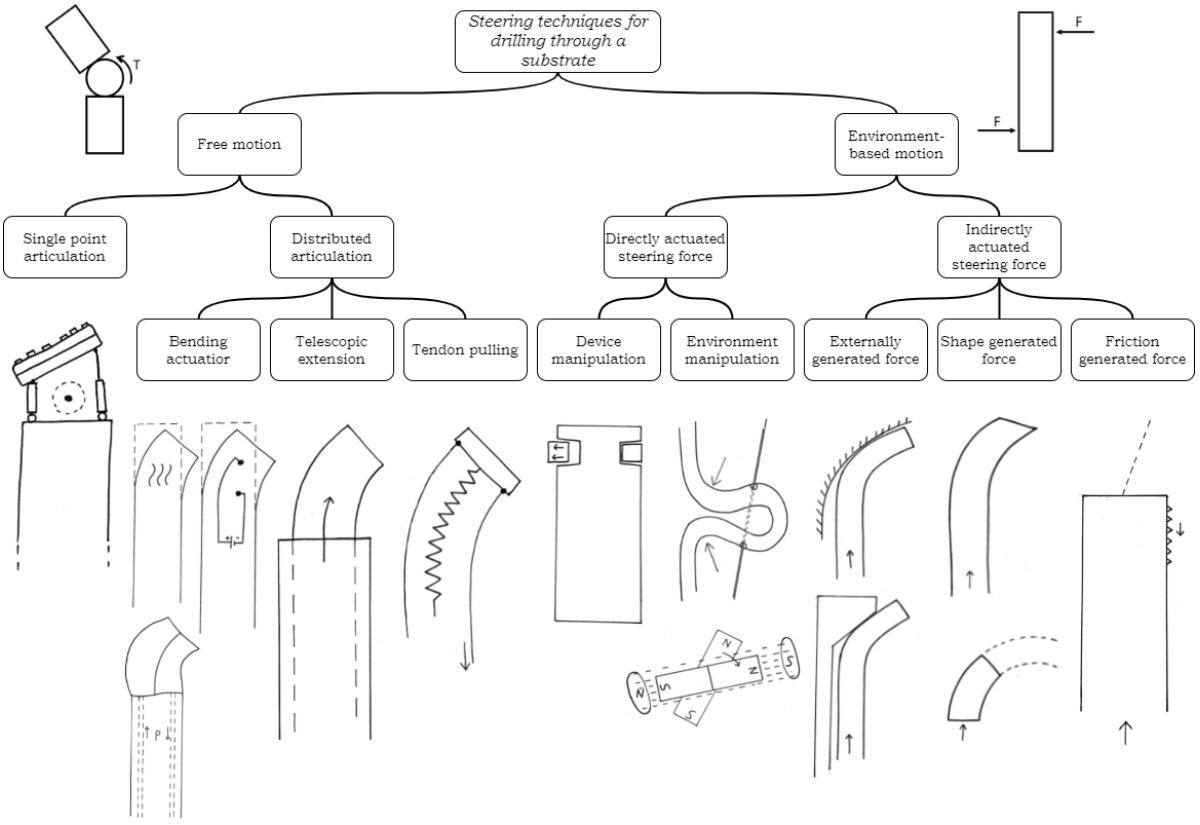

Figure 2.1: A categorized overview of existing methods for steering a drilling device through a substrate.

where the body of the drill can be deformed as actuation. This can be done by applying heat, an electric charge or by inflating and deflating hollow chambers. The second sub-category is telescopic extension, where two or more bodies are concentrically nested and can slide in the longitudinal direction. One example is a pre-curved flexible body that is pushed through a rigid tube. Extending this flexible body from the rigid tube makes that it produces a curved path. The third sub-category is tendon pulling, where tendons are guided through a flexible body and attached to its distal end. By selectively pulling these cables, the flexible body can be deformed to produce a curved shape.

Within the category of "environment-based motion," a first subdivision is defined between direct- and indirect actuated steering. Directly actuated steering is where an actuator directly applies a force to the environment to push itself into a new direction. Within this category, a division is made between device manipulation, where the device itself creates a mechanical steering force and environment manipulation, where the forces are applied from the environment to the device. Within environment manipulation methods were found that mechanically manipulate the environment or where the magnetic field is locally manipulated. The second subdivision within the category environment-based motion is indirectly actuated steering forces, meaning that the steering forces are the result of another motion or force that has no primary function as a steering actuator. The first sub-division within this category is externally generated force where the drilling device is blocked or guided into a new direction by an external device that deviates the forward push force of the drill. The second sub-category is shape-generated force, where the shape of the drill body or drill head causes the push force to induce a steering force from the environment. This can be established by providing the drill head with an asymmetric taper or wedge shape or by the drill body having a predefined curvature. The third sub-division is a friction force. Here the friction on the circumference of the drill body can be altered locally to induce a moment force on the drill head as a result of the forward motion and the sum of friction forces.

The forward feed force of the drill needs a sideways deviation force component added to have it change its direction. Forces for drilling in bone are relatively high compared to laparoscopic devices used in soft tissues. Therefore it is also expected that the deviation force needs to be relatively high, as this force should scale with the magnitude of the feed force.

The high force required for steering through bone makes that many of the steering methods presented in Figure 2.1 will not suffice in generating a large enough deviation force to deflect the drill. A downside of some methods is that a steering actuator is needed alongside the drill actuator which can increase the stiffness of the construction. The most important downside is the added complexity of integrating and using additional actuators in a bending device. A successful attempt for a steerable bone drill found in the literature is the use of tendons in combination with a drill body formed by a series of connected rigid segments by Alambeigi [24] [25]. For this drill, a tendon force of 25 N is needed to reach a 40° trajectory deviation. A more simplistic method is desired, preferably one where no additional actuators are required within the drill body or drill tip.

2.1.2. Manipulation of the drill head oscillation

The oscillating drill presented in Section 1.3 provides a good solution direction for finding a method of steering without an additional steering actuator. The oscillating drill constantly produces a sideways force due to the rotation of the drill head. The cutters produce a friction force tangential to the cylindrical wall of the cutter head, analogous to a wheel on a surface as seen in Figure 2.2. The friction force induced by the drilling action on the forward stroke is currently cancelled out by an equal and opposite force during the reversed stroke. Introducing an oscillation with a difference between the two oscillating inputs to the drill head can create a force difference between the forward and reverse stroke. Taking the sum of many repetitions from the continuous oscillation, a force difference should be capable of achieving a net sideways force as presented in Equation 2.1.

$$\sum F_{sideways} = \sum F_{forwardstroke} + \sum F_{reversestroke} \neq 0 \tag{2.1}$$

With the original design, this sideways force would achieve very little, because of the leaf spring's orientation. It is oriented such, that the drill head will push in a direction where the leaf spring provides high stiffness, as indicated in Figure 2.3a. To allow this force to push the drill head sideways, the leaf spring must be able to bend in this direction. Therefore the sideways force needs to act in the same plane where the leaf spring is the thinnest and most flexible. The proposed solution is to re-orient the drill head and leaf springs as displayed in Figure 2.3b.

Different methods of manipulating the oscillating input to the drill head have been studied to find promising methods for generating the sideways force for steering the drill. Only the oscillating motion of the drill

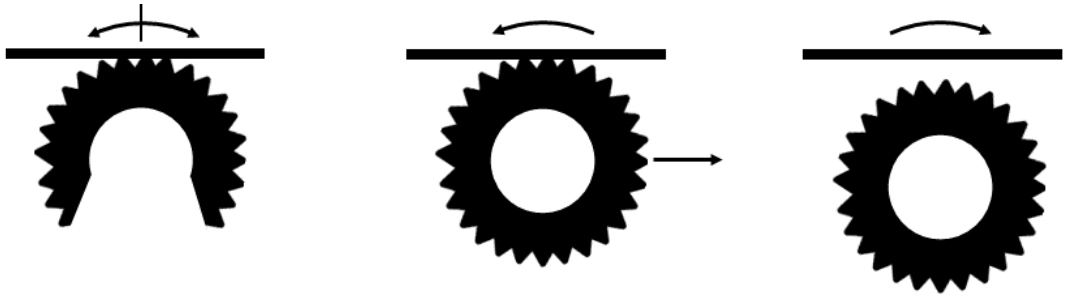

(a) (b) (c)

Figure 2.2: Three schematic top views of the drill head. (a) When the oscillating drill head is in contact with an object, it does not produce a net sideways motion or force. (b) A sideways motion or force is generated when the drill head rotates continuously as if it were a wheel. (c) No sideways motion or force is generated when the drill head is not in contact with the object. Combining the effect of (b) and (c) within an oscillation is expected to generate a net sideways steering force and direction deviation.

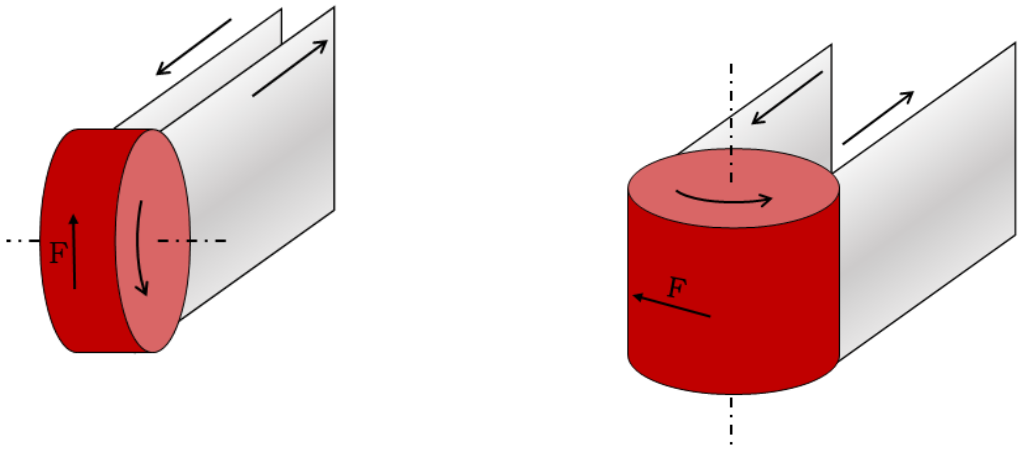

(a) (b)

Figure 2.3: Configuration (a) shows the orientation of the drill head in the original design. The deviation force F will have a negligible steering effect due to the high stiffness provided by the leaf springs in this direction. Configuration (b) has the drill head in a different orientation, allowing the leaf springs to bend with the deviation force generated in the drill head.

head and the interaction with the bone have been considered in this analysis. The interaction with the leaf springs that transfer the oscillation to the drill head has for now been omitted. The standard formula to define an oscillation is shown in Equation 2.2. The y value provides the magnitude of the oscillation at a particular instance of x. x Is here in degrees within the domain 0° to 360°. This oscillation waveform can be manipulated by changing the amplitude (a), changing the frequency (b) or changing the phase ($\frac{c}{b}$). Dimensionless relative values are used in this analysis as they should work on any scale.

$$y(x) = a\sin(bx - c) \tag{2.2}$$

A motion study has been performed in Solidworks, where the drill head received two oscillating displacement inputs as if it were attached to the two leaf springs. At first, the oscillation of the drill from Müller [18] was simulated by generating two oscillations that each drive one of the hinge points of the drill head. The oscillations are equal in amplitude, causing the drill head to rotate over a 30° angle. The two signals are 180° out of phase. The frequency remains 1 as velocity can be disregarded for now. This results in a purely oscillating rotation of the drill head as displayed in Figure 2.4a. The motion study was continued by assessing the effects of a change in amplitude, a change in phase and a change in frequency in one of the two oscillations. The theoretical calculations that can be used to determine the drill head position and orientation can be found in Appendix A.

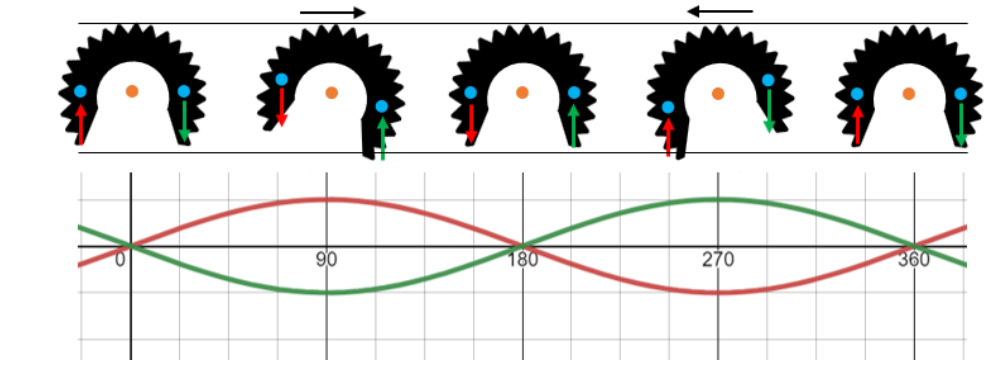

(a)

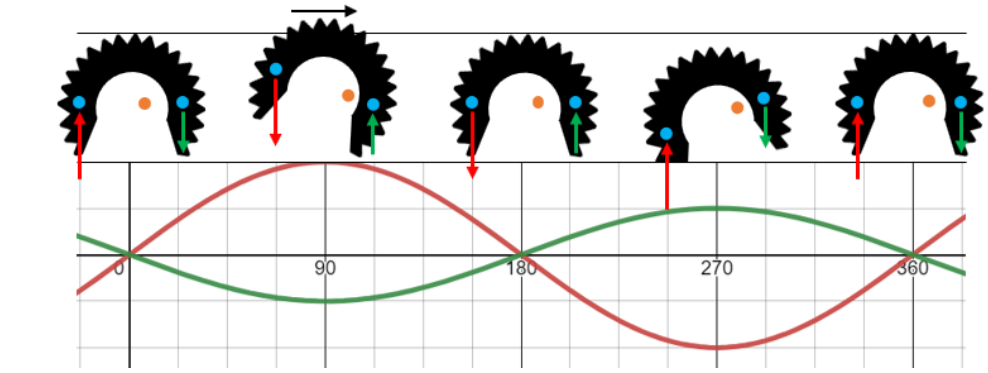

(b)

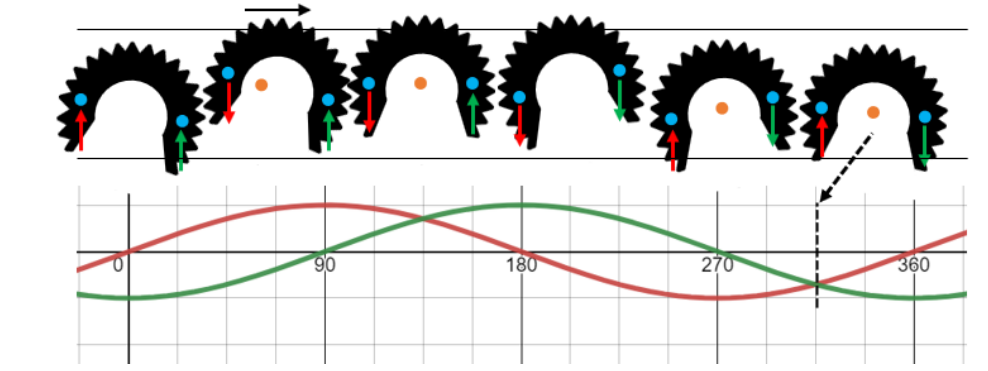

(c)

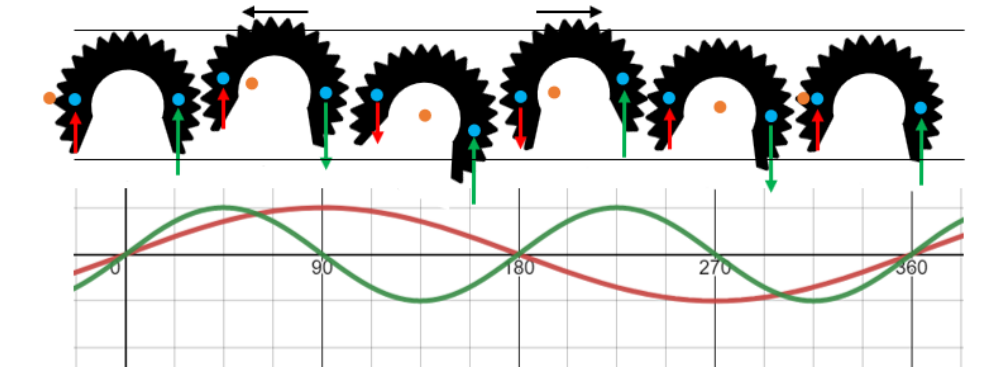

(d)

Figure 2.4: Four graphs display the results of the motion study on the effects of different oscillation patterns of the drill head. The results are replicated for improved visualisation. The drill head icons are in the top-view perspective and correspond to the position and orientation provided by the two waves from the wave graph. The blue dots represent the attachment points where the oscillation is received. The orange dot is the centre of rotation at that instant. The arrows provide the direction of motion towards the next position of the drill. The green arrow corresponds to the green wave in the graph and the red arrow to the red wave. The black arrow shows the instance and direction where the sideways force is predicted to cause the largest trajectory deviation. Graph (a) is the reference motion where the drill head receives two oscillations 180°out of phase with the same amplitude and the same frequency. Graph (b) shows two oscillating inputs, where the left (red) oscillation has twice the amplitude of the right (green) oscillation. Graph (c) shows the effect of two oscillating inputs with a phase difference of 90°. Graph (d) shows two oscillating inputs with a frequency difference. The frequency of the green oscillation is double the frequency of the red oscillation.

Amplitude difference: As displayed in Figure 2.4b, the difference in amplitude creates a shift in the location of the centre of rotation (orange dot) away from the centre of mass but between the two input points (blue dots). This causes the drill to not only rotate but also translate forwards and backwards. This creates a forward stroke, where the drill pushes itself into the substrate and a backwards stroke where it releases itself. It is expected that the increased friction during this forward stroke pushes the drill slightly sideways to the left, which is not counteracted during the reversing stroke. Additional to this, the drill moves a greater distance on the left side compared to the right. In theory, this should cause more material to be removed on the left compared to the right. This may create a lower resistance path to the left, increasing the steering effect of this motion profile. The expectation is that increasing the amplitude difference, increases the steering effect. This is however limited to the maximum amplitude that can be supplied to the drill head.

Phase difference: In Figure 2.4c an example with a phase difference of 90° is shown. A phase difference of 0° causes the drill to fully punch without rotation. This effect should be avoided. A phase difference of 180° is what is used in the reference graph where the drill head fully rotates. Between 0° and 180° phase difference, a translating motion together with the rotation of the drill head is created. The drill alternates between a translation forwards and backwards, where it rotates in-between. This means that it moves forward and rotates counterclockwise whilst engaged in high friction with the substrate creating a large friction force sideways. After this, the drill retreats and rotates clockwise with little friction. It is likely that a phase difference will cause a deviation force. The best results are expected with a phase difference in the range between 90° and 180° as the punching effect becomes too prominent below 90°. Beyond 180° the steering effect reverses direction.

Frequency difference: The frequency of a signal can be changed by speeding up or slowing down one of the oscillating inputs. This also creates a shift in phase, therefore the timing of this process matters in reaching a desired frequency and phase shift. Furthermore, there are two types of frequencies possible: The first is a harmonic frequency, where the two signal frequencies are integer multiples of each other and non-harmonic frequencies where the two are non-integer multiples of each other. The use of non-harmonic frequencies did not look promising as the two waves constantly shift in phase. Over time this creates an effect where the drill head continuously changes its behaviour as the waves harmonize and de-harmonize. This causes the drill head to occasionally oscillate in periods with near 180° phase difference and more or less punch in periods with near 0° phase difference. The sideways force is not repeatedly present or can even be reversed, making non-harmonic oscillations not suited for further trial. The harmonic oscillations are more consistent in their behaviour, but, as can be observed in Figure 2.4d, the oscillation shows a leftward directed force and a rightward directed force being generated. A frequency difference larger than a factor of two does not show more promising results. At the start of the motion pattern between 0° and 45°, the drill shows a punching behaviour where it translated forward with little rotation. This effect is undesired as it generates an impact, which is not the intended use of the drill head. Shifting the phase does not eliminate this issue entirely. Because of the lack of the desired net steering force and the tendency to punch, a frequency difference does not show promising behaviour.

This motion analysis of the drill head behaviour shows a potential to generate the desired sideways force for steering the drill when one of the inputs is changed in phase or amplitude. Combining the two effects may provide improved performance. However, the hypothesis of this sideways force being generated is still to be verified in practice. A prototype drill and accompanying oscillator have been designed and built to further research the effects of the amplitude and phase difference on the drill motion and drilling performance.

2.2. Schematic overview of the design

The prototype drill and oscillator were first divided into multiple back-box modules with each module coupled to a function of the device. In this manner, each module can be designed separately, after which the combination of these modules will form the concept design for the complete drill device. An overview of the module division is presented in Figure 2.5.

- **The oscillator assembly:** The device that generates the oscillating motion.
  - **Motor module:** The motor module generates motion and provides a torque or force to drive the complete mechanism.
  - **Motion adjustment module:** The motion adjustment module is responsible for converting the motor motion into two oscillations. The adjustment of the amplitude and phase of these two oscillations is also a function of this module.
- **The drill assembly:** The device that drills into the bone.
  - **Motion transfer module:** The motion transfer module is responsible for transferring all drilling and steering motion from the oscillator assembly to the drill head module. This means that the drill oscillation, drill feed and steering actuation are all supplied through this motion transfer module. To follow the drill head through the curve, the motion transfer module must be flexible in the desired steering direction.
  - **Drill head module:** The drill head is responsible for cutting the bone and inducing the steering force by rotationally oscillating in specific patterns.

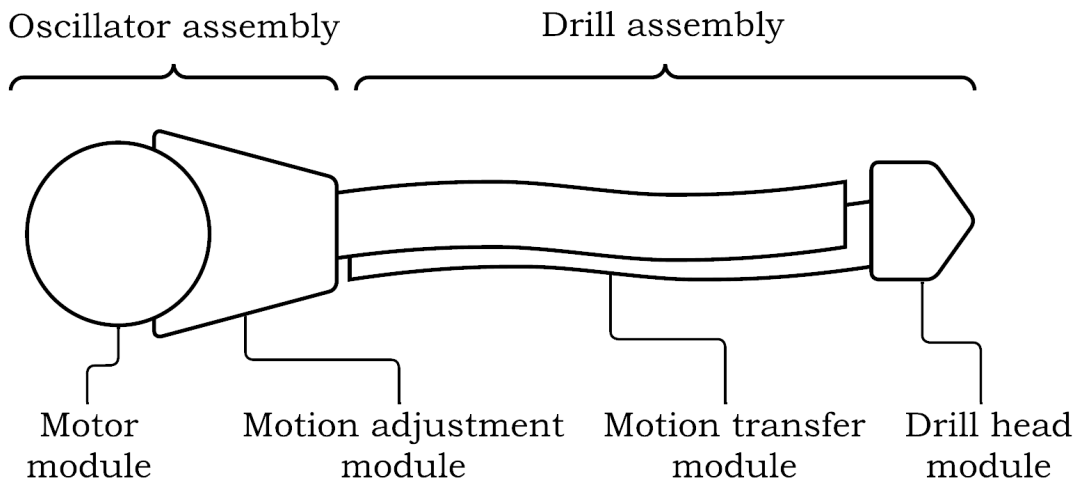

Figure 2.5: An overview of the sub-assemblies and modules of the oscillating steerable bone drill.

2.3. Design requirements

Three main functions of the drilling device are provided in the list below. The drilling device should fulfil all three functions to render this design successful.

- **Cutting artificial bone:** The cutter shape and motion must be adapted to cut through an artificial bone sample, called bone phantom. A Sawbones rigid polyurethane foam block will be used to represent bone, as it features a cellular structure like in cancellous bone. A grade of 10 PCF provides the best mechanical properties to represent osteoporotic cancellous bone [26]. However, a slightly lower grade of 5 PCF was chosen for ease of testing. The drill should be able to reach at least 50 mm depth, preferably up to 80 mm.
- **Steering the cutter:** The steering motion must be produced from changes in the cutting motion, eliminating the need for a separate steering actuator. The oscillator must be able to generate two oscillations with an adjustable amplitude with a magnitude difference of at least a factor of two and an adjustable phase difference with at least a setting for 180°and 90°phase difference.
- **Push the cutter forward:** The cutter must be pushed into the artificial bone sample from the outside. The push force must be transferred to the cutter ensuring contact between the cutter and the artificial bone. The pushing system must not suppress the steering functionality.

Furthermore, a set of practical requirements was set up with regard to testing the prototype.

- **Prototype requirements:** The design will be tested with a prototype model. For testing the effects of steering through adjustment of the phase and amplitude, a high degree of adjustability is desired. Both the amplitude and phase between the two generated oscillations need to be adjustable, preferably with three or more different settings.
- **Adjustability requirements:** With a highly adjustable design comes a high degree of complexity. Therefore, the individual mechanisms and components will be kept as simple as possible to avoid overcomplicating the design. Options with fewer parts and fewer interactions will be preferred.
- **Maximum hole size:** The drill will be designed to be used in spinal fusion surgeries. For its dimensions, the most critical part is the pedicle. The drill should fit safely through a pedicle and should not damage or breach the cortical bone. As a case study, a spinal fixation of the L3-L5 lumbar vertebrae is taken, where the drill should fit through the smallest pedicle of these vertebrae. As found by Zhou *et al.* [27] the pedicles in the L3 lumbar vertebra are the smallest of these three with an average width of 8.7 mm for females. Since the drill creates a rectangular hole, the diagonal of the rectangular hole can therefore not be larger than this maximum diameter. The shapes of the pedicle and the rectangular hole through it are displayed in Figure 2.6.

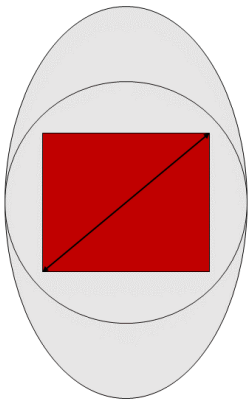

Figure 2.6: A schematic display of the smallest pedicle size, the drill head needs to fit through with its rectangular shape. The oval represents the pedicle based on dimensions from [27]. The circle represents the hole size boundary of 8.7 mm diameter. The red square is the size of the drill cross section.

3
Concept design

3.1. Oscillator assembly design

3.1.1. Oscillator motor design

The configuration of the oscillator assembly resulted in a selection of one of three motor design concepts.

1. **Directly oscillating drive:** The directly oscillating drive concept, depicted in Figure 3.1a, consists of two linear actuators that directly supply an oscillating linear motion to the drill assembly. Suitable actuators would be voice coils which are capable of directly supplying the correct amplitude and frequency to the drill module. The voice coils can be fed from an oscillating electrical signal meaning that the phase difference and amplitude difference can be adjusted on the go with very little effort. This solution provides the ideal properties of a drill actuator. However, it requires expensive and sensitive equipment.

2. **Two rotational motors:** The two rotational motors concept assumes that two rotational motors both with their own amplitude adjustment are driven with exact control of the phase between the two motors, as displayed in Figure 3.1b. This is however very difficult to establish at higher frequencies. High-frequency motors are extremely difficult to control in phase, whilst the motors that can be controlled in phase, such as stepper motors, cannot provide the requested motor speeds. This means that this concept is not feasible.

3. **Single rotational motor:** The single rotational motor concept assumes a purely mechanical solution that takes its input from a single rotational motor as seen in Figure 3.1c. The mechanism must split the input to create two outputs that can be individually manipulated. A mechanism must provide a means for adjusting the phase between the two outputs and a means of adjusting the amplitude of both outputs.

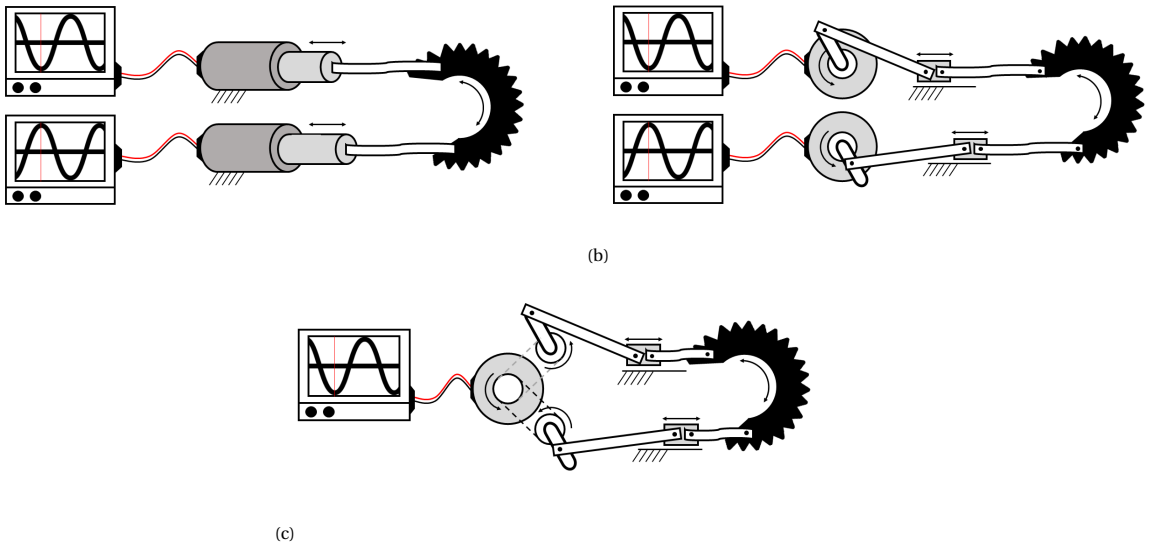

(a) (b)

(c)

Figure 3.1: Three schematic overviews of the concepts for generating the motion of the oscillator. (a) Depicts the directly driven oscillating drill concept. (b) Is an oscillator concept based on two position-driven motors. (c) Is the oscillator concept based on a single rotational motor with a split output.

The third concept single rotational motor was chosen based on its feasibility and affordability of the concept. The order of implementing the phase adjustment and amplitude adjustment matters in this concept. Adjusting the phase between two mechanical oscillations was found to be only possible when the mechanism is rotating. This is because, in a sine function, the angular position of a rotation determines the phase of an oscillation. It is therefore most practical to implement this adjustment before the motion is converted to a translating oscillation. With the amplitude adjustment, this is the other way around. A rotating object provides a signal by projecting a non-centre point, onto a stationary line or surface. This means that the rotation itself does not provide an amplitude, only when it is converted to a linear oscillation. In Figure 3.2, the flow of motion is schematically displayed. From the single motor, two rotating outputs are created. One of the rotations can be adjusted in phase to create a relative phase difference. Both rotations are then converted to an oscillation. The amplitude adjustment can be performed when the rotation is converted to a translational oscillation or thereafter. The drill assembly is directly attached to the output of the oscillator assembly.

3.1.2. Phase adjustment mechanism concepts

The following five methods were considered for establishing a phase difference between two rotating outputs from a single continuous rotational input. They are listed in order of complexity. Figure 3.3 gives an overview of these options.

- Parallel meshing, such as gears, chains and belts (Figure 3.3a).
- In-line meshing, such as a spline and Hirth coupling (Figure 3.3b).
- A planetary gear set (Figure 3.3c).
- A differential (Figure 3.3d).
- A swashplate (Figure 3.3e).

Considering the simplicity of the mechanisms, the meshing type of phase adjustment options are the simplest. The secondary advantage is that they feature a fixed number of adjustment points, so no measurement is needed to know what the set phase difference is. A meshing connection can be made from readily available off-the-shelf components. A proof of principle model made of Lego was used to assess a gear meshing mechanism. It was found that removing and attaching the gears on a round shaft causes positional inaccuracies. Therefore, a splined shaft connection was chosen as the solution for the phase adjustment. This can be created using a small gear that is fixed to the shaft as the spline and a 3D printed negative as the hub. A gear with 20 teeth provides positions with 18° increments, allowing the phase to be adjusted to 90°, 108°, 136°, 144°, 162°and 180° within the desired range.

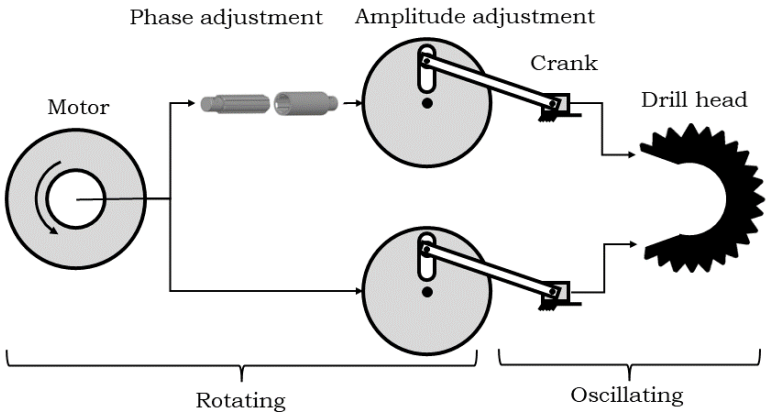

Figure 3.2: This schematic shows how the order of motion conversions within the oscillator generates two mechanical oscillations that can be adjusted in phase and amplitude.

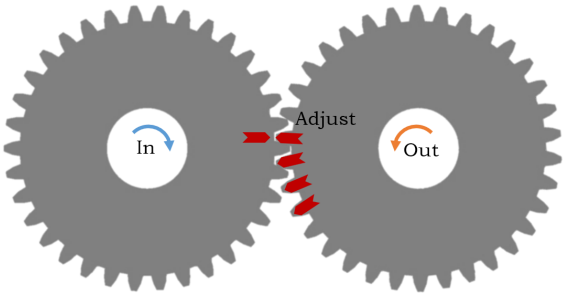

(a) Image adapted from `flaticon.com`

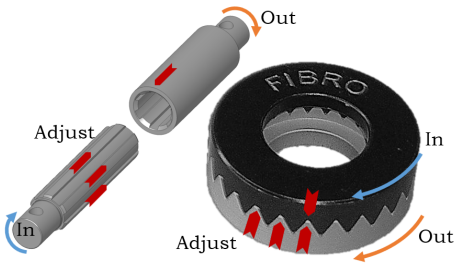

(b) Images adapted from Wikimedia Commons, Author spline: Silberwolf and Author hirth: Pfedelbacher

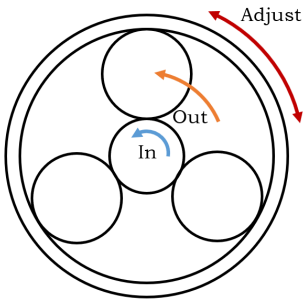

(c)

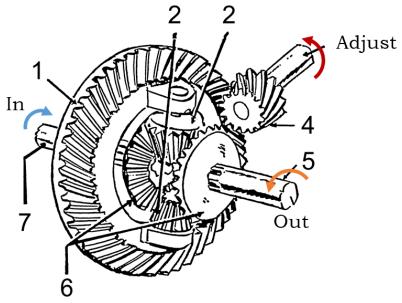

(d) Image adapted from Wikimedia Commons, Author: Pearson Scott Foresman

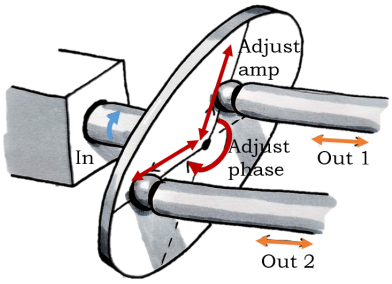

(e)

Figure 3.3: An overview of the five options considered for adjusting the phase between the two oscillations. The blue arrow indicates the input, the orange arrow indicates the output and the red arrows indicate the adjustment method. Images (a) and (b) are meshing-type adjustments, where the teeth have to be disconnected to adjust the relative rotation between the input and output (phase). (c) is a planetary gear mechanism where the ring gear is used for adjusting the phase. (d) is a differential where axle 4 is used for adjustment of the phase. (e) is a swashplate mechanism. The plate is attached to the motor shaft (in) with an angular deviation, causing it to make a wobbling motion. When the linear rods are kept in position and pressed against the rotating plate, they output two oscillations. The phase between two oscillations can be adjusted by setting the relative angle between two rods. Adjusting the amplitude of the output can be done by sliding the rod in the radial direction.

3.1.3. Amplitude adjustment mechanism concepts

The following four methods were considered for adjusting the amplitude of a mechanical oscillation. They are listed in order of complexity. Figure 3.4 gives an overview of these options.

1. An adjustable crank arm length (Figure 3.4a).
2. An adjustable cantilever beam (Figure 3.4b).
3. A hypocycloid mechanism (Figure 3.4c).
4. A swashplate (Figure 3.3e).

The adjustment methods that are mechanically the simplest, are the adjustable crank arm and the adjustable cantilever beam. Both can be used with a set of fixed set-points, which is an advantage as the settings are then always the same. The hypocycloid mechanism is complex in itself, requiring an additional scotch yoke to function, further increasing the complexity of the mechanism. It provides a continuous range of adjustment settings, requiring measurement to know what the exact setting is which makes adjustment more cumbersome. The swash plate mechanism solves both the amplitude and phase adjustment at once, which seemingly makes this an attractive solution. However, it is also a complex mechanism. The adjustment rods both need to be adjustable in the radial and tangential direction. It then becomes very difficult to adequately connect the drill assembly to these rods, making this not a viable option. A proof of principle model from Lego with adjustable cantilever beams was tested. It featured a slidable adjustment for the amplitude. This setup had some drawbacks as the beams require a lot of space to provide enough adjustment settings within a human-friendly scale. The attachment points for the leaf springs are each time in a different location depending on the setting. This can be solved by an added linear guide, but this over-complicates the mechanism. The preferred design eventually combines an adjustable crank with a fixed ratio cantilever beam. The crank is made of a disk which features holes on its flat surface at different distances from the centre. Each hole corresponds to a different amplitude setting to which the connector rod can be attached. The motion generated by the crank then needs to be reduced which is done by the cantilever beam.

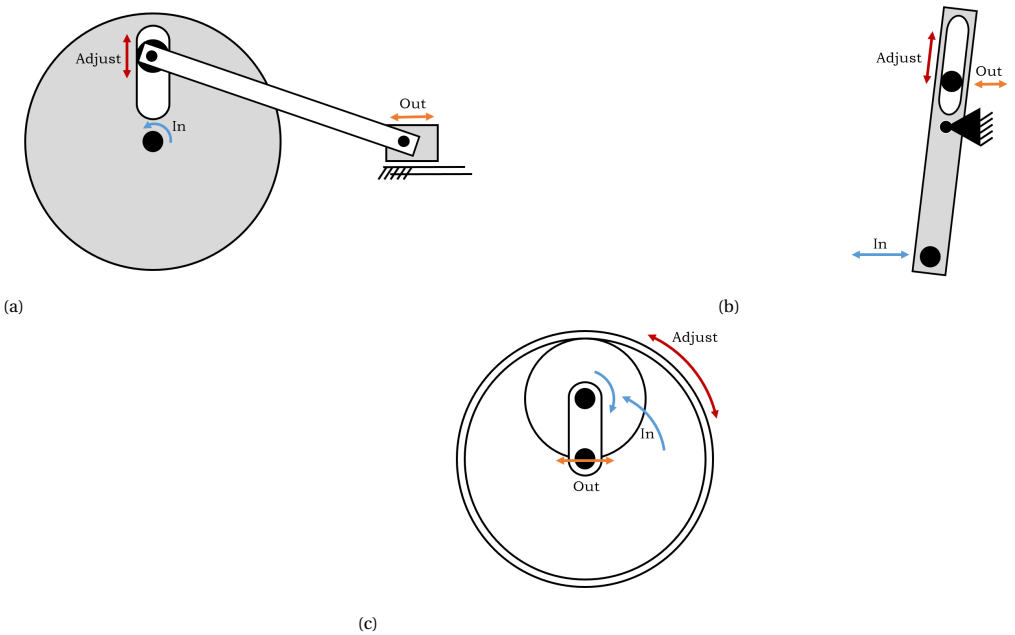

Figure 3.4: An overview of three options considered for adjustment of the amplitude of a mechanical oscillation. (a) a crank mechanism with adjustable amplitude. (b) a cantilever rod with adjustable amplitude. (c) A schematic display of a hypocycloid gear mechanism. A single planet gear rolls along the ring gear. The diameter of the planet gear is equal to the radius of the ring gear. A crank arm with the same length as the radius of the planet gear is rigidly attached to the planet gear causing the end of the crank to oscillate in a straight line. With a scotch yoke, this motion can be projected onto a line in any orientation within the same plane. Rotating the ring gear causes the relative angle between the oscillation of the crank arm and the scotch yoke to change, thereby changing the amplitude of the motion coming from the scotch yoke.

3.2. Drill assembly design

3.2.1. Drill head concept design

The drill head design is derived from the design of a flexible oscillating drill by Müller [18], comprising of a cylindrical drill head with the cutters placed on the cylinder wall. The cutter oscillates rotationally around the cylinder's central axis with the feed in the radial direction. The existing drill head does, however, not comply with the size restriction and must therefore be redesigned. The oscillating motion of the drill head is kept similar to the original design with a 30° stroke angle. With larger angles, the drill head motion can no longer be approximated by a linear model which unnecessarily increases the complexity. A small stroke angle could provide insufficient travel distance for the cutters.

The drill head must fit through a pedicle. Therefore, the size of the drill head was set to fit within a cylinder of 5 mm high and a 6 mm diameter. When drilling, a 180° section of this cylinder will be in contact with the bone. The 30° stroke angle makes that at least 210° of the cylinder needs to have the ability to cut. A 150° wedge from the rear side of the cylinder is removed to free up space for attaching the motion transfer system. The resulting cylinder is shown in Figure 3.5.

To find a suitable geometry for the cutters on the drill head, analogous insights were sought from existing tool and cutter designs. The cutting motion is difficult to compare to existing tools as a rotational oscillation is rarely used. In search of similar tools, the following characteristics were defined for the drill head. The first characteristic is that the cutter is driven by an oscillating motion which can be seen in saws, files, oscillating multi-tools and cast saws. The second characteristic is that the cutter needs to cut in both directions, which is a very rare property which is mostly seen in grinding-type tools and occasionally in saws. The third characteristic is the scale of the cutter: fine cutters are meant for precise removal of material and rough cutters are meant for fast removal of material. Figure 3.6 is an overview of existing tool types categorized based on the latter two properties: cutting direction of the tool and roughness of the cutter. This overview was used for finding inspiration and for defining a design direction for the cutter geometry.

Tuijthof *et al.* [29] experimented with different types of cutters in cancellous bone and found that the thrust force was higher for burr type cutters compared to drill and mill type cutters. Since the drill must be bendable it is preferred to keep the thrust force low to decrease the risk of buckling. It is therefore beneficial to use a cutter profile rather than a fine grinding or file profile for the cutter teeth.

The oscillating back and forth motion of the drill head is best resembled by a saw that is wrapped around a cylindrical body as displayed in Figure 3.7. This analogy with a saw is used to determine the shape of the cutters. Low cutting resistance is preferred since the motion transfer system can deliver a limited feed force due to its slenderness. Finding an efficient cutter that converts the majority of its energy into cutting, rather than producing heat from friction is therefore the goal. A low cutting temperature is also preferred to prevent bone necrosis. Bone necrosis is when bone is permanently damaged by heat exposure. This already happens when bone is exposed to temperatures of 50°C for over 30 seconds. Experiments from Krause *et al.* [30] focused on finding parameters that keep the cutter temperature low for bone cutters. One of these parameters is the rake angle, which is explained in Figure 3.8. The study saw a reduction in temperature when a rake angle of -10° was used compared to a rake angle of -30°. Therefore a -10° rake angle is chosen for the cutters. Since the cutters also need to cut in the reversed direction, the cutters will be symmetrical.

Because of the oscillating motion of the drill head, the distance travelled for each individual cutter must

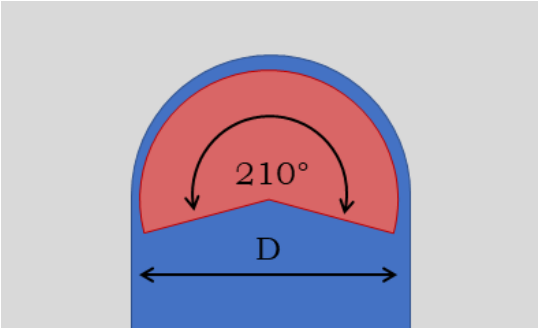

Figure 3.5: The sketch displays a top view of the drill head (red) in a drilled hole (blue) through the bone phantom (grey). The drill head is based on a cylinder of 6mm diameter and 5mm height. A 210° section of the cylinder face is used for cutting, making that the remaining 150° section can be removed from the design.

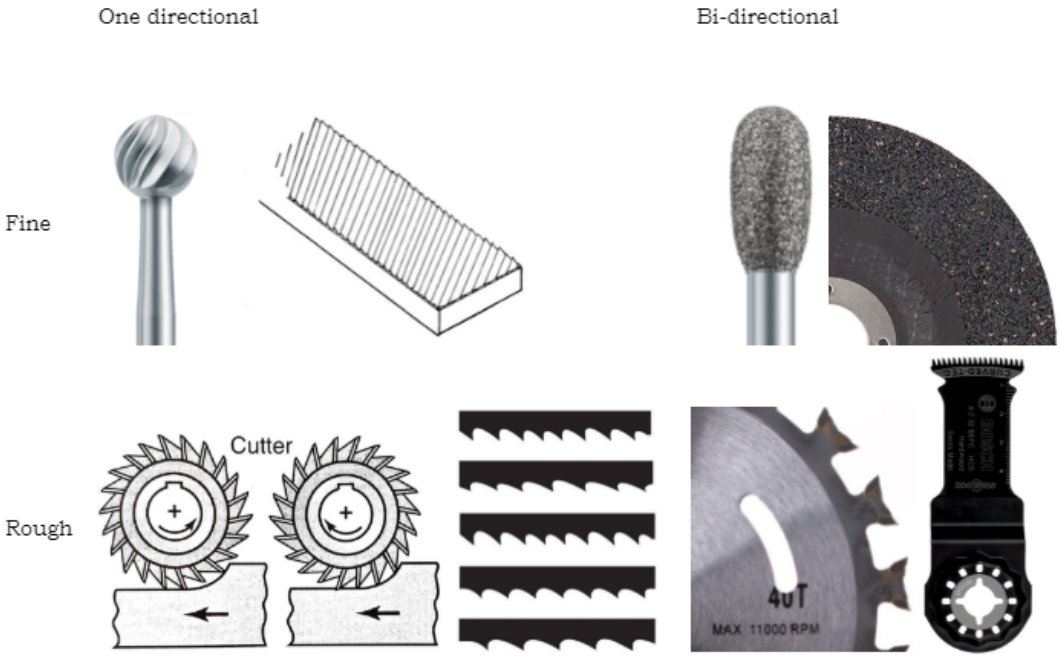

Figure 3.6: This figure shows multiple types of cutters divided into four quadrants based on their classification. The horizontal axis defines uni-directional and bi-directional cutter types and the vertical axis divides between relatively fine and rough cutter profiles. Image sources: burr top left and top right are adapted from Nouvag AG, grinder top right and cutter bottom right are adapted from Bosch-professional, cutters bottom left are adapted from [28], saw blades bottom are adapted from Tenyu-tools.

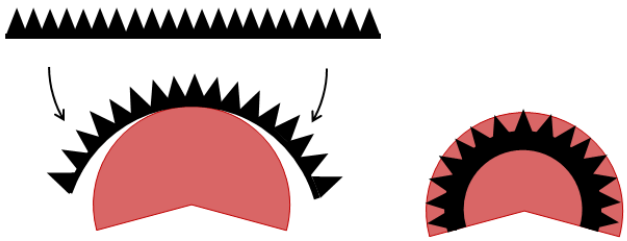

Figure 3.7: A saw-like cutter profile is wrapped around the drill head to form the cutting face of the drill.

be greater than the separation distance between the cutters. This means that the cutters must be at the maximum 30° apart. This however does not hold up when the amplitude is reduced when testing the steering effect. The maximum cutter separation is therefore based on the minimally supplied amplitude which was determined to be one-third of the normal amplitude (10°). Additionally, some redundancy is desired: each piece of material needs to be struck by two cutters. The drill head cutter profile is defined by the cutter rake angle and the cutter separation. The height of the cutters follows from this value but is limited by the design of the connection with the leaf springs. Eventually the separation angle was set to 6.74°resulting from the before mentioned considerations and cutter height constraints.

The drill will receive a translating oscillation from the two leaf springs of the motion transfer system as indicated in Figure 3.9. The expected input for normal operation is here represented by two arrows indicating the direction of motion of each leaf spring. The separation distance between the two attachment points for the leaf springs is 3 mm and is indicated by S. The diameter is 6 mm and is indicated by D. Table 3.1 shows an overview of the used stroke length values.

The concept design of the drill head is based on a cylinder with a diameter of 6 mm and a height of 5 mm. A wedge is removed, leaving a 210°section of the cylinder intact, considering it oscillates over a 30°angle. The teeth are symmetrical with a rake angle of 10°and a minimum separation of 6.74°. The attachment points for the motion transfer system are 3 mm apart, requiring the stroke length of the oscillation to be 0.75 mm.

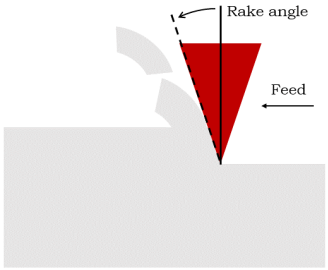

Figure 3.8: A schematic representation of a cutter. The bone (grey) is cut by a cutter (red) in the feed direction. The rake angle indicated in the image is a negative rake angle, meaning that the face of the cutter is slanted forward towards the material.

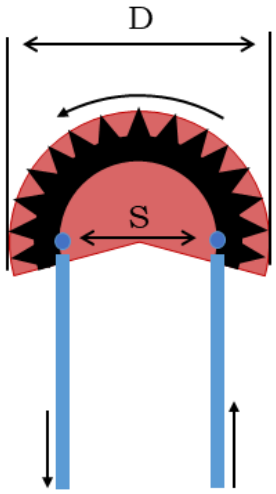

Figure 3.9: A schematic top view of the drill head rotation as a result of the input from the leaf springs. The motion is indicated with the solid arrows and dimensions with the open arrows. This motion is amplified by a factor $\frac{D}{S}$ based on the separation of the leaf springs S and the diameter of the drill head D.

3.2.2. Flexible motion transfer system concept design

The motion transfer system is responsible for transferring the actuation motion and forces required for the three main functions that are needed for the steerable drill. These functions are cutting, feeding and steering. All three functions will be fed through this single motion transfer system through two methods:

- The oscillation actuates the drill head. The linear oscillation of the two parallel plates is converted to a rotating oscillation of the drill head, causing the teeth to cut away material and generate the cutting friction that is used for steering the drill head.
- The leaf springs themselves are responsible for transferring the feed force and position in the longitudinal direction. The leaf springs therefore have a high stiffness in the longitudinal direction and low stiffness in the steering direction. The feed force is limited by the critical buckling force of the plates.

An important aspect of the design proposed here is that the bending direction of the parallel leaf springs should be in the same plane as the sideways force generated with the drill head motion as explained in Figure

Table 3.1: The drill head's rotational motion expressed in arc length and corresponding angle as a result of the input stroke length from the leaf springs.

Setting	Drill rotation arc length	Drill stroke angle	Input stroke length
normal	1.5 mm	28.6°	0.75 mm
2/3 amp.	1.0 mm	19.1°	0.50 mm
1/3 amp	0.5 mm	9.5°	0.25 mm

2.3. This proposed design requires a high stiffness for transferring the drilling oscillation to the drill tip and a low stiffness for bending as a result of the generated steering forces in the same direction. For this design to work, the connections between the leaf springs, drill head and the oscillator need to be redesigned. Figure 3.10 is a schematic drawing of the leaf springs divided into three sections. The frontal section diverges to connect between the parallel section and the drill head. The parallel section will provide the majority of length for deep drilling and provides the most flexibility in bending. The rear section again diverges to attach to the oscillator.

At first, the parallel section of the leaf springs was considered. The leaf springs must be as flexible as possible, whilst still providing sufficient resistance against buckling. The construction of the leaf springs should be constrained, to allow only the transnational oscillating motion of the leaf springs. As indicated in Figure 3.11, having the leaf springs separated will result in the drill head remaining in the original orientation instead of pointing towards the desired direction. The majority of the leaf spring length should thus be close together. Additionally, with such separation the leaf springs would have to be constrained using an intermediate body, to prevent the leaf springs from buckling into each other which would make the drilling direction unpredictable.

The method for constraining the leaf springs together used by Müller appeared to work well. With one leaf spring providing holes and the other leaf spring slots, a bolt or rivet connection can hold the leaf springs together and allows them to slide.

When using the leaf springs in this manner, desiring a very low bending resistance but also using the leaf springs to transfer the feed force, the most limiting factor is buckling of the leaf springs. Whilst the deviation from buckling is limited by the walls of the drilled hole, the behaviour and force direction can become unpredictable when the leaf springs are pressed into multiple curves. Test results from Müller show that the feed force is 0.5 N in 5 PCF bone phantom at 22000 rpm and around 2 N for 10 PCF bone phantoms. It is therefore preferable when the leaf springs can sustain a 2 N load or more. The length of the drill was determined at 80mm. These values can be used together with equations 3.1 and 3.2 to find a suitable thickness of the leaf springs to prevent buckling of the structure. The detailed calculations can be found in Appendix B. The outcome is that two leaf springs made of spring steel of 0.2 mm thickness can support a load of up to 2.89 N which is above the expected 2N.

$$F_{critical} = \frac{\pi^2 * E * I}{(K * L)^2} \tag{3.1}$$

$$I = \frac{b * h^3}{12} \tag{3.2}$$

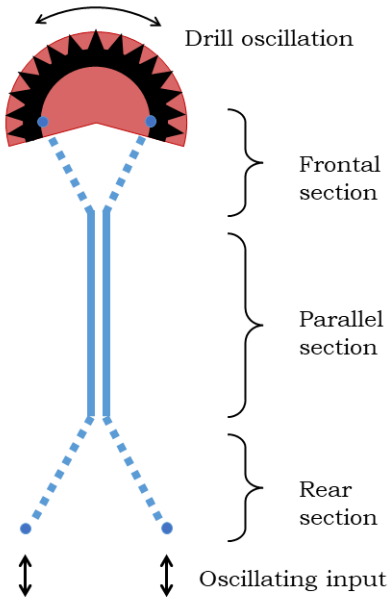

Figure 3.10: A schematic top view of the different sections of the leaf springs.

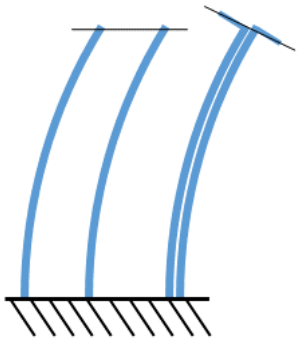

Figure 3.11: A schematic view of parallel leaf springs in a bend position. The left image with separated leaf springs and the right image with the leaf springs close together.

For estimating the bending behaviour of the leaf spring a linear bending model was used. The Euler-Bernoulli static beam equation for cantilever beams is expected to suffice. It should be noted that this model is purely meant to gain a rough estimate and is therefore limited in its use and does not account for large deflections. For estimating the buckling behaviour of the drill assembly, the Euler critical load model was used. Equations 3.3 and 3.2 can be used to gain a rough estimate of the force required to create a displacement in the drill tip. A detailed description of the calculations can be found in Appendix B.

$$\delta = \frac{F * l^3}{3 * E * I} \tag{3.3}$$

Secondary to the parallel section, the frontal section was designed. The leaf springs are designed to be close together to optimally accommodate bending. However, the drill head requires the input points from the leaf springs to be separated to produce a moment on the drill head. This contradiction requires the leaf springs to transition from touching to separated. Three different methods to achieve this were proposed. The first is a hinged connection between the drill head and the leaf springs, the second is a bending connection and the third is a bending connection with an additional guide part. The three options are displayed in Figure 3.12.

The preferred option is to use hinge points, as this system provides the lowest resistance of motion. However, fabricating such a connection at this scale is impractical at the least. The hinge pin would have to be attached to the edge of a 0.2 mm thick leaf spring and be constrained within the drill head such that it can get in to attach, but cannot get loose during its use. An alternative approach would be to utilize the flexibility of the leaf springs, to create the hinge. Instead of a hinge point, the leaf spring will bend so the drill head

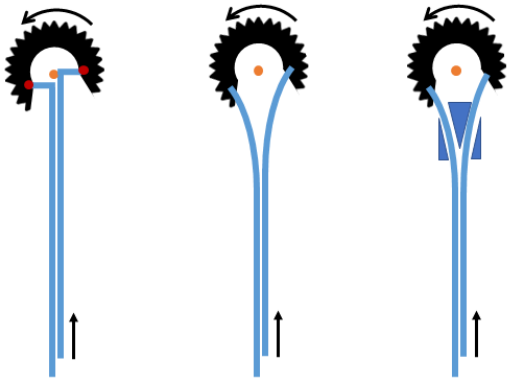

Figure 3.12: Three different options were considered for connecting the drill head and the leaf springs. From left to right: the hinged connection, the bending connection and the guided bending connection.

can rotate. This does provide a problem as the drill head will then have the tendency to swing left and right instead of rotating in place. The first solution to this bending problem is to constrain the drill head itself. Preventing the drill head from swinging should force the drill head to make a rotating motion instead. This constraint can be provided by the walls of the drilled hole and with a retractable sleeve structure outside of the hole. An alternative to this approach is to constrain the leaf springs in the frontal section from bending, forcing the leaf springs to produce a translating motion and thereby forcing the drill head to rotate. However, such a guide part complicates the construction by introducing additional parts that have to be secured and constrained. Therefore the second approach from Figure 3.12 is used.

Lastly, the rear section of the leaf springs is designed. This connection receives the oscillating output from the oscillator mechanism and converges this to the parallel section of the leaf springs. At this end, an external guide structure can be easily used as it can be secured on the oscillator mechanism. Preferably, the connection can be disassembled to store the drill separately and prevent damage during transportation or storage.

For attaching the leaf springs to the oscillator mechanism, a pin connection was chosen. Each leaf spring can be inserted into a slot on the output of the oscillator mechanism. A hole in the leaf spring aligns with a hole in the connector. A pin then joins the two together. The advantage of this connection is that it provides a good forward and backward tolerance, whilst allowing some rotating motion. In this manner, the leaf spring can be directly connected to the reduction rods without requiring intermediate parts.

The guide for the leaf springs provides a constraint to only allow the leaf springs to translate in one direction. It converges the separated leaf springs together with a set of channels in a Y-shaped configuration. In the middle at the point of the split, the top of the guide is open so the leaf springs can be separated manually when inserted, to guide both ends in a different direction.

The concept design of the flexible motion transfer system consists of two leaf springs made of 0.2 mm thick spring steel, 5 mm high, and 80 mm long. For the majority of their length, they are kept parallel with a bolt or rivet connection. They split into a Y-shape at the front to connect to the drill head. The flexibility of the leaf springs is used as a hinge, with the constraints provided by the surrounding bone. At the rear side of the leaf springs, they are constrained by a guide to connect them to the oscillator mechanism.

4

Prototype design

4.1. Prototype design

4.1.1. Oscillator assembly

Figure 4.1 shows an exploded view of the oscillator mechanism. The prototype for the oscillator is built around a central frame (1) consisting of a 10 mm thick upright slab and a 6mm thick bottom plate. The structure is printed from generic PLA on an Ultimaker 3. The motor (2) is a Reely RS380PM-4531F-57D. It attaches to the frame directly with two M2.5 bolts (11). The motor axle protrudes through the frame to the other side where the bottom gear (6) is mounted. The gear is a steel 50 teeth module 0.5 gear. Between the motor axle and the first gear, a custom adapter was used to mount the gear with a 4mm hole to the 2.3 mm motor axle. The gear and axle adapter are secured with set screws.

The second axle (4), which is above the motor, drives the crank mechanism. The length of this axle is kept as small as possible at only 22 mm, thereby keeping a small width of the crank. Two bearings (3) are housed in the frame and support the axle in the radial direction and counteract any moments acting in the radial plane. The bearings are pressed into the frame from both sides and are separated by a ridge in the hole. The axle can be pushed through both bearings with a fairly loose fit. The axle is secured to the bearings with two retainer rings (5). The axle and bearings are then constrained by the ridge in the frame and retainer rings such that only rotational motion is possible.

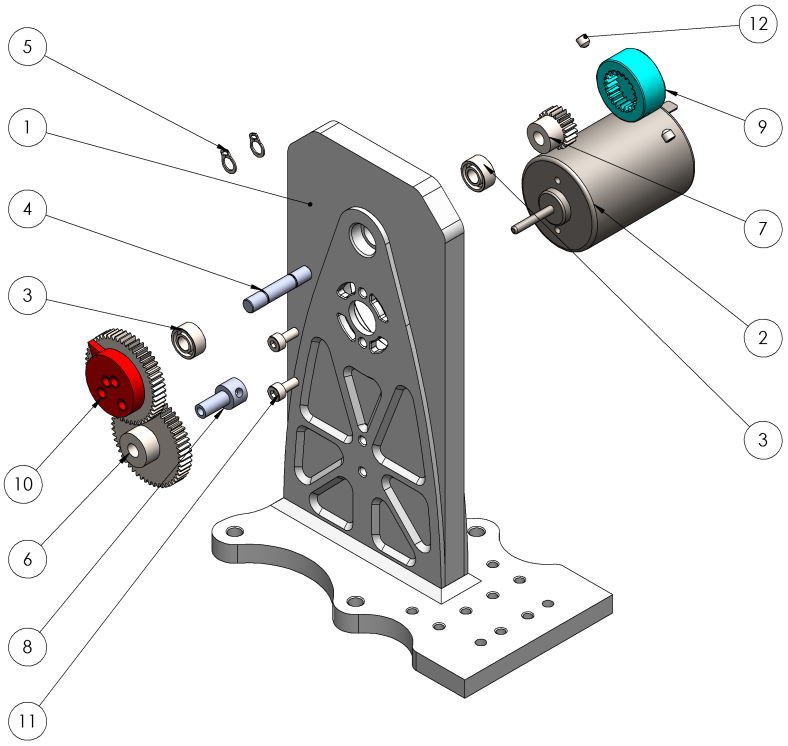

Figure 4.1: An exploded view of the drive system of the prototype oscillator with adjustable amplitude and phase between the two outputs. The red and blue parts are responsible for the amplitude and phase adjustment. The colours are meant for contrasting different parts and referencing parts between figures. The annotations are explained in the text.

On either side of the axle, a gear is attached. The large gear is driven by the motor gear via a 1:1 transmission ratio. A 3D printed plate (10) is glued to this gear and it provides holes for the crank to attach to. Each hole has a different distance from the centre corresponding to a different amplitude for the crank. The four holes create a crank arm length between 1.5 mm and 6mm with 1.5 mm increments. The holes are placed at a 90°angle from each other to prevent overlapping of the holes. This means that when the amplitude is adjusted, the phase changes as well.

The gear (7) on the other side of the axle is smaller with 20 teeth and is used as a spline connection. The splined hub (9) slides over gear (7) and forms the crank. The splined connection is a shape-locked connection to directly transfer the rotation from the axle, therefore, the phase can be easily adjusted. The splined hub is secured by two set screws (12) to prevent it from sliding off. The other side of the hub (9) provides holes with a different distance to the centre to connect the crank similarly to the large gear (10). The only difference is that the splined hub does not feature the hole for a 6 mm crank distance. The splined hub provides 20 set points, meaning that the phase can be adjusted in 18°increments.

The adjustment methods for the phase and amplitude are designed for manual operation. The size of the used components does not correspond well with the amplitudes that need to be fed to the drill head. The crank produces a mechanical oscillation with a stroke length of 9 mm in the normal setting, which is a 4.5 mm crank arm length. The drill head only needs to rotate approximately 30°, which corresponds with a stroke length of the leaf springs of 0.75 mm. A reduction ratio of 12:1 needs to be established to provide the correct input to the leaf springs. A cantilever system was chosen to provide this motion reduction. Figure 4.2 provides an exploded view of these rods that form the motion reduction mechanism. Two sets of two hinged rods provide transmission of motion from the crank to the leaf springs. The connector rod (6) converts the rotational motion of the crank to a mechanical oscillation. The reduction rod (4) provides a 12:1 reduction on the oscillating motion. At the top, the reduction rod is connected to the connector rod via a hinge pin (7). At the bottom, the reduction rod is constrained by a fixed hinge (3, 5). The distance between the top and bottom hinges is 90 mm. 7.5 mm Above the bottom hinge, the reduction rod provides a connection to the leaf springs with a slot through which the leaf spring can be inserted and a bolt hole where it can be secured to the rod with a hinged connection. The connector rods, reduction rods and bottom hinge are made with a Fromlabs SLA machine using though 1500 V2 resin. This machine produced parts that are sufficiently accurate and provides connections with press-fitted steel pins to form play-free hinges.

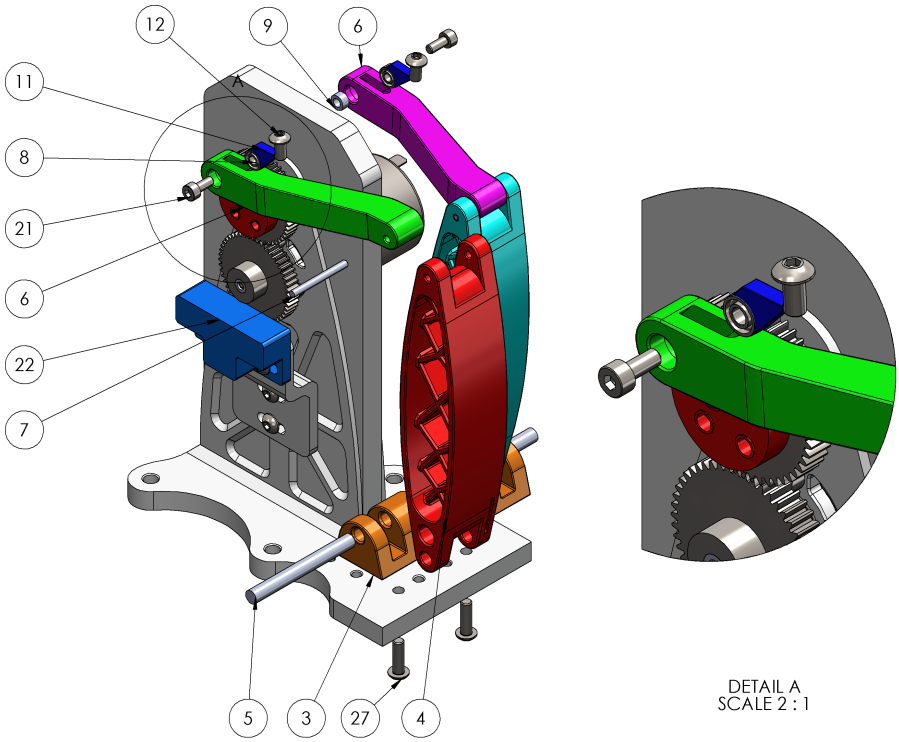

Figure 4.2: The mechanism of rods and hinges that converts the rotational motion of the crank to an oscillation with the correct amplitude for the drill. The annotations are explained in the text.

The bottom hinge (3) is secured to the frame with two M3 bolts (27). A 4mm steel pin (5) provides the hinged connection. For the top hinge, a 2mm steel pin (7) provides the hinge connection. Since the top hinge oscillates, this pin is smaller and lighter than the bottom hinge. The reduction rod (4) is hollow to reduce mass. It is wide and features a structure of ribs on the inside to provide rigidity. This is needed as the connector rod (6) produces an offset force and moment due to its angled shape. The structure of the reduction rod provides sufficient rigidity against these unwanted forces. The hinged connections are designed to precisely fit together, such that there is no mechanical play in the hinges but with some additional friction as a trade-off. All parts in the linkage mechanism are removable and can be replaced when required.

The connection between the linkage mechanism and the crank is displayed in Figure 4.2. The connector rod houses a bearing (8) that can be secured in a slot with the help of a small wedge (11), which is locked with an M2.5 bolt (12). The bearing is connected with the crank via an M2.5 bolt (21) that directly screws into the holes of the top gear crank and the splined hub crank. A spacer (9) is used to prevent the connector rods from rubbing against the crank parts. The bearing separates the rotating parts from the oscillating parts, providing a low friction connection.

The magnetic switch (22) can be used as a velocity sensor. The first gear has a magnet glued to its hub which, together with this magnetic switch, is used to measure the rotational velocity.

4.1.2. Drill assembly

The oscillator mechanism provides two adjustable mechanical oscillations which are transferred to the drill head via two slidably connected leaf springs. The leaf springs themselves are 0.2mm thick, 5mm high and 127mm long (55.3mm long for the parallel section). According to the theoretical calculations for buckling and stiffness, this is the lowest available stiffness that still allows for sufficient buckling resistance. Figure 4.3 shows an exploded view of the drill assembly. The two leaf springs (32) are displayed in green and pink, corresponding to the signal they receive from the green and pink connector rods. The two leaf springs are connected to each other with two M1.6 bolts (33) and nuts (34). One of the leaf springs features holes for the bolts and the other features slots to allow both leaf springs to only slide in the longitudinal direction. This means that the leaf spring with the holes also moves the bolts back and forth. The leaf springs slide along each other with direct metal-to-metal contact. To lower friction, super lube synthetic oil lubricant with PTFE is applied between the leaf springs.

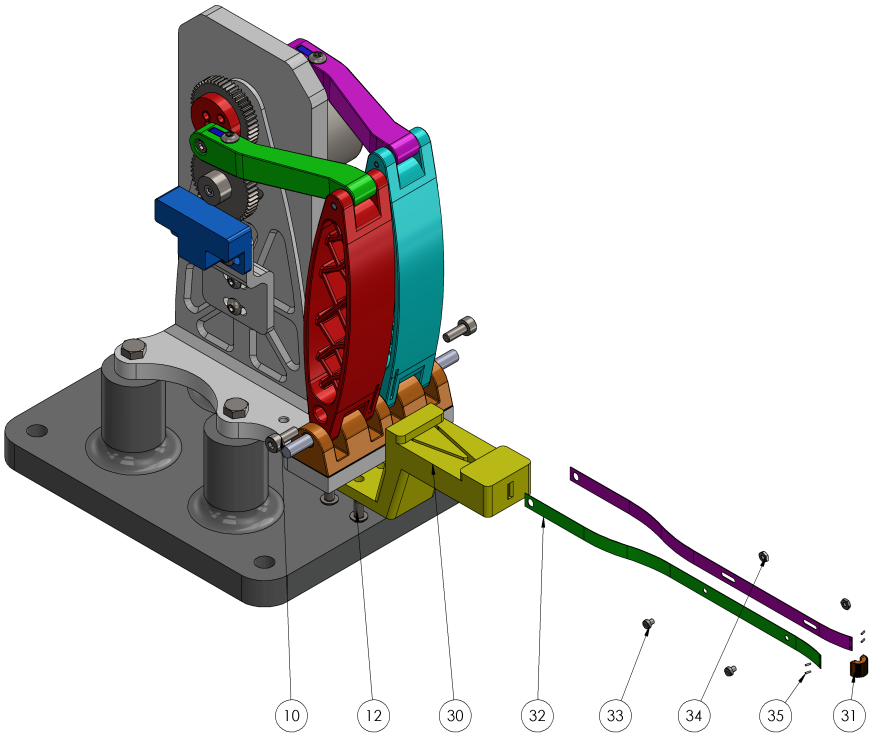

Figure 4.3: An exploded view image of the drill and drill guide. The annotations are explained in the text.

The attachment points of the leaf springs to the drill head (31) are separated by 3.0mm. The leaf springs are inserted into slots of 0.9mm deep and are each secured with two pins of 0.5mm diameter (35). The core of the drill head cylinder is empty and features a wall that is concentric with the cylinder's outer shape. This allows for the removal of the pins, so the leaf springs and drill can be separated later if components need to be changed.

The leaf springs are each attached to one of the reduction rods of the oscillator with an M2.5 bolt (10). Since these attachment points are separated from each other by a distance of 9.6mm, the leaf springs need to be guided to stay together and parallel. This is the function of the guide (30). It constrains the leaf springs in their motion and spring effects that can be present in the curved parts of the leaf springs. The guide is attached to the frame with four M3 bolts (32). The drill assembly can be slid through the guide to remove and attach the drill assembly to the oscillator. The guide is open at the top for access to the leaf springs, as they need to be manually separated when the drill is mounted. The oscillator mechanism is mounted on an adapter plate (coloured dark grey) that allows it to be mounted securely to a linear stage or other test setups.

4.1.3. Complete prototype

The oscillator assembly was manufactured mostly from 3D-printed parts and standard steel components. Manufacturing of the drill assembly was outsourced to a team of instrument makers. The parts of the drill assembly were mostly produced by wire-electronic-discharge-machining (wire-EDM). An overview of the assembled prototype is provided in Figure 4.4. The sub-figures show the prototype from different perspectives. A complete parts list and drawings with annotated measurements can be found in Appendix C.

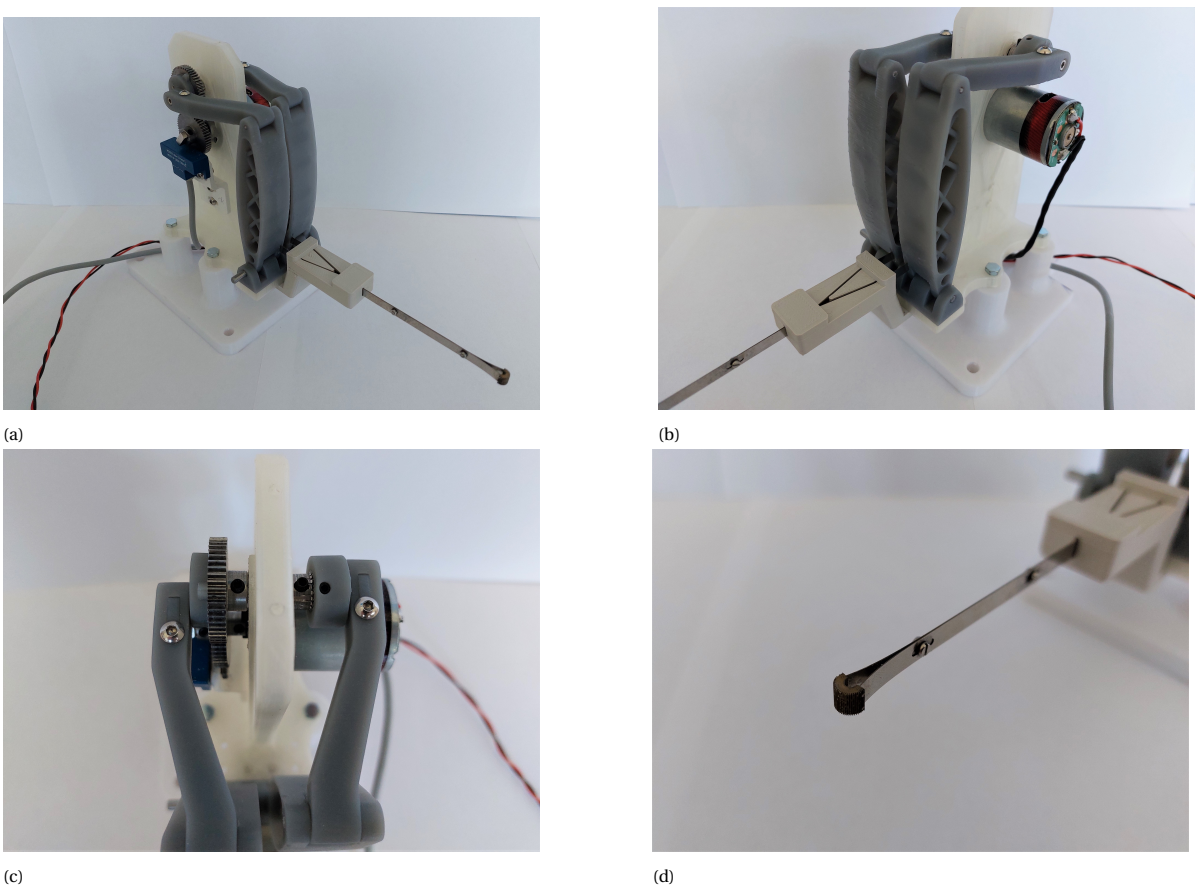

(a) (b) (c) (d)

Figure 4.4: Four photographs of the prototype of the oscillator and drill assembly from different perspectives. Photographs (a) and (b) are of the right and left side respectively. (c) Is a close-up of the crank and (d) is a close-up of the drill head.

4.2. Proof of principle experiments

4.2.1. Preliminary practical experiments

Preliminary test goal and hypothesis: The goal of the preliminary tests was to observe how the drill behaves with different settings and to find a suitable motor speed. Secondary, it was tested to see if a pilot hole would be required for the drill. The expectation was that verification testing would mainly involve drilling tests for assessing the effectiveness of the steering principles hypothesised in Section 2.1.2.

Preliminary test variables: The dependent variable is the motion of the oscillator and the drill. The motor speed needs to be consistent with little variation of speed and needs to be continuous as it may not stall. The dependent variable is the voltage supplied to the motor. To start up the motor a manual push is allowed. The speed variation is tested with the drill in contact with a bone phantom and with the drill in free air. With the secondary test, the dependent variable is the ability of the drill to remove material. The independent variable is the that the drill is started with or without a pilot hole. During testing, the motion and behaviour of the drill is visually observed.

Preliminary test setup and procedure: The setup for the preliminary tests involved the prototype oscillator and drill clamped to a work surface. The bone phantom was held by hand and pressed onto the drill head. The drill was also supported by hand. A variable voltage power supply was used to provide power to the motor. The oscillator was set to an amplitude of 0.75mm on both outputs and a phase difference of 180°. A pilot hole was created by cutting a 6 by 5 mm rectangle of 5 mm depth from the bone phantom with a knife.

Preliminary test results: The oscillator can reliably produce a consistent motion at a voltage of 2.5V and higher with the drill in free air. When in contact with the bone phantom, at least 3.0V is needed for a steady motor speed. The observed motion of the drill head from the preliminary tests was a swinging type of motion, where the drill head swings left to right as indicated in Figure 4.5, this was expected. The drill did not drill when it was constrained by a pilot hole. Without a pilot hole, the drill produces a a slotted hole with a large width compared to its height as seen in Figure 4.6. As the drill head progresses into the bone sample, the width of the hole reduces until there is no space left for the drill to swing. At this point, the drill is embedded in the surrounding material and can no longer remove material. It is unable to drill deeper than 6mm.

Proposed design changes: The most likely explanation for the drill's behaviour is that the frontal section of the leaf springs is too stiff and thereby prevents the drill from rotating around its centre axis to produce the desired drilling motion. The drill only swings from side to side, which stops when the drill head is physically blocked by the side walls of the drilled hole. The rotating motion has been proven to work by Müller [18] with a similarly designed drill head which is forced to produce this rotating motion. The general assumption is that lowering the stiffness of the frontal part of the leaf springs makes that this section can more easily bend and therefore the desired rotational motion of the drill head can be produced. A risk is that decreasing the stiffness of the leaf springs, causes the drill to rotate around its contact point with the bone as shown in the right image in Figure 4.5. To some extent, this can be solved by adjusting the feed force during the drilling depth tests.

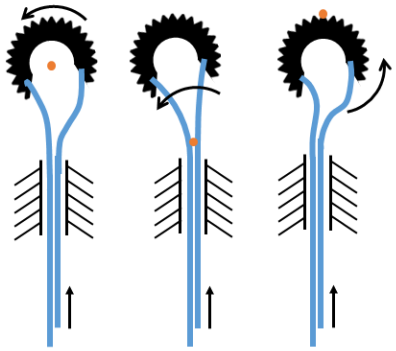

Figure 4.5: A schematic view of the behaviour of the drill tip attached to the leaf springs. On the left, side the preferred motion is displayed, where the supplied translation is fully converted to a rotation of the drill head. In the middle, the observed motion is displayed where the drill head swings due to bending of the leaf springs and the right image shows the observed motion when the drill head gets embedded and rotates around the contact point with the bone sample or when the feed force is too high.

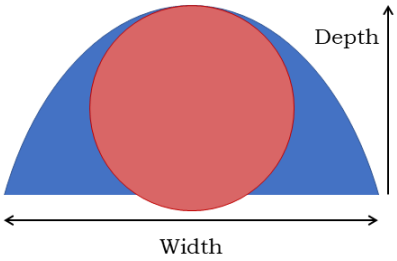

Figure 4.6: A schematic top view of the drilled hole (blue) and the drill head (red). The hole starts wide and gradually decreases in width.

Based on this assumption, two design directions are proposed: The first is that by reducing the stiffness of the whole front section of the leaf springs, the leaf springs can more easily be bent into to let the drill head make the correct rotational motion rather than the swinging motion when constrained by drilled hole. The second hypothesis is that by creating hinge points in the leaf springs by locally reducing the stiffness, the point of rotation can be relocated to be in between these hinge points. The point of rotation can then be placed very close to the centre of the drill head. Multiple design variants will be evaluated with a simulation before adapting the drill.

4.2.2. Simulation of design improvements

Simulation goal and hypothesis: The goal of the bending simulation was to improve the design of the drill to drill a deeper hole. The resources for practical tests were limited, therefore only two alternative designs could be tested in practice. The outcome of the simulation selects a maximum of two designs for further practical experiments. Only static results of the bending behaviour were tested in the simulation. The design hypothesis is mentioned in Section 4.2.1. Either the creation of hinge points or the decrease of stiffness in the frontal section of the leaf spring will provide an improvement of the drill head motion and the possibility to create a deeper drill hole.

Simulation variables: The dependent variable is the sideways displacement of the drill head. The displacement value measured in millimeters from the top center node of the drill head is used. The independent variable is the geometry of the frontal section of the leaf spring. Seven different designs have been tested and compared with this simulation. The seven designs are shown in Figure 4.7. Design 1 is the original unchanged leaf spring which will be used as a reference for the simulation and the experiments. Design *A* features a slot for reducing the stiffness of the whole section. Design *B* features a slot with varying stiffness over the length of the section, with the lowest stiffness near the drill head. Design *C* is inverted from Design *B*, where the thickness is locally doubled instead of removed. This creates two bending hinges at both ends of the rigid section. Design *D* works similar to *C*, by creating an integral hinge by locally lowering the stiffness at both ends of the frontal section. This approach is more practical to fabricate. Design *E* is similar to *D* but only features a single hinge near the drill head.

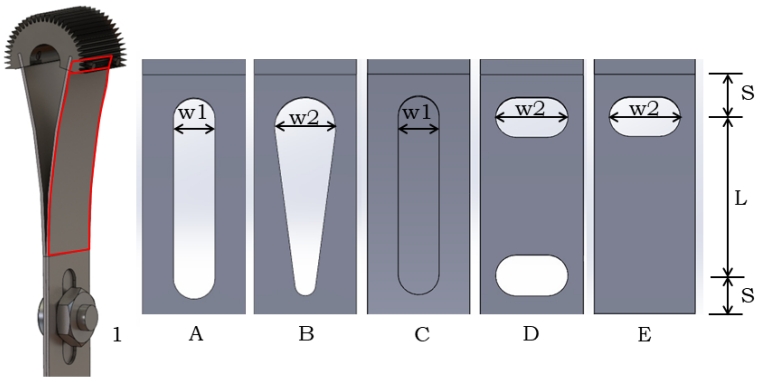

Figure 4.7: A side view of the leaf spring top section with different structures for altering the stiffness and bending behaviour. Designs *A-E* are compared to *1* during the simulation. w1 is 2.5 mm, w2 is 3.0 mm, S is 2.0 mm and L is 8.0 mm.

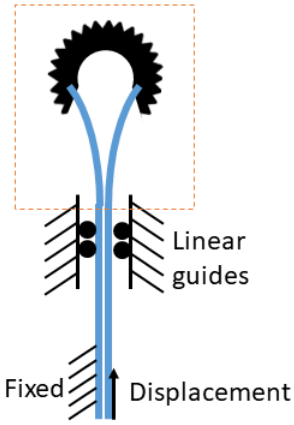

Figure 4.8: A schematic diagram (top view) of the model that is used in simulating the bending behaviour of the drill. The leaf springs are only allowed to translate along a sliding connection. One leaf spring is clamped at the bottom and the other is displaced by a set amount. The orange box shows the focus area of the experiments.

Simulation setup and procedure: The model simulates the displacement of the drill head based on the displacement input of the leaf springs. The bending behaviour of the leaf springs and the resulting motion of the drill head was simulated in Solidworks 2021 using the non-linear bending simulation in standard settings. The CAD model of the drill head and leaf springs was slightly altered to shorten the simulation time: The cutters were removed along with the bolts, furthermore, the connection between the leaf spring and drill head was simulated as a continuous structure. A schematic diagram of the simulation setup can be found in Figure 4.8. The model only simulates the behaviour of the drill head and the front section of the leaf springs where they separate from parallel to the attachment points on the drill head. The straight parts of the leaf springs are only allowed to slide in the longitudinal direction, but cannot bend. The bottom of the left leaf spring is fixed and the right leaf spring is translated forward by a set value of 0.75 mm, which corresponds to the maximum stroke length supplied by the oscillator in normal settings.

Simulation data processing: Screenshots are taken from the deformed state of the drill and the neutral state without forces and displacements acting. The displacement values are taken from the top centre position of the drill head from the node displacement values reported by Solidworks. Two overlaying images are used to compare the displacement of the drill head and the bending shape of the leaf springs. Drill 1 is used as a reference against the screenshots of Designs *A* to *E*.

Simulation results: The results from the simulation are displayed in Figure 4.9. The figure displays the deformed states of Designs *A* to *E* with Design 1 in the background as a reference. Table 4.1 contains the values of the displacement of the front of the drill head for each of the six designs. Design *A* shows the largest displacement which is almost 10% higher compared to Design 1. Design *B* shows almost no difference in displacement compared to Design 1. Design *C* shows the lowest displacement which is almost 33% lower compared to Design 1. Design *D* has a displacement that is slightly lower than Design 1. Design *E* has the second lowest displacement which is 18% lower compared to Design 1.

Table 4.1: Displacement results from the simulation. The displacement values are from the top centre of the drill head.

Design	Deviation
1	2.44 mm
A	2.67 mm
B	2.48 mm
C	1.64 mm
D	2.26 mm
E	2.00 mm

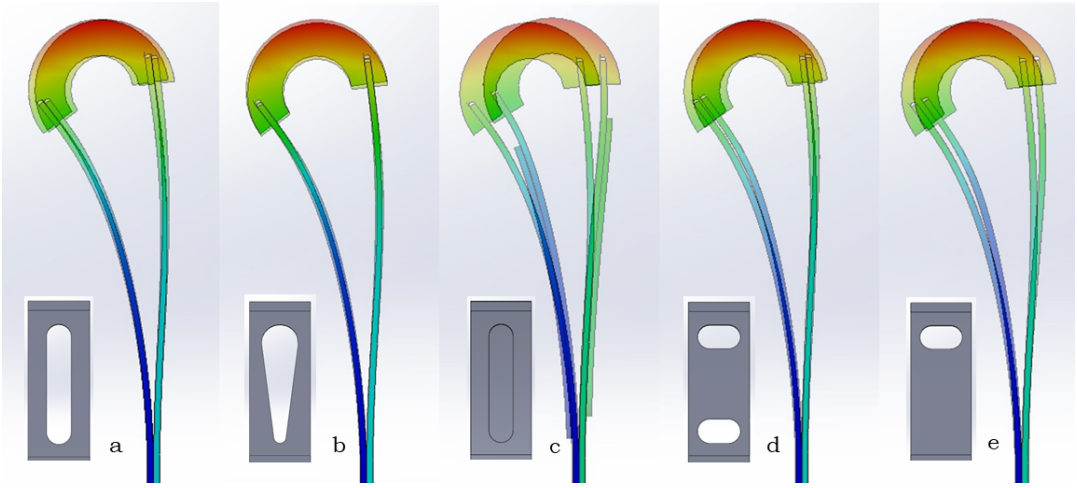

Figure 4.9: Screenshots from the resulting displacements from the simulation. Design one is used as a reference, each of the leaf spring designs is placed over the result of design one. On the bottom left of each image, is the corresponding leaf spring design.

4.3. Prototype improvements

Design *A* has the lowest stiffness, therefore this is the preferred option to test the first design direction proposed in Section 4.2.1. Design *C* has the lowest deviation however, adding thickness to a thin bending structure is difficult and cumbersome to fabricate. The second best result: Design *E* is therefore used for testing the second design direction proposed in Section 4.2.1. Figure 4.10 shows the two newly proposed drill designs that were further evaluated with the practical experiments. These new designs are compared to Drill 1 and will be referred to as Drill 2 and Drill 3, as indicated in Figure 4.10.

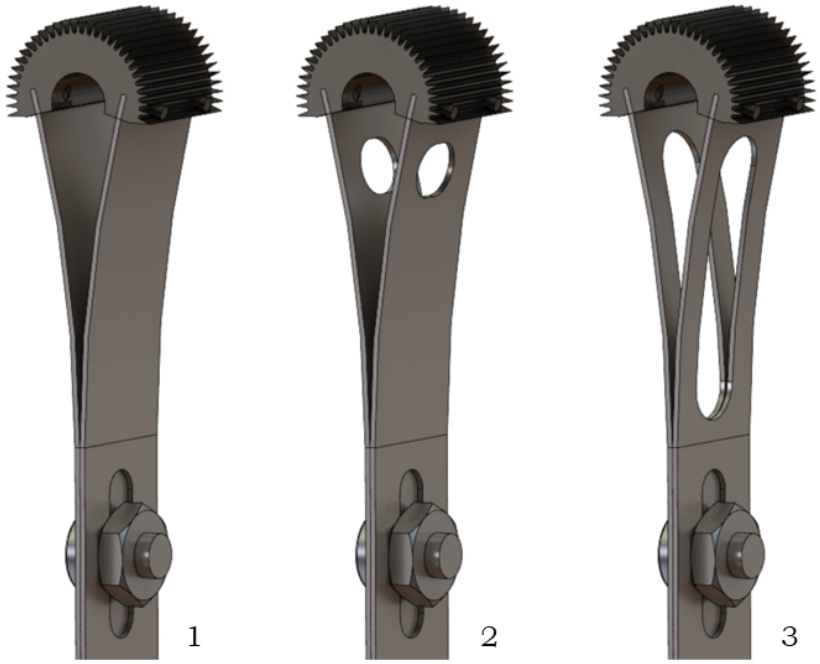

Figure 4.10: The three drill designs that are tested and compared during the evaluation experiments. Drill 1 is used as a reference. Drill 2 corresponds to Design *E* and Drill 3 corresponds to Design *A*

5
Evaluation

5.1. Drilling depth experiments

5.1.1. Experiment goal and hypothesis

The drilling depth experiments are used to verify the drilling performance of the alternative drill designs that are proposed based on the simulation experiments. The goal is to assess if the design changes allow the drill to drill a deeper hole in a cancellous bone phantom. The hypothesis is that the design changes resulting from the simulation will provide an improvement of the drilling motion and will therefore produce a deeper hole.

5.1.2. Experiment variables

The dependent variables to measure are the depth (mm) and the width (mm) of the drilled hole as indicated in figure 4.6. The independent variable is the geometry of the frontal section of the leaf springs, for which three designs are compared. These three designs are Drill 1, 2 and 3 in Figure 4.10.

5.1.3. Experiment setup and procedure

The drill prototype is set up as shown in Figure 5.1. The full length of the leaf springs is constrained to only permit motion in the longitudinal direction. This setup diminishes the risk of buckling of the leaf springs, allowing higher forces to be applied with the drill. The oscillator is set to normal settings with a stroke length of 0.75 mm and a phase difference of 180°. The motor is provided with 3.0V.

The procedure starts with turning on the drill at 3.0V. A sample piece of 5 PCF bone phantom is then slowly pressed onto the front of the drill head. A stopwatch is started as the drill makes contact. The bone phantom is manually pushed forward over the table surface against the drill tip to carefully balance the drill force. This is needed to make sure the drill is removing material and does not get embedded. If the drill gets stuck, the pressure onto the drill head needs to be released until the drill head moves again. This is maintained for 6 minutes, or until the drill is stuck and cannot be recovered for over 20 seconds. The elapsed time will be noted down. The experiment will be repeated 5 times for each design to reduce the effect of the variability of the manual operation. Afterwards, the hole depth and width are measured.

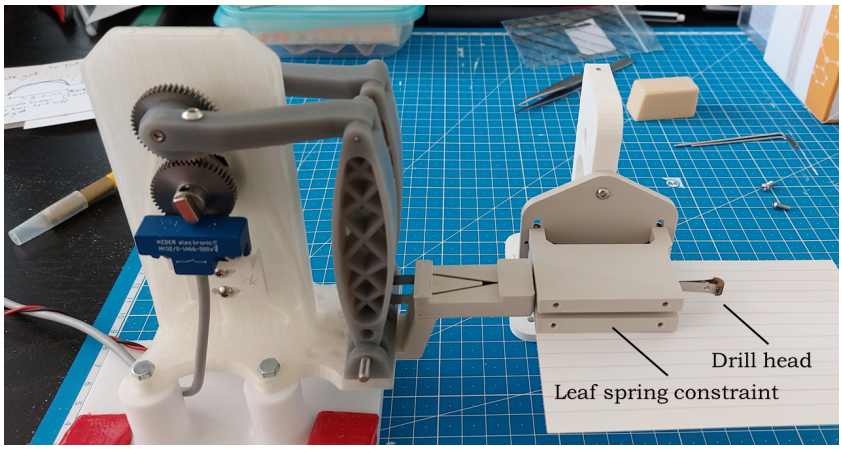

Figure 5.1: A photograph of the fully constrained test setup, where the parallel section of the leaf springs is only allowed to translate and cannot bend. Only the drill head on the right can move. The two blocks between the drill guide and the drill head contain a groove that only allows the leaf springs to slide in the longitudinal direction. A note card with a line structure is used to align the photographs before measurements are taken.

5.1.4. Experiment data analysis

The hole depth and width will both be measured using callipers. The hole may be irregular, therefore the median value of three measurements will be collected for the measurement. The hole depth measurements are converted to box plots to visualize the median depth and variability for each of the three drill designs. The same is done for the hole width. A two-tailed t-test is performed to assess if a significant difference in the drilling depth is reached.

5.2. Drill head motion experiments

5.2.1. Experiment goal and hypothesis

The goal is to observe the drill head motion with an amplitude difference and a phase difference and compare it with the motion patterns as hypothesised in Section 2.1.2. A static test and a dynamic test will be performed. The static test involves measuring the drill head positions in static conditions. The dynamic test involves measuring the drill head deviations when the motor is turned on. A secondary goal is to check for inconsistencies in the motion of the drill head.

The hypothesis is that despite the swinging motion, the steering patterns that result from the amplitude and phase difference can be observed with a static motion test. This is only partially representative of the dynamic motion the drill exhibits, therefore a dynamic test is used as a comparison. Inconsistencies in the drill head motion should result in a skewed drill head motion with inequalities between the left and right position and angle. By repeating the test with the drill flipped over its longitudinal axis, the results should tell if the inconsistencies arise from the drill's construction, the clamp or the oscillator.

5.2.2. Experiment variables

For the static test, the dependent variables are the positions of the drill head measured at a quarter turn of the crank (0°, 90°, 180° and 270°). The position of the drill head is measured as a position and a rotation (x, y, θ) in millimeters and degrees. Figure 5.2 explains the measurement of these variables. The first set of independent variables is the phase and amplitude of the generated signals. A reference test with normal settings, a stroke length of 0.75mm on both signals with a 180° phase difference, is made first to compare the effects. For testing the effects of the amplitude difference, a stroke length of 0.75mm on the left and a stroke of 0.25mm on the right is used. For testing the phase difference, a difference of 144° between the left and the right phase is tested. The second independent variable is the geometry of the frontal section of the leaf springs, using Drill 1, 2 and 3. The third independent variable is the connection of the drill with the oscillator where the drill can be attached in the standard or flipped position with the left side of the drill attached to the right side of the oscillator and the right side to the left.

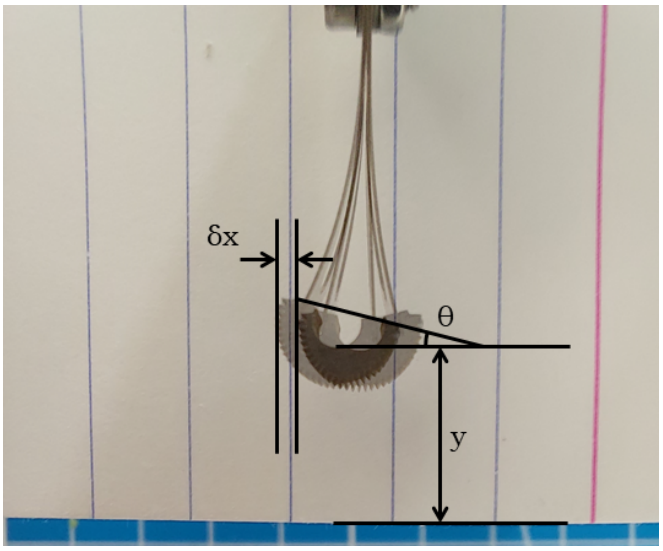

Figure 5.2: An example of how the position measurements are taken from the static test. One photo is used as a reference and the measured photo is overlaid at 50% transparency and aligned with the reference photo. From this, the position and angle of the drill can be determined.

For the dynamic tests, the dependent variables are the maximum x-deviation (mm) of the drill head to the left and right. The drill head moves fast, making it difficult to measure exact positions with the still images from an ordinary phone camera. Therefore only the extreme ends of the swinging motion are measured on the left and right. The independent variables for this test are the same as for the static motion test.

5.2.3. Experiment setup and procedure

The experiment uses the prototype setup as displayed in Figure 5.3. This is the same setup used in the preliminary tests, making it easier to compare results. The drill is clamped directly behind the front bolt to allow motion of the frontal part of the leaf springs and drill head but to prevent bending of the parallel section of the leaf springs and provide consistency in the drills neutral position. For static tests, three sets of measurements are taken for each drill design. First, the drill is set to normal settings, then with an amplitude difference and lastly, a phase difference will be tested. Each set of tests will follow a similar procedure: The crank will be rotated in 90° increments until three full rotations are made. For each step, a photo of the drill head is captured from directly above the drill head. for the dynamic test, the drill is driven by the motor at 2.5V when it is not in contact with the bone phantom. The drill is recorded from straight above for 10 seconds.

5.2.4. Experiment data analysis

The pictures from the static tests are used for measuring the relative positions of the drill head in pixels, referenced to its neutral position. Measurements of the drill head are used to scale the positions to millimetres. The x- and y-data points are then plotted in a graph to visually display the positions of the drill head motion. The angle deviations are plotted in a box plot to display the magnitude and variability. A two-tailed t-test is performed to assess if a significant difference in the angular deviations is present.

For the dynamic test, the maximum deflection of the drill head to the right and left is measured from stills of the recording. The position of the drill head can be measured by comparing the displacement of the drill against its neutral position. The diameter of the drill head is used to convert the measured value to millimetres. The values are plotted in a bar graph to assess if the various settings show differences in the deviation of the drill head.

To assess the motion for discrepancies, the left and right angular deviations are compared for different variables from the static motion results in normal settings. The first comparison is between the three drill designs, the second is between the drill in standard and flipped position for all drills and the third comparison is between the left and right deviation of each drill. A two-tailed t-test is used to assess if the differences that are present are significant.

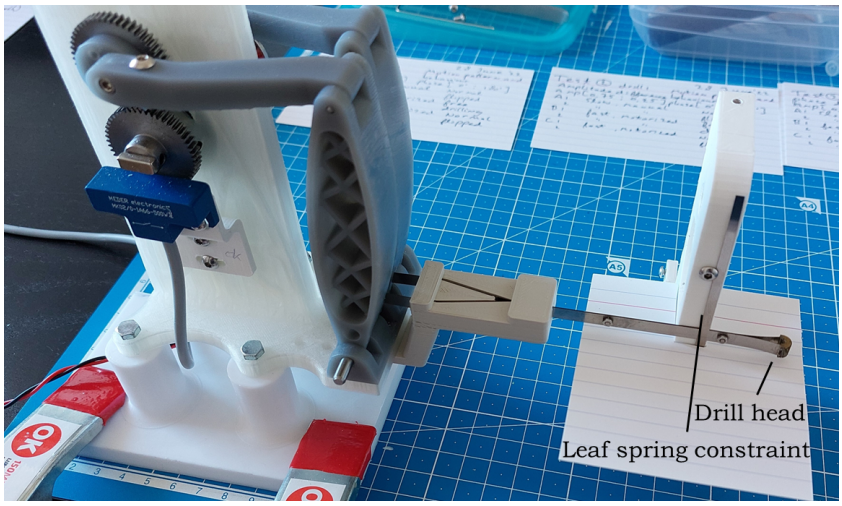

Figure 5.3: A photograph of the experiment setup with on the left the oscillator mechanism and on the right the drill. The leaf springs are constrained by clamping them to a pillar on the desk that only allows a sliding motion. The note card provides a reference to align the photographs before measurements are taken.

5.3. Drilling depth results

The data resulting from the drilling depth test can be found in Table 5.1. The list of test result values for all experiments can be found in Appendix D. Figures 5.4a and 5.4b show a box-plot of the hole depth and width for each of the different drill designs. The variation in results for the first drill design is higher as these results come from the preliminary experiments which had a similar, but a more lenient test protocol. A two-tailed t-test was performed to see if the design changes lead to a significant difference in the drilling depth. The p-value for Drill 2 compared to Drill 1 is above 0.5 and the p-value for Drill 3 compared to Drill 1 is 0.13. Both are above 0.05, making them insignificant. When comparing the depth results of Drill 3 to Drill 2, the p-value is 0.088, which is also not significant. An observation made during testing was that Drill 3 seemed to recover from getting stuck easier than the other drill designs. Drill 3 also displayed multiple modes of vibration (see Figure 4.5) when stuck, whilst the other drills only vibrated in one way when stuck. This observation led to an additional depth test with Drill 3. This resulted in a reached depth of 7.80 mm after 12 minutes of drilling for the first hole and 6.84 mm for the second hole.

Table 5.1: A table of the measured hole depth and width values from the drilling depth experiments. The results are separated for each of the three drill designs and also contain the recorded drilling time. The tests for drill design 1 did not include time recording.

Drill design	Drilling time min.sec	Hole depth mm	Hole width mm
1	-	2.67	6.2
	-	4.38	7.75
	-	5.62	7.85
	-	3.4	9
2	5.30	3.53	8.05
	4.30	4.02	7.5
	3.57	4.05	8.05
	6.00	5.05	8.55
	6.00	4.25	8.1
3	4.43	3.61	9.40
	6.00	5.56	9.98
	6.00	5.39	10.55
	5.35	3.75	9.88
	6.00	5.66	9.50

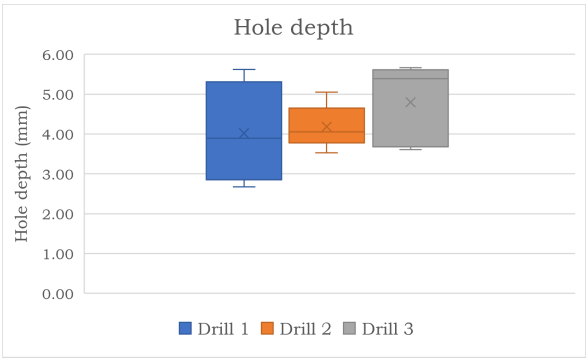

(a)

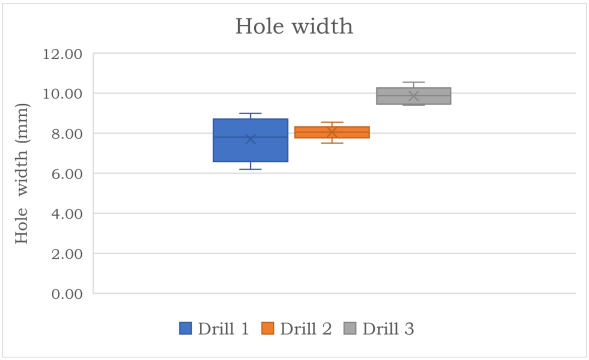

(b)

Figure 5.4: Two box-plots showing the measured results of the drilling depths (a) and hole width (b) for each of the three drill designs.

5.4. Drill head motion results

The goal of the drill head motion test was to observe the effects on the drill head motion with an amplitude difference and a phase difference. The position data recorded during the static motion experiments is plotted using a scatter plot of the x- and y-coordinates. These plots are shown in Figure 5.5, containing positions based on the theoretical model described in Appendix A and positions recorded during the static motion test from the three drill designs. With some of the test results, the positions show clustered groups corresponding to the 90° increments of the crank. This can be seen in the plot of the normal test of drill 2 in Figure 5.5c, where three groups of points can be distinguished. The position data for Drill 2 with a phase difference applied, Figure 5.5c shows rather more a path trace instead of groups.

The results from the dynamic motion tests can be found in Figure 5.6. The maximum deviation of the left and right can be compared for each of the three drill designs. Differences between the normal, amplitude and phase test values can be seen as well as the results with the drill in standard and flipped position.

The motion of the drill was verified by looking for inconsistencies between the motion patterns of the drill head in normal settings. Figure 5.7 shows the x-y-positions of the drill head, comparing drill designs 1, 2 and 3 in normal settings. Figure 5.8 provides three box plots comparing the angles of the drill head for different test settings. Figure 5.8a compares the absolute drill angles between the three different designs. The expectation from Section 4.2.2 was that the design for Drill 2 would show a lower deviation of the drill head than Drill 1 and Drill 3 would show the same deviation as Drill 1. However, the deviation angles of Drill 1 and 2: 7.8° and 7.9° on average respectively, are not significantly different with a p-value larger than 0.5. The deviation angles of Drill 3 are significantly larger than those of Drill 1 with an average angle of 10.0° and a p-value of 0.0375. This is a 28% increase in the drill angle. Figure 5.8b compares the angular deviations between the drill attached in the standard position and the flipped position for the combination of all three drill designs in normal settings. There is no significant difference between the angles of the drill head in normal and flipped positions. The p-value is greater than 0.5. Figure 5.8c compares the drill angles between left and right at a crank angle of 90° and 270°. A difference between the left and right deviation angle is visible for each of the three drill designs, where the left deviation is greater than the right deviation. The p-value for the deviation between the left and right of drill 1 is 0.021 and the p-values for drills 2 and 3 are both below 0.05, showing a significant difference among all three drill designs.

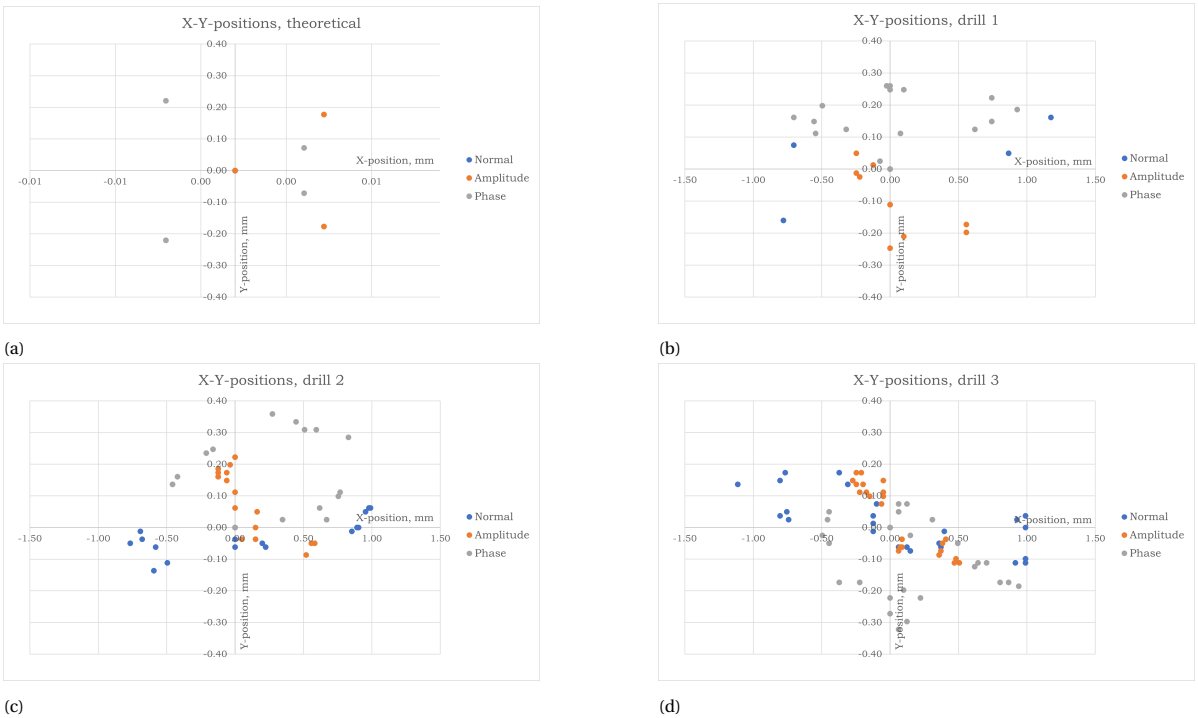

Figure 5.5: Four plots displaying the x-y-positions of the drill head at 90° rotation intervals of the crank. Plot (a) displays the positions determined by the theoretical model of the drill head motion. Mind the scale difference of the x-axis. Plots (b), (c) and (d) contain the results Drills 1, 2 and 3. The colours reference the settings: normal (blue), amplitude difference (orange) and phase difference(grey).

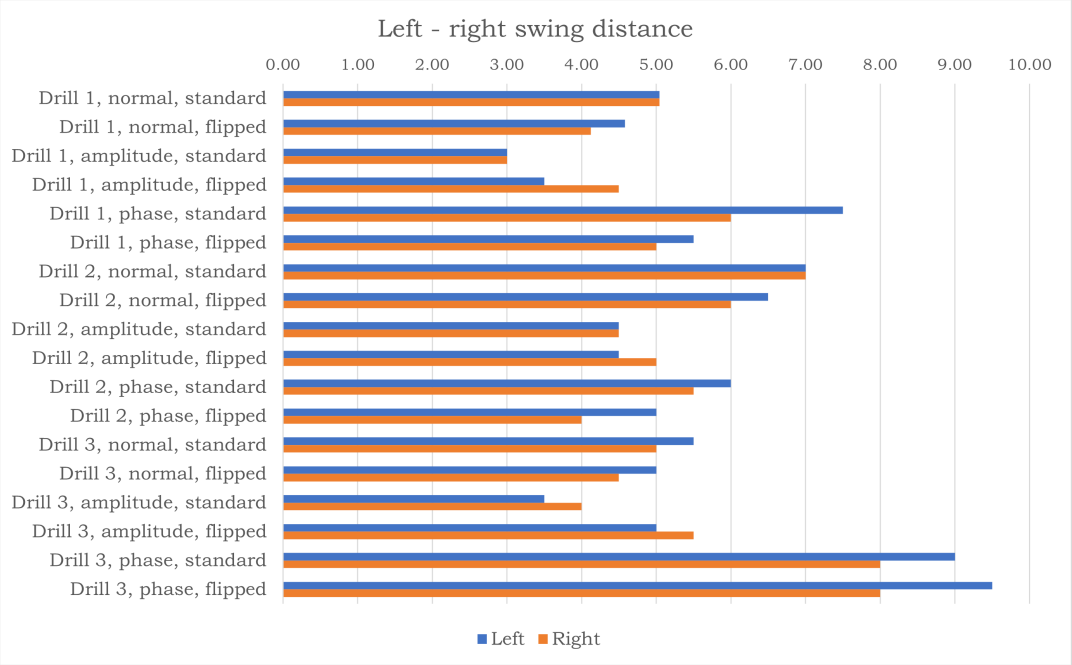

Figure 5.6: A bar graph containing the values for the maximum left and right deviations measured from the dynamic motion tests. The values for each of the three drill designs (designs 1, 2 and 3) and each of the three test types (normal, amplitude and phase) are displayed. Every test was performed with the drill in standard and flipped position.

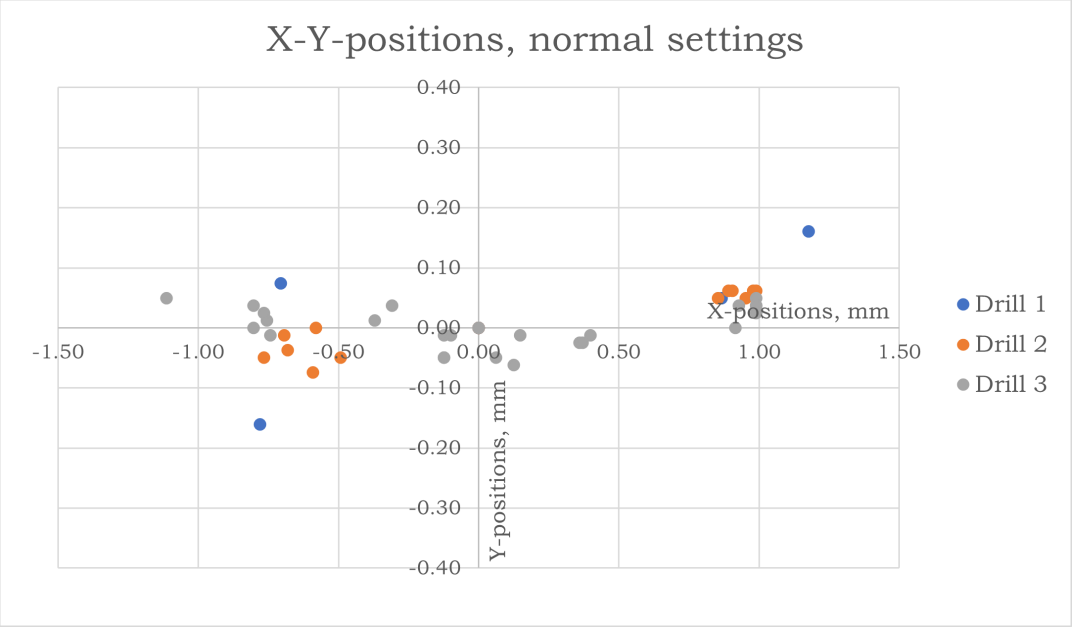

Figure 5.7: A scatter plot with the x-y-positions of the drill head of Drill 1, 2 and 3 from the static motion tests in normal settings. The data from the drill in standard and flipped position are here combined.

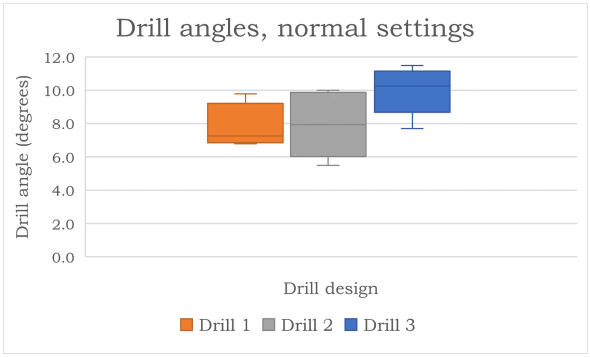

(a)

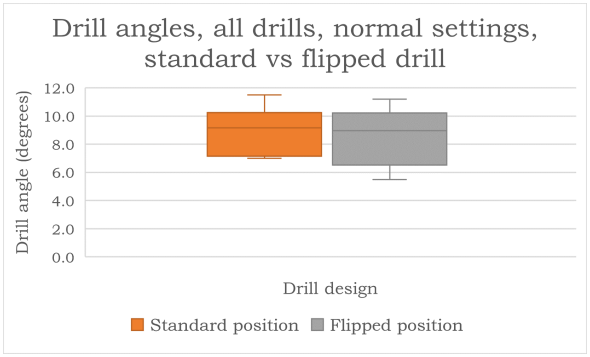

(b)

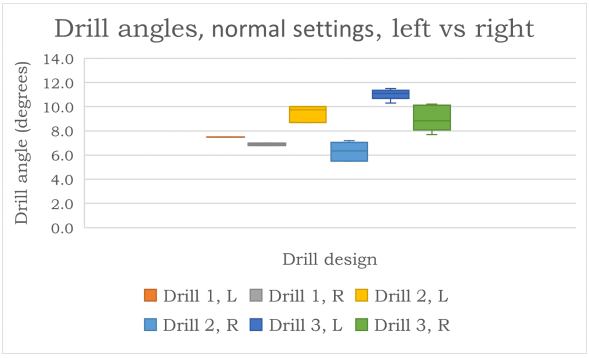

(c)

Figure 5.8: Three box plots comparing angular deviations of the drill head from the static motion test in normal settings. Plot (a) contains the absolute drill angles corresponding to a crank rotation of 90° and 270°, comparing the three drill designs. Plot (b) contains the absolute drill angles of all drills, comparing the angles for the standard and flipped positions. Plot (c) contains the angular deviations for all three drill designs, comparing the left and right angular deviations in absolute values.

6
Discussion

6.1. Main findings

The project goal was to design and evaluate a steerable oscillating bone drill that can create a curved hole in artificial cancellous bone. A prototype drill and oscillator were designed, built and evaluated. The results show that the reachable drilling depth is insufficient to evaluate the steering capability of the prototype, nonetheless, the results demonstrate a motion pattern that is expected to produce a steering effect. Two alternative designs for the drill prototype have been proposed and evaluated to increase the drilling depth. The results show an increase in the drilling depth for one of the adapted designs, however, it was not significant.

When comparing the deviation distances of the drill head in the x-direction, no large differences arise between the three drill designs. Yet, when comparing the deviation angles, Drill 3 shows a significant increase in the rotation angle of the drill head. The combined rotation and translation make the cutting teeth travel a longer distance with Drill 3 than with the other designs. Additionally, the drill is capable of generating multiple vibration modes (see Figure 4.5) when drilling in a hole and it showed that Drill 3 can produce a hole beyond the depth where the other designs got embedded. Combining these observations makes that Drill 3 is favoured over the other designs.

Comparing the results of the oscillation types (normal, amplitude difference and phase difference) shows clear differences in the produced motion patterns. The amplitude difference drastically reduces the drill head deviation distance. This is a logical result of the reduced amplitude on one of the oscillations but incidentally will also reduce the drilling speed. This effect is visible in the x-y-position plots from the static motion test as well as in the maximum swing distance observed in the dynamic motion test. It is therefore not likely that applying an amplitude will produce satisfactory drilling depth and steering results. The phase difference does not display a clear difference in the deviation distance of the drill head in the x-direction. On the contrary, the deviation in the y-direction is increased. This makes that the drill produces an oval motion pattern which is expected to be the most effective in generating a steering effect.

The set of tests devised to verify the produced motion of the drill and the oscillator showed some discrepancies within the results. Overall, no large abnormalities were observed. A consistent difference in the deviation to the left and the right is present among all the drills. The leftward motion produces larger angular deviations, but smaller positional deviations compared to the right. When the drill angle is compared between the standard and flipped position, no significant difference is present. This indicates that the discrepancies are produced by the drill constraint or by the oscillator and not by the drill itself. These discrepancies slightly hinder the results as they increase the variance of the data when comparing absolute deviation values.

6.2. Limitations

The results show improved motion behaviour of Drill 3 compared to Drills 1 and 2. However, this does not show a significant change in the reached drilling depth. The significance can be an attribute of the methodology: increasing the number of repetitions provides a better estimate of the variance and the mean. Another method of reaching significant results is by increasing the drilling time. Drill 1 always got embedded in under six minutes, however, when the goal changed to increasing the drilling depth, the drilling time should have been increased as well, to allow for this depth to be reached.

The motion of the drill head was recorded with the drill in free air. This is not representative of the situation whilst drilling, where the drill is constrained within the material. A test setup for studying the behaviour of the drill whilst drilling into material might have benefited the study in the attempt to understand and manipulate the drill's motion. Still, the drill's behaviour was partially observed with the drilling depth tests, because of the limited drilling depth. The results from this study show that the motion of the drill head with a phase difference will likely produce a steering effect, but this cannot be concluded.

6.3. Recommendations

Further research is needed to conclude if manipulation of the oscillating motion is effective in generating a curved drill path. The oscillator designed in this study can be used to generate the oscillations and adjust the phase and amplitude. Drill 3 shows promising results for creating a deep drill hole. Only when a deep drill hole is successfully produced, it makes sense to continue experimenting with steering the drill. Drill 3 still does not drill reliably, as it occasionally gets stuck, but it shows that a decrease in stiffness of the connection between the drill head and leaf springs is beneficial for the drill motion. The displacement supplied by the leaf springs results in bending of the leaf springs and a rotation of the drill head. The bending should be minimized, causing the displacement that is fed to the drill head to be maximally converted into the rotational motion. This can be established by using hinges in the connection between the drill head and the leaf springs. Figure 6.1 shows how such a hinged connection could look like.

When the drill is capable of drilling deeper holes, the drill guides used in the experiment setup will not suffice. A retractable guide is the preferred solution to constrain bending of the drill outside of the bone to limit buckling of the leaf springs. The guide can than support the the leaf springs up to the bone and adjust its length to the depth of the drill.

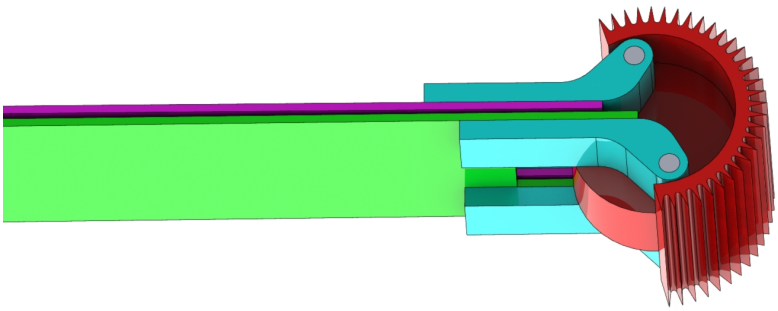

Figure 6.1: A design change proposed for improving the reliability of the drill is to create a hinged connection between the drill head and the leaf springs. The leaf springs are pink and green. The hinges are blue and the drill head is marked red.

7
Conclusion

The goal of this project was to design and evaluate a steerable oscillating bone drill that can create a curved hole in artificial cancellous bone. The underlying idea was that, by a difference in amplitude or phase between the two oscillations that are supplied to the drill head, a deviation force can be created. The drill head motion is then used for both drilling and steering, eliminating the need for a separate steering actuator. This resulted in the design of a prototype for a flexible drill and accompanying oscillator. The oscillator produces two oscillating outputs that can be individually adjusted in amplitude and phase. The flexible drill is built up of two parallel sliding leaf springs that transfer the two oscillations from the oscillator to the drill head. These oscillations cause the drill head to rotate and swing from left to right. The thin leaf springs allow the drill to bend, which is required to let the drill steer.

The preliminary results showed that the drill got embedded in the drilled hole, only reaching a maximum depth of 5.6 mm. This depth is insufficient for measuring a steering effect. Therefore, two alternative drill designs were proposed and evaluated to increase the drilling depth. The design adaptation that provides the most promising result, is to drastically lower the stiffness of the connection between the drill head and the leaf springs. The experiments showed that this solution significantly increased the rotation angle of the drill head by 28%, increasing the travel distance of the cutters. Furthermore, it was observed that the adapted drill did not get itself embedded as easily as the original design, allowing it to reach greater drilling depths.

An amplitude or phase difference applied by the oscillator causes the drill head to produce a different motion pattern. The pattern from the amplitude difference (left: 0.75 mm, right 0.25 mm) shows a decrease in the deviation distance which likely has a diminishing effect on the effectiveness of the drill. A phase difference of 144°between the two oscillations, causes the drill to produce an oval motion pattern which is expected to be the most effective in generating a steering effect.

This project provides a great basis for the future development of a drill that can steer without a steering actuator. The next step forward with this design should be to incorporate hinges between the leaf springs and the drill head, to maximise the rotational motion of the drill head.

Bibliography

[1] Fabio Galbusera and Hans-Joachim Wilke. *Biomechanics of the spine : basic concepts, spinal disorders and treatments*. Engels. First edit. London: Academic Press, 2018. ISBN: 9780128128527. DOI: 1032810215. URL: https://search.ebscohost.com/login.aspx?direct=true&scope=site&db=nlebk&db=nlabk&AN=1627751%20https://public.ebookcentral.proquest.com/choice/publicfullrecord.aspx?p=5359390%20https://www.sciencedirect.com/science/book/9780128128510%20https://nls.ldls.org.uk/we.

[2] Ilya Laufer and J J Verlaan. *Posterior MIS for Thoracolumbar, unstable, high ESCC*. URL: https://surgeryreference.aofoundation.org/spine/tumors/metastatic-tumors/thoracolumbar-unstable-high-escc/posterior-mis?searchurl=%2FSearchResults.

[3] Han Jo Kim, Marinus de Kleuver, and Keith Luk. *Insertion of pedicle screws*. URL: https://surgeryreference.aofoundation.org/spine/deformities/adolescent-idiopathic-scoliosis/basic-technique/insertion-of-pedicle-screws.

[4] Stryker Medical. *Xia ő 3 Spinal System Surgical Technique*. Tech. rep. Allendale, 2018. URL: https://inspine.nl/cms/wp-content/uploads/2020/01/TLXIA_ST_4.pdf.

[5] Daniel M. McKenzie et al. "Robotics in spine surgery: A systematic review". In: *Journal of Clinical Neuroscience* 89 (July 2021), pp. 1–7. ISSN: 0967-5868. DOI: 10.1016/J.JOCN.2021.04.005.

[6] Paul Anderson. *Spinal Instrumentation: Basic Concepts & Biomechanics by Paul Anderson, M.D. - YouTube*. Aug. 2015. URL: https://www.youtube.com/watch?v=q0-EdCJyfgA&ab_channel=SeattleScienceFoundation.

[7] Alexander Aichmair et al. "Aortic perforation during lateral lumbar interbody fusion". In: *Journal of spinal disorders & techniques* 28.2 (Mar. 2015), pp. 71–75. ISSN: 1539-2465. DOI: 10.1097/BSD.0000000000000067. URL: https://pubmed-ncbi-nlm-nih-gov.tudelft.idm.oclc.org/24326238/.

[8] Aleem K. Mirza et al. "Management of major vascular injury during pedicle screw instrumentation of thoracolumbar spine". In: *Clinical Neurology and Neurosurgery* 163 (Dec. 2017), pp. 53–59. ISSN: 0303-8467. DOI: 10.1016/J.CLINEURO.2017.10.011.

[9] J. Y. Du et al. "Treatment strategies for early neurological deficits related to malpositioned pedicle screws in the lumbosacral canal: A pilot study". In: *Bone and Joint Research* 5.2 (Feb. 2016), pp. 46–51. ISSN: 20463758. DOI: 10.1302/2046-3758.52.2000477/ASSET/IMAGES/LARGE/10.1302{_}2046-3758.52.2000477-FIG1.JPEG. URL: https://online.boneandjoint.org.uk/doi/abs/10.1302/2046-3758.52.2000477.

[10] Frank H Netter. *Atlas of Human Anatomy*. 4th ed. Philadelphia: Saunders Elsevier, 2006, pp. 153–179. ISBN: 978-1-4160-3385-1.

[11] Noojan Kazemi. *Biomechanics of Spinal Instrumentation - Noojan Kazemi, MD - YouTube*. Seattle, Aug. 2020. URL: https://www.youtube.com/watch?v=cf5ZqRkSf_M&ab_channel=SeattleScienceFoundation.

[12] Elke Rometsch et al. "Screw-Related Complications After Instrumentation of the Osteoporotic Spine: A Systematic Literature Review With Meta-Analysis". In: *Global Spine Journal* 10.1 (Feb. 2020), pp. 69–88. ISSN: 2192-5682. DOI: 10.1177/2192568218818164. URL: http://journals.sagepub.com/doi/10.1177/2192568218818164.

[13] Jizhou Wang, ů Xiaoqi He, and Tianwei Sun. "Comparative clinical efficacy and safety of cortical bone trajectory screw fixation and traditional pedicle screw fixation in posterior lumbar fusion: a systematic review and meta-analysis". In: *European Spine Journal* 28 (2019), pp. 1678–1689. DOI: 10.1007/s00586-019-05999-y. URL: https://doi.org/10.1007/s00586-019-05999-y.

[14] Yiren Chen et al. "Minimally Invasive Lumbar Pedicle Screw Fixation Using Cortical Bone Trajectory: Functional Outcomes". In: *Cureus* 10.10 (Oct. 2018). ISSN: 2168-8184. DOI: 10.7759/CUREUS.3462. URL: https://pubmed.ncbi.nlm.nih.gov/30564541/.

[15] Vishwajeet Singh et al. "Surgical Trend Analysis for Use of Cement Augmented Pedicle Screws in Osteoporosis of Spine: A Systematic Review (2000-2017)". In: *AO Spine* 9.7 (2019), pp. 783–795. DOI: 10.1177/2192568218801570. URL: https://us.sagepub.com/en-us/nam/open-access-at-sage.

[16] Yamaan S. Saadeh et al. “Effect of Fenestrated Pedicle Screws with Cement Augmentation in Osteoporotic Patients Undergoing Spinal Fusion”. In: *World Neurosurgery* 143 (Nov. 2020), e351–e361. ISSN: 1878-8750. DOI: 10.1016/J.WNEU.2020.07.154.

[17] Andrea Lorenz et al. “Pull out Strength of Dual Outer Diameter Pedicle Screws Compared to Uncemented and Cemented Standard Pedicle Screws: A Biomechanical in vitro Study”. In: *Orthopaedic Surgery* 9 (2017), pp. 229–236. DOI: 10.1111/os.12322.

[18] Rob Müller. “Bio-Inspired Flexible Vertebral Drill: The design, manufacturing and evaluation of a prototype”. PhD thesis. Delft University of Technology, 2022. URL: https://repository.tudelft.nl.

[19] Alexander Sendrowicz et al. “Surgical drilling of curved holes in bone a patent review”. In: *https://doi-org.tudelft.idm.oclc.org/10.1080/17434440.2019.1596794* 16.4 (Apr. 2019), pp. 287–298. DOI: 10.1080/17434440.2019.1596794. URL: https://www-tandfonline-com.tudelft.idm.oclc.org/doi/abs/10.1080/17434440.2019.1596794.

[20] Awaz Ali, Dick Plettenburg, and Paul Breedveld. “Steerable Catheters in Cardiology: Classifying Steerability and Assessing Future Challenges”. In: *IEEE Transactions on Biomedical Engineering* 63.4 (Apr. 2016), pp. 1–1. ISSN: 0018-9294. DOI: 10.1109/TBME.2016.2525785. URL: http://ieeexplore.ieee.org/document/7399367/.

[21] Xiaohua Hu et al. “Steerable catheters for minimally invasive surgery: a review and future directions”. In: *Computer Assisted Surgery* 23.1 (Jan. 2018), pp. 21–41. ISSN: 2469-9322. DOI: 10.1080/24699322.2018.1526972. URL: https://www.tandfonline.com/doi/full/10.1080/24699322.2018.1526972.

[22] Marta Scali et al. “Needle-like instruments for steering through solid organs: A review of the scientific and patent literature:” in: *Journal of Engineering in Medicine* 231.3 (Jan. 2017), pp. 250–265. DOI: 10.1177/0954411916672149. URL: https://journals-sagepub-com.tudelft.idm.oclc.org/doi/10.1177/0954411916672149?url_ver=Z39.88-2003&rfr_id=ori%3Arid%3Acrossref.org&rfr_dat=cr_pub++0pubmed.

[23] Tianshou Ma, Ping Chen, and Jian Zhao. “Overview on vertical and directional drilling technologies for the exploration and exploitation of deep petroleum resources”. In: *Geomechanics and Geophysics for Geo-Energy and Geo-Resources* 2.4 (Dec. 2016), pp. 365–395. ISSN: 23638427. DOI: 10.1007/s40948-016-0038-y. URL: https://link-springer-com.tudelft.idm.oclc.org/article/10.1007/s40948-016-0038-y.

[24] Farshid Alambeigi et al. “A Curved-Drilling Approach in Core Decompression of the Femoral Head Osteonecrosis Using a Continuum Manipulator”. In: *IEEE Robotics and Automation Letters* 2.3 (July 2017), pp. 1480–1487. ISSN: 2377-3766. DOI: 10.1109/LRA.2017.2668469. URL: http://ieeexplore.ieee.org/document/7855629/.

[25] Farshid Alambeigi and Mehran Armand. *Steerable Device for Treatment of Hard-Tissue-Related Diseases and Minimally Invasive Surgery*. Sept. 2018. URL: https://worldwide.espacenet.com/patent/search/family/063370484/publication/WO2018160269A1?q=alambeigi.

[26] Purvi SD Patel and David WL Hukins. “Compressive properties of commercially available polyurethane foams as mechanical models for osteoporotic human cancellous bone”. In: (2008). DOI: 10.1186/1471-2474-9-137. URL: http://www.biomedcentral.com/1471-2474/9/137.

[27] S. H. Zhou et al. “Geometrical dimensions ,of the lumbar vertebrae - Analysis of data from digitised CT images”. In: *European Spine Journal* 9.3 (2000), pp. 242–248. ISSN: 09406719. DOI: 10.1007/s005860000140. URL: https://pubmed-ncbi-nlm-nih-gov.tudelft.idm.oclc.org/10905444/.

[28] Serope Kalpakjian. *Manufacturing engineering and technology*. 6th ed. Upper Saddle River: Prentice-Hall, 2010. ISBN: 9780136081685.

[29] G.J.M. Tuijthof, C. Frühwirt, and C. Kment. “Influence of tool geometry on drilling performance of cortical and trabecular bone”. In: *Medical Engineering & Physics* 35.8 (Aug. 2013), pp. 1165–1172. ISSN: 13504533. DOI: 10.1016/j.medengphy.2012.12.004. URL: https://linkinghub.elsevier.com/retrieve/pii/S1350453312003323.

[30] William R. Krause et al. “Temperature elevations in orthopaedic cutting operations”. In: *Journal of Biomechanics* 15.4 (Jan. 1982), pp. 267–275. ISSN: 00219290. DOI: 10.1016/0021-9290(82)90173-7. URL: https://linkinghub.elsevier.com/retrieve/pii/0021929082901737.

A
Motion calculations

Hypothetical drill head oscillation motion

The drill head motion model only takes into account the oscillating translation input directly to the drill head and the resulting motion of the drill head. Figure A.1 depicts the resulting rotational oscillation of the drill head. This model is used to determine the theoretical motion pattern of the drill head by calculating the position and orientation. The input displacements are forward and backward in a single direction. First the positions of the input points of the drill head are determined. The left and right position are determined separately. The attachment point moves radially around the center of the drill head with an arc distance corresponding to the input displacement. With the position of the left and right attachment point determined, the position of the center point is interpolated between the two. Lastly the orientation of the drill head is determined, by taking the angle between a horizontal line and the line that can be drawn through the two attachment points.

The fixed parameters of the model are the dimensions of the drill head. In this case the outer diameter is 6mm and the distance between the two attachment points is 3mm. Both attachment points receive a sign wave oscillation as input. The stroke distance ($amplitude * 2$) can for each input be set to the values 0.25, 0.50, 0.75 and 1.0 mm which are the same settings that can be produced by the prototype. For each input, the phase can be adjusted to 0°, 90°, 108°, 126°, 144°, 162°and 180°. For normal operation, the left input is set to 0°and the right input to 180°and a stroke length of 0.75mm. These parameters can be inserted into a sine function, provided in Equation A.1. The oscillation is simulated by inputting values for x between 0°and 360°.

$$y = a\sin(bx - c) \tag{A.1}$$

Determining the positions of the attachment points starts with determining the y-position of each input, using Equation A.1. Next, the x-position is determined by taking the value of this y-position as the arc length with a radius of 1.5mm and projecting this position onto the y-axis. In practice this means taking the cosine (with an amplitude corresponding with the radius) of the previously determined y-value over the radius as in Equation A.2. The center of the drill head in neutral position is considered 0, the left input position is thus negative and the right input position is positive.

$$x = r\cos(y/r) \tag{A.2}$$

The center position is taken by addition of the left and right positions, both for x and y. The angle of the drill head is determined by calculating the angle of a line trough both attachment points. This is done with the arc tangent as seen in Equation A.3.

$$\theta = \arctan\frac{\delta y}{\delta x} = \arctan\frac{y_l - y_r}{x_r - x_l} \tag{A.3}$$

These calculations were made in Excel to produce a list of position values over a full motion cycle of 360°with 45°increments. Example results for the standard setting is provided in Figure A.2.

Motion relations between prototype components

A model was made to relate the stroke lengths of the different components of the prototype based on their dimensions. This allowed to quickly determine the required size for components and to assess the impact of adjustments. The flow of motion for the prototype starts with the motor which rotates the crank. On the crank the amplitude of the oscillation can be adjusted. This oscillation is reduced by a cantilever bar. It is then transferred by the leaf springs of the flexible motion transfer system to the drill head. The motion is increased at the drill head.

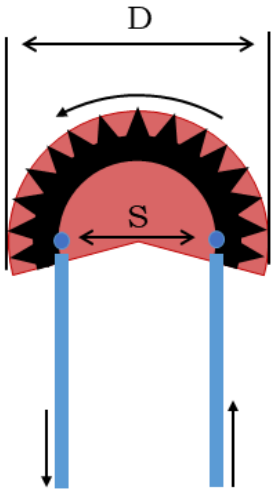

Figure A.1: A schematic top view of the drill head rotation as a result of the input from the leaf springs. The attachment points are the two blue dots. D is the diameter of the drill head and S is the separation distance between the two attachment points.

Motion model: select amplitude and phase for left and right input to the drill head											
				Output:	Lx	Ly	Rx	Ry	Cx	Cy	alpha
Wave function	Left	Right		Input (deg)	mm	mm	mm	mm	mm	mm	deg
Setting stroke	0.75	0.75		0	-1.50	0.00	1.50	0.00	0.00	0.00	0.00
Setting phase	0	180		45	-1.50	0.27	1.50	-0.27	0.00	0.00	10.03
				90	-1.50	0.38	1.50	-0.38	0.00	0.00	14.06
				135	-1.50	0.27	1.50	-0.27	0.00	0.00	10.03
				180	-1.50	0.00	1.50	0.00	0.00	0.00	0.00
				225	-1.50	-0.27	1.50	0.27	0.00	0.00	-10.03
				270	-1.50	-0.38	1.50	0.38	0.00	0.00	-14.06
				315	-1.50	-0.27	1.50	0.27	0.00	0.00	-10.03
				360	-1.50	0.00	1.50	0.00	0.00	0.00	0.00

Figure A.2: An overview of the resulting values of the drill head position and orientation of a full motion cycle.

Cutter dimensions									
Outter diam	6	mm			plate	drill	drill	crank	crank
separaition	3	mm			stroke	angle	stroke	stroke	radius
nominal stroke	0.75	mm			mm	deg	mm	mm	mm
				high	1	38.19719	2.0	12	6
				nominal	0.75	28.64789	1.5	9	4.5
Mechanism dimensions				small	0.5	19.09859	1.0	6	3
				smallest	0.25	9.549297	0.5	3	1.5
Reduction ratio	12								
Reduction CD	90	mm							
Reduction DE	7.5	mm							

Figure A.3: An overview of the dimensions and ratio's in the prototype and the resulting motion of the components.

The parameters that can be adjusted are the drill outer diameter, the separation distance between the attachment point to the drill, the nominal stroke length, the reduction ratio and the longest length of the reduction rod.

All calculations are based around the drill head input motion, as this value is the same for the drill assembly and the oscillator assembly. This was set for a standard stroke length of 0.75mm. The adjustment setting for the amplitude should correspond to stroke lengths of 0.25, 0.50, 0.75, and 1.00 mm. Based on the dimensions of the drill, the drill stroke distance is calculated by assuming the input stroke distance directly corresponds to the arc length travel distance. This arc length travel distance is multiplied by the ratio between the separation distance and the outer diameter. This arc length travel distance is also used to calculate the rotation angle of the drill head. On the side of the oscillator the reduction ratio of the reduction rod is used to calculate the stroke length that needs to come from the crank. Halve the stroke length is the crank radius. A screenshot of the resulting overview is provided in Figure A.3.

B

Buckling and bending calculations

Euler critical load calculation

For calculating the maximum allowable force before buckling of the flexible motion transfer system, the Euler critical load calculations were used. The structure comprising of two parallel leaf springs is a slender construction. Without the steering force, the only load is the feed force in axial direction for which the maximum is calculated. Equation B.1 is the Euler critical load calculation which was used to determine this maximum allowable force. The variable E is the Young's modulus, which is $1.8e11$ Pa for spring steel. The variable I is the area moment of inertia, determined by Equation B.2. The width b was kept at 5 mm and the heigth h was varied. The variable L is the length of the leaf spring which is desired to be 80 mm long with a minimum of 50 mm. The constant K is the column effective length factor and is determined by the boundary conditions at both ends of the leaf spring.

$$F_{critical} = \frac{\pi^2 * E * I}{(K * L)^2} \tag{B.1}$$

$$I = \frac{b * h^3}{12} \tag{B.2}$$

The Euler critical load calculation was used for determining the required thickness for the leaf springs. Thin leaf springs are desired, as they need less force to bend. The original drill design had 0.3 mm thick leaf springs and this thickness was gradually lowered in the calculation based on the available stock. The critical load value was calculated for the two leaf springs together, meaning that the load is equally shared amongst the two leaf springs as shown in Figure B.1. It is important not to double the thickness in the calculation, since the two leaf springs are slidably connected and thus do not resist shear forces. One end is clamped by the drill guide and the other end is free leading to a theoretical length factor K of 0.7, but the recommended value of 0.8 was used. A thickness of 0.3 mm leads to a maximum force of 9.76 N, a thickness of 0.2 mm leads to a maximum force of 2.89 N and a thickness of 0.1 mm leads to a maximum force of 0.36 N. In theory a leaf spring thickness of 0.2 mm should provide sufficient resistance to the feed force.

A check was performed on the buckling resistance of a section of leaf spring between the two sliding joints. The maximum length of such section is 4 mm with a thickness of 0.2 mm. The recommended K factor is 0.65 as both ends are clamped by the slidable bolt connection. The maximum load on such section is 8.76 N which is well beyond expected values.

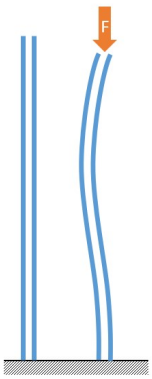

Figure B.1: A schematic display of the two leaf springs sharing the feed force. They buckle as one structure.

The buckling calculations are rough estimates based on theoretical values and static conditions. The drill will likely experience more dynamic and unpredictable conditions which is difficult to account for in the early design stage.

Euler-Bernoulli static beam calculation

A simple linear bending calculation with the Euler-Bernoulli static beam equations was performed to gain some insight in the expected forces that are needed to create a small directional deviation. Te beam deflection was determined with Equation B.3. The deflection is determined with a constant sideways force and the length is incrementally increased. This is to simulate the drill extending into the bone. Two trajectories were created, one with a constant sideways force of 0.2 N and one with a constant sidaways force of 0.1 N. These are $\frac{1}{10}^{th}$ and $\frac{1}{20}^{th}$ of the expected 2 N feed force. The maximum insertion depth is set to 50 mm.

$$\delta = \frac{F * l^3}{3 * E * I} \tag{B.3}$$

The calculations resulted in Figure B.2 where two drill trajectories are displayed. For the 0.1 N sideways force, a directional deviation is likely measurable beyond 30 mm depth when the deviation is above 1 mm. At 50 mm depth (or beam length), the deviation is almost 7 mm. For the 0.2 N sideways force, the deviation becomes measurable beyond 25 mm depth. At 50 mm depth, the deviation is almost 14 mm. Of course these calculations are rough estimates of the behaviour of the drill and should be revised based on the observed and measured results.

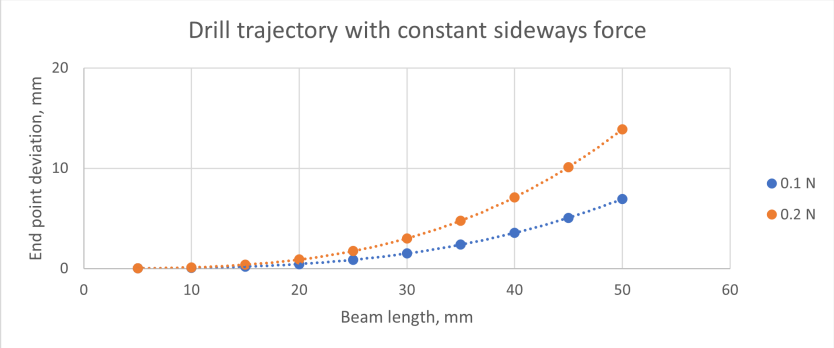

Figure B.2: The expected drill tip deviations based on the drill extending with a constant sideways force acting on the drill tip. Forces of 0.1 N and 0.2 N are used in the calculations.

C

Technical drawings

ITEM NO.	PART NUMBER	DESCRIPTION	QTY.
1	Frame A		1
2	Reely RS380PM-4531F-57D		1
3	Bottom hinge pt1		1
4	Reduction rod		2
5	Bottom hinge pin		2
6	Connector rod pt1		1
7	Top hinge pin		2
8	ISO 15 RBB - 382.5 - 10,SI,NC,10_68		2
9	Crank spacer		2
10	Connector rod pt1		1
11	ISO 4762 M3 x 8 - 8N		2
12	Connector rod pt2 retainer		2
13	ISO 7380 - M3 x 6 - 6N		6
14	ISO 15 RBB - 384 - 10,SI,NC,10_68		2
15	Shaft 4mm		1
16	Circlip DIN 471 - 4 x 0.4		2
17	ISO - Spur gear 0.5M 50T 20PA 4FW --- S50B10H9L4.0N		2
18	ISO - Spur gear 0.5M 20T 20PA 4FW --- S20B9H9L4.0N		1
19	Shaft coupler		1
20	Spline sleeve crank		1
21	Crank		1
22	ISO 4762 M2.5 x 6 - 6N		4
23	Magnetic switch		1
24	Switch holding plate B		1
25	ISO 7380 - M3 x 8 - 8N		4
26	ISO - 4032 - M3 - W - N		2
27	ISO 4029 - M3 x 3-N		2
28	ISO 7380 - M3 x 10 - 10N		4
29	Adapter plate		1
30	ISO 4015 - M4 x 20 x 20-N		4
31	Drill guide		1
32	Drill head		1
33	Leafspring		1
34	Leafspring		1
35	DIN EN ISO 1207 - M1.6 x 2 - 2N		2
36	Hexagon Thin Nut ISO 4035 - M1.6 - N		2
37	Pin 0.5mm		4

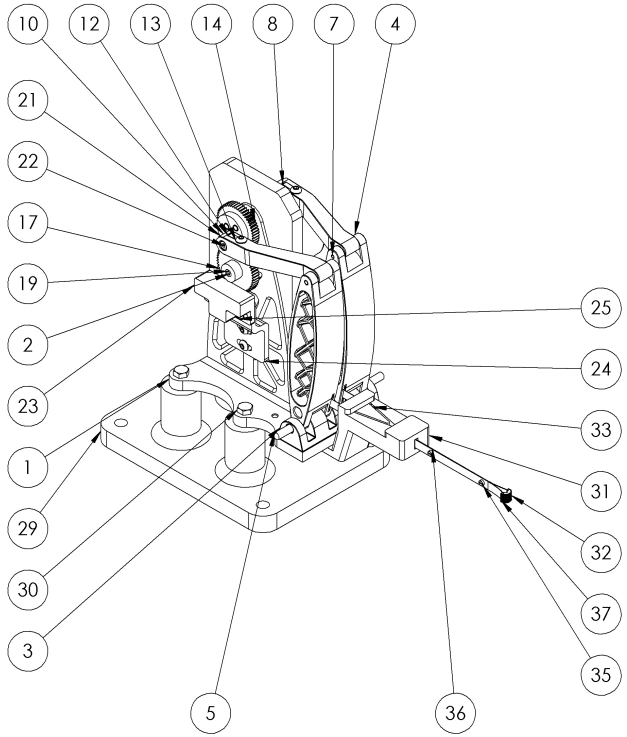

UNLESS OTHERWISE SPECIFIED:
DIMENSIONS ARE IN MILLIMETERS
SURFACE FINISH:
TOLERANCES:
LINEAR:
ANGULAR:

FINISH:

DEBURR AND BREAK SHARP EDGES

DO NOT SCALE DRAWING

REVISION

	NAME	SIGNATURE	DATE
DRAWN			
CHKD			
APPVD			
MFG			
Q.A			

TITLE:

Complete drill assembly and BOM

MATERIAL:

DWG NO.

A3

WEIGHT:

SCALE:1:2

SHEET 1 OF 1

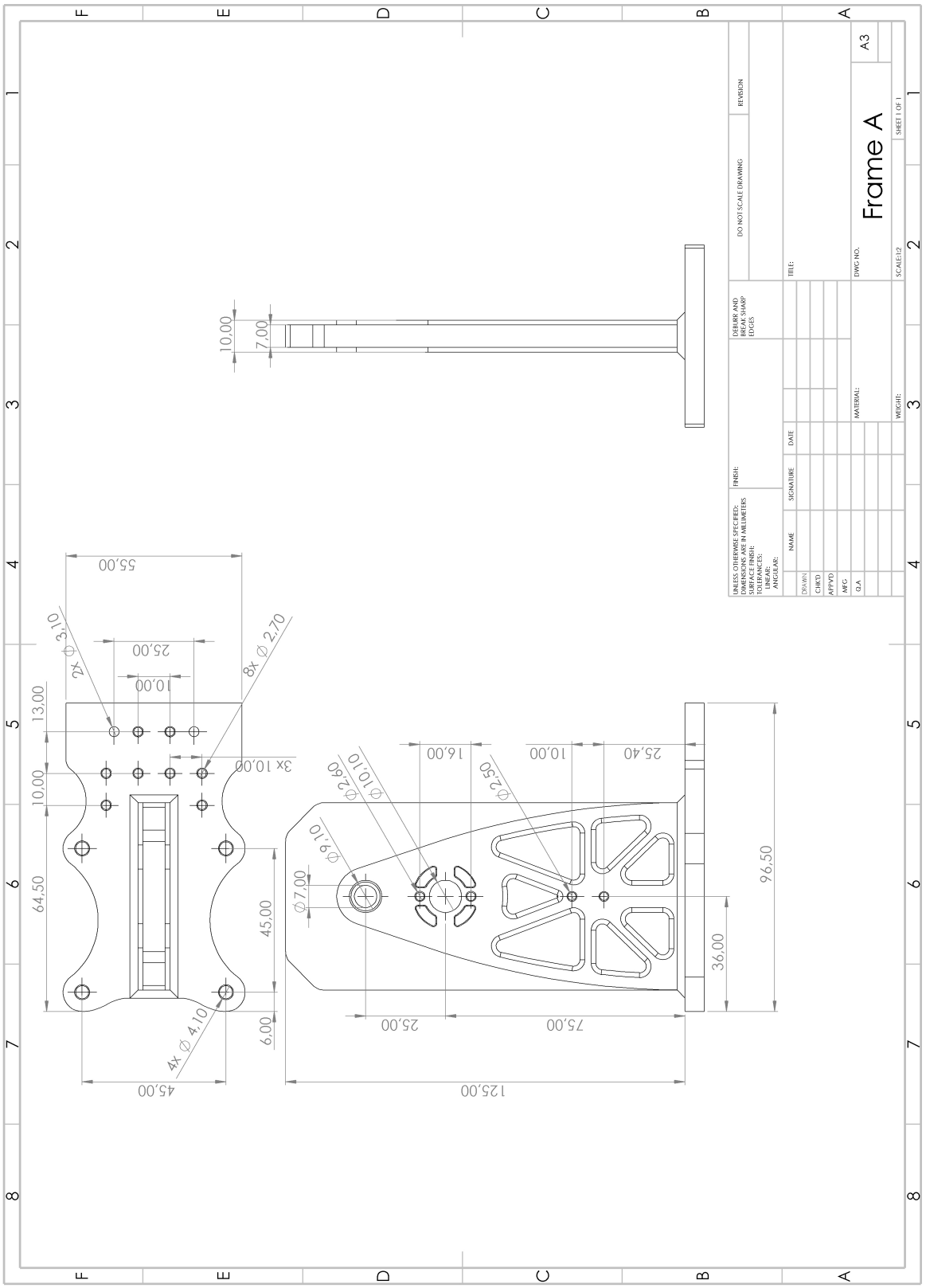
Frame A
A3
SCALE:1:2
SHEET 1 OF 1
DO NOT SCALE DRAWING
REVISION
DEBURR AND BREAK ALL SHARP EDGES
UNLESS OTHERWISE SPECIFIED:
DIMENSIONS ARE IN MILLIMETERS
SURFACE FINISH:
TOLERANCES:
LINEAR:
ANGULAR:
FINISH:
MATERIAL:
DWG NO.
TITLE:
NAME
SIGNATURE
DATE
DRAWN
CHK'D
APP'VD
MFG
Q.A
WEIGHT:
55,00
25,00
10,00
2x ⌀ 3,10
8x ⌀ 2,70
3x 10,00
13,00
10,00
64,50
45,00
6,00
4x ⌀ 4,10
45,00
10,00
7,00
⌀7,00
⌀9,10
⌀10,10
⌀2,60
⌀2,50
16,00
10,00
25,40
96,50
36,00
25,00
75,00
125,00

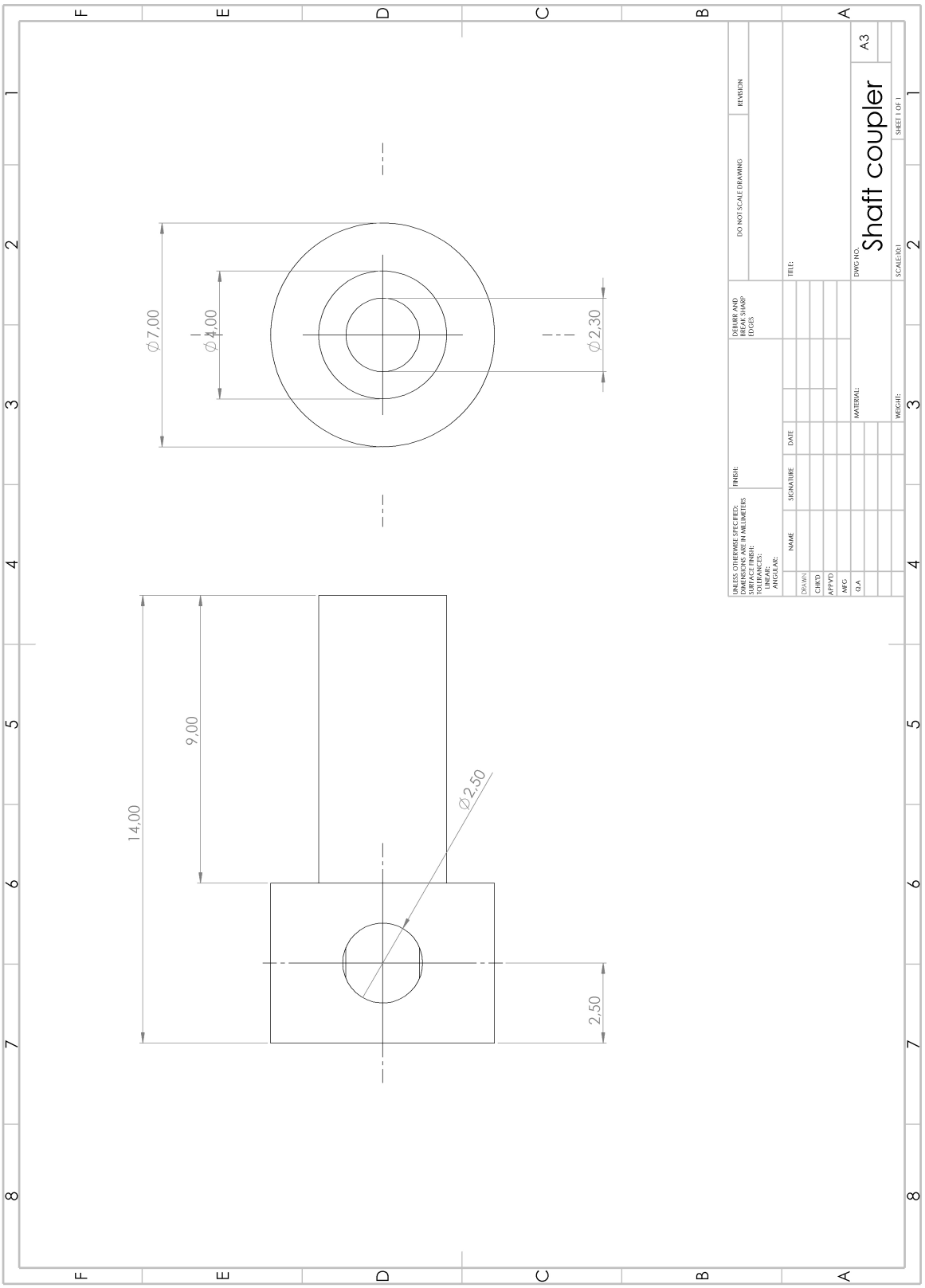
Ø7,00
Ø4,00
Ø2,30
9,00
14,00
Ø2,50
2,50
Shaft coupler
A3
SCALE:10:1
SHEET 1 OF 1
DO NOT SCALE DRAWING
REVISION
DEBURR AND BREAK SHARP EDGES
UNLESS OTHERWISE SPECIFIED:
DIMENSIONS ARE IN MILLIMETERS
SURFACE FINISH:
TOLERANCES:
LINEAR:
ANGULAR:
FINISH:
NAME
SIGNATURE
DATE
DRAWN
CHKD
APPVD
MFG
Q.A.
MATERIAL:
WEIGHT:
TITLE:
DWG NO.

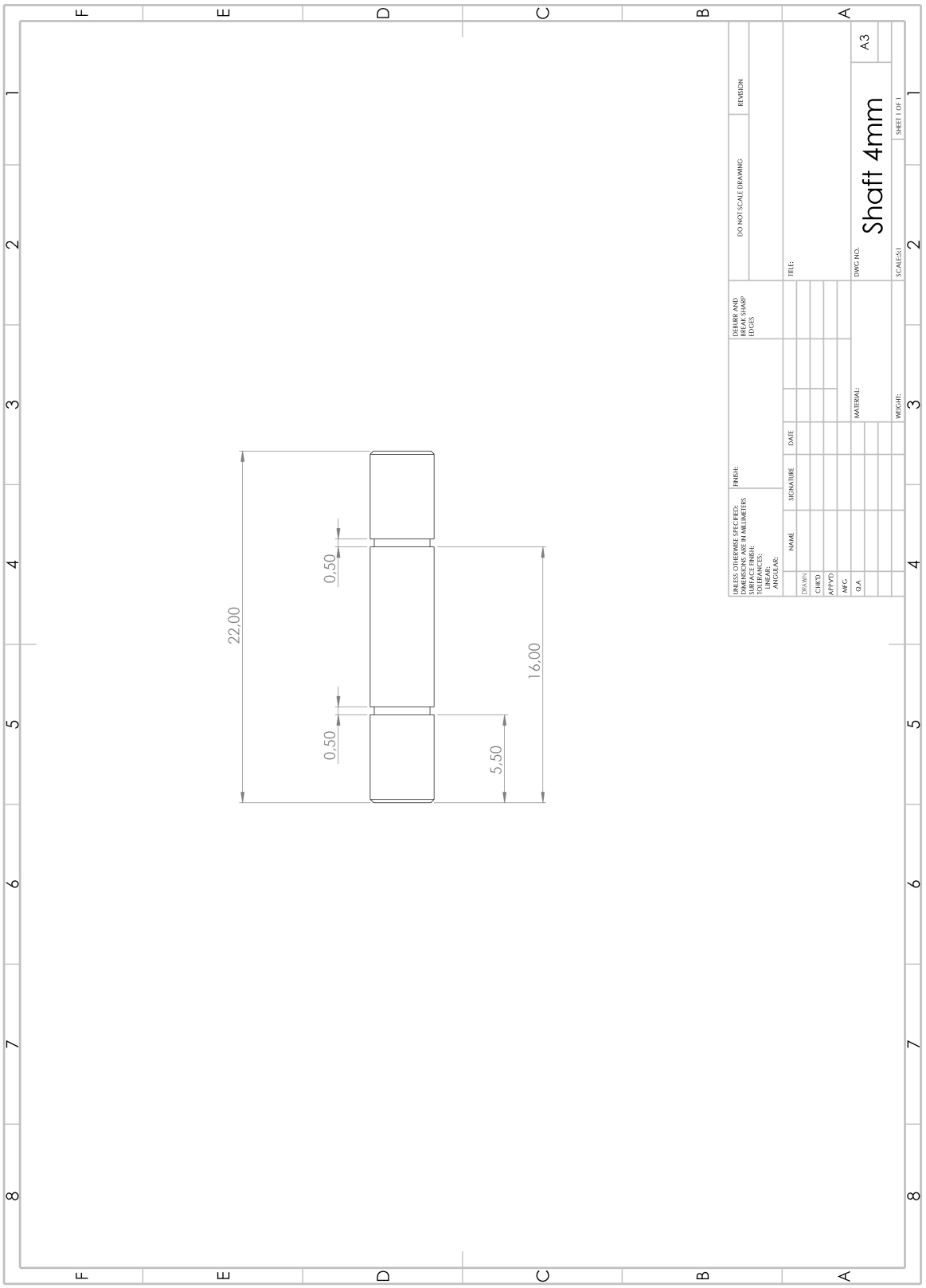
22,00
0,50
0,50
16,00
5,50
Shaft 4mm
A3
DO NOT SCALE DRAWING
REVISION
DEBURR AND
BREAK ALL SHARP
EDGES
FINISH:
UNLESS OTHERWISE SPECIFIED:
DIMENSIONS ARE IN MILLIMETERS
SURFACE FINISH:
TOLERANCES:
LINEAR:
ANGULAR:
NAME
SIGNATURE
DATE
DRAWN
CHK'D
APP'D
MFG
Q.A
MATERIAL:
DWG NO.
TITLE:
WEIGHT:
SCALE:1:1
SHEET 1 OF 1

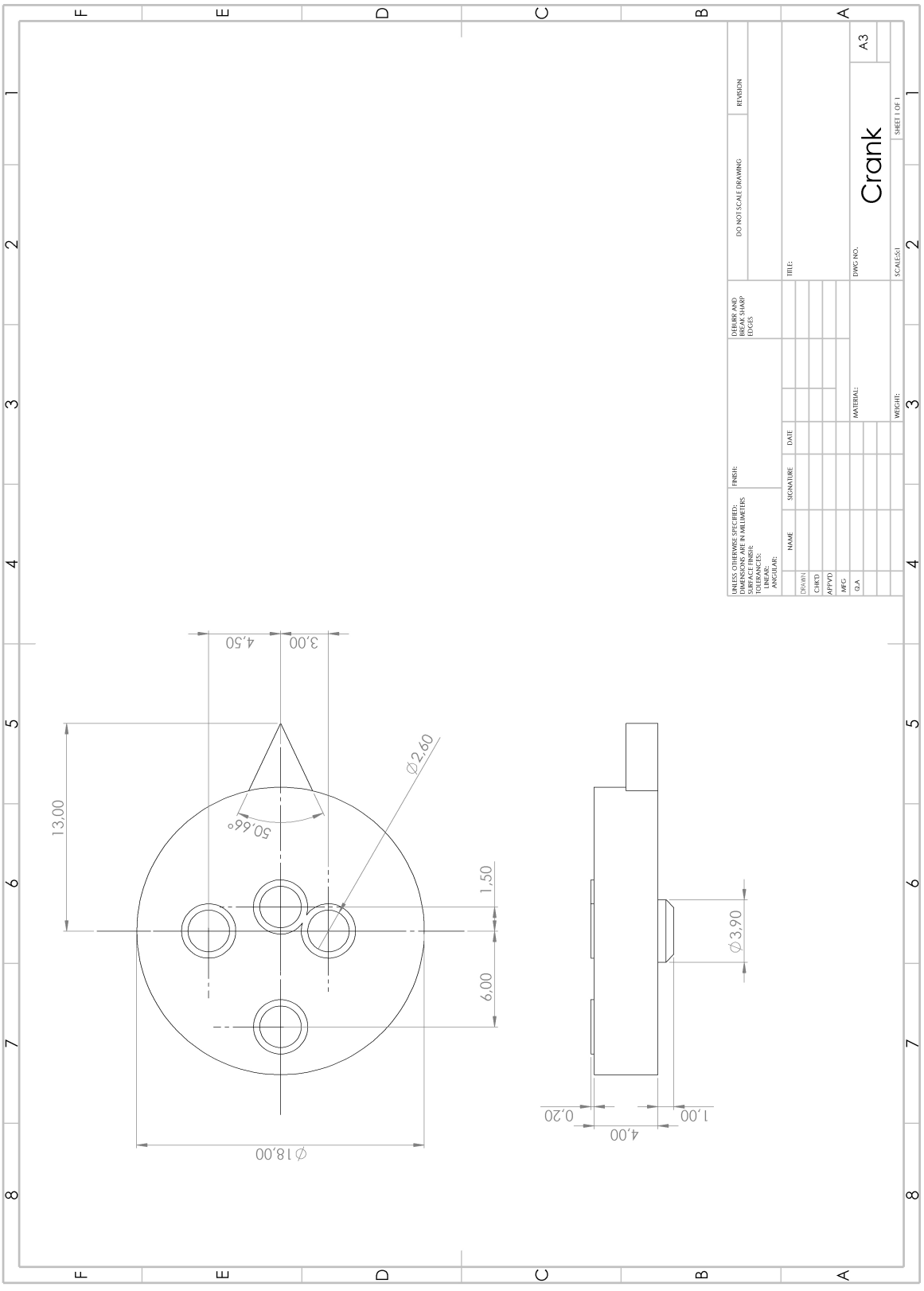
Crank
A3
DWG NO.
TITLE:
REVISION
DO NOT SCALE DRAWING
SCALE:5:1
SHEET 1 OF 1
MATERIAL:
WEIGHT:
DEBURR AND BREAK SHARP EDGES
FINISH:
UNLESS OTHERWISE SPECIFIED:
DIMENSIONS ARE IN MILLIMETERS
SURFACE FINISH:
TOLERANCES:
LINEAR:
ANGULAR:
NAME
SIGNATURE
DATE
DRAWN
CHKD
APPVD
MFG
Q.A
3,00
4,50
13,00
50,66°
Ø2,60
1,50
6,00
Ø18,00
Ø3,90
0,20
1,00
4,00

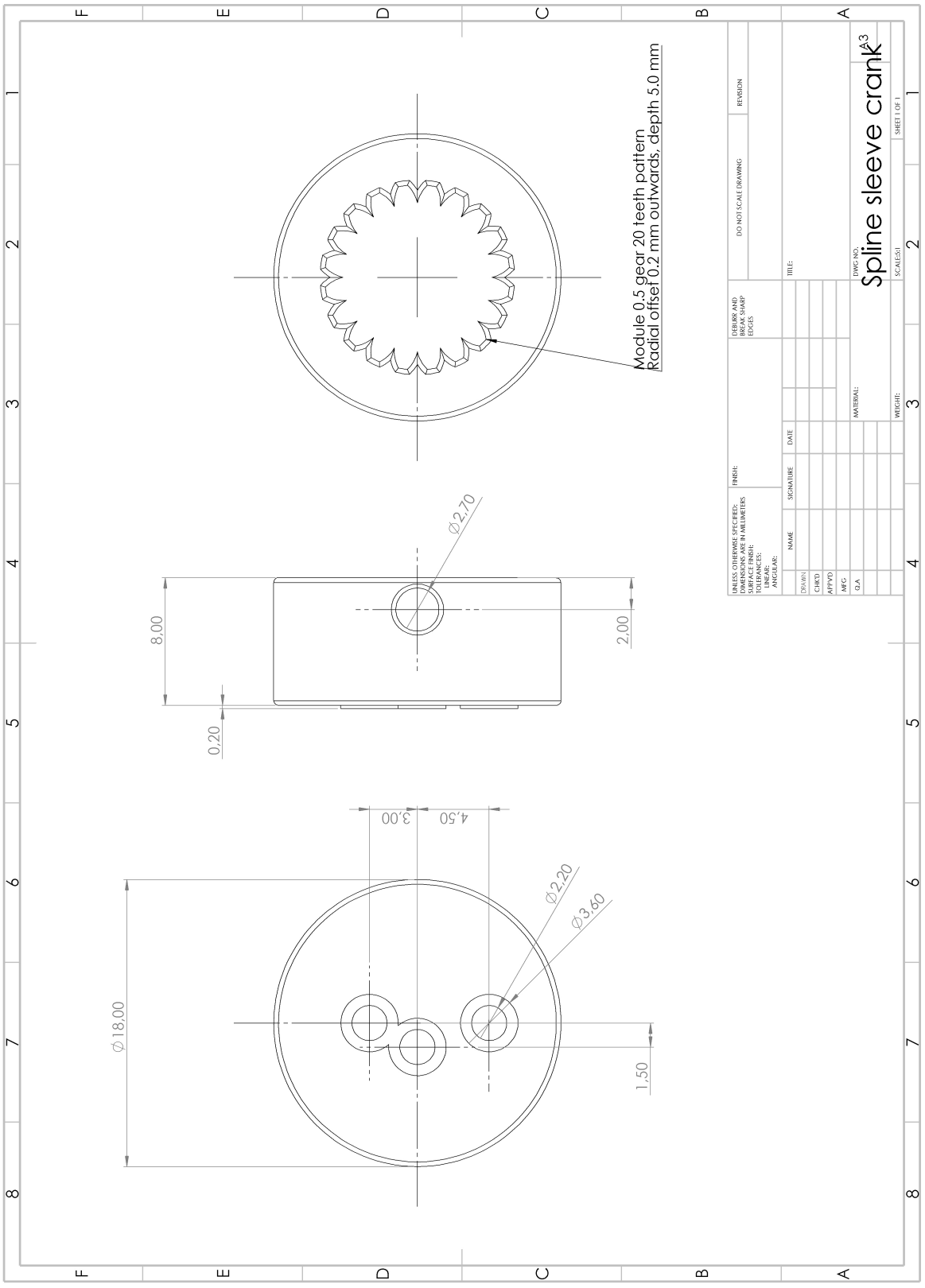
Module 0.5 gear 20 teeth pattern
Radial offset 0.2 mm outwards, depth 5.0 mm
Ø2.70
8.00
2.00
0.20
4.50
3.00
Ø2.20
Ø3.60
Ø18.00
1.50
Spline sleeve crank
A3

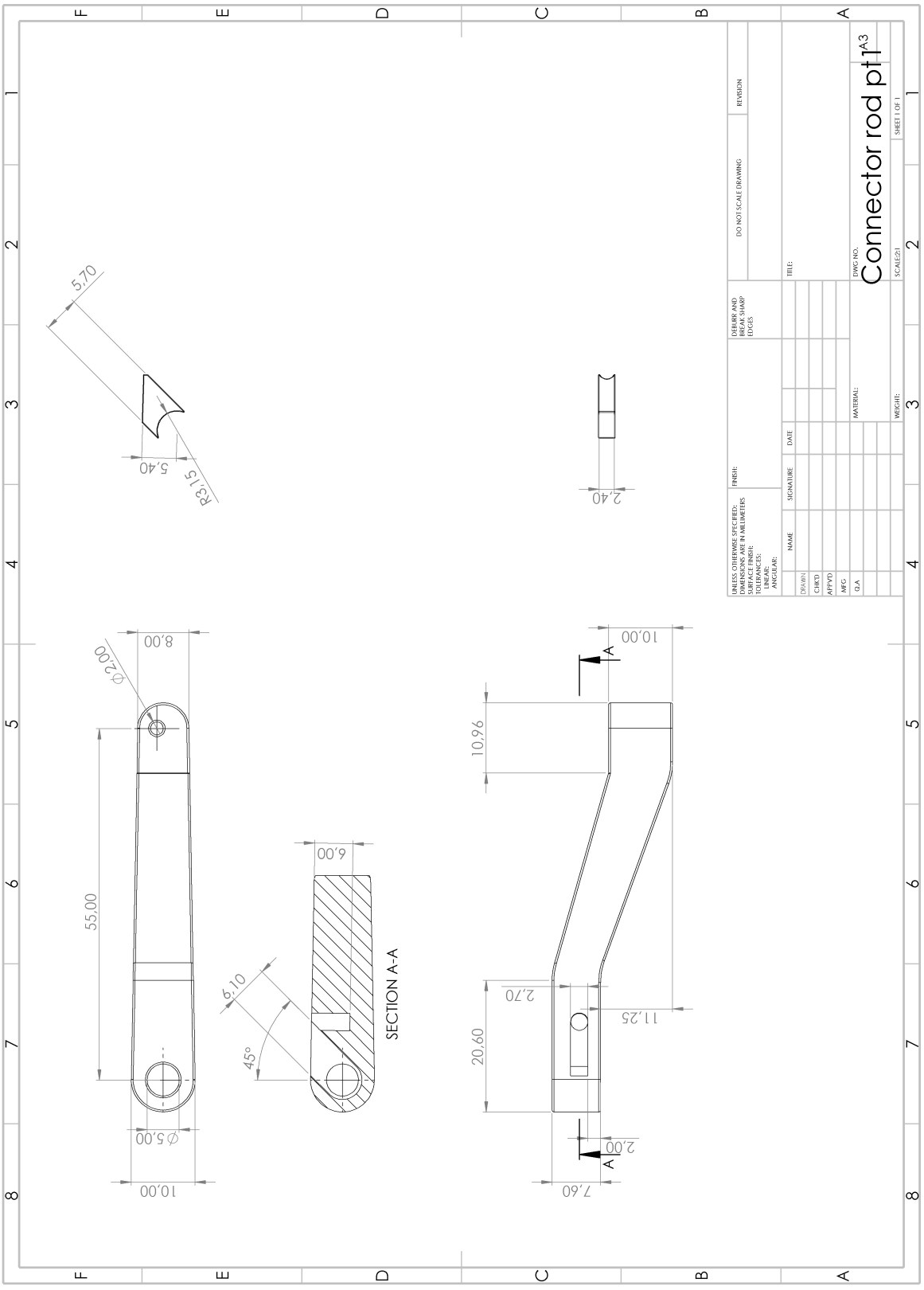
Connector rod pt1
A3
SECTION A-A
5,70
5,40
R3,15
2,40
8,00
Ø2,00
55,00
Ø5,00
10,00
6,00
6,10
45°
10,00
10,96
2,70
20,60
11,25
2,00
7,60
DO NOT SCALE DRAWING
REVISION
DEBURR AND BREAK SHARP EDGES
UNLESS OTHERWISE SPECIFIED:
DIMENSIONS ARE IN MILLIMETERS
SURFACE FINISH:
TOLERANCES:
LINEAR:
ANGULAR:
FINISH:
NAME
SIGNATURE
DATE
DRAWN
CHKD
APPVD
MFG
Q.A.
MATERIAL:
WEIGHT:
SCALE:2:1
SHEET 1 OF 1
DWG NO.
TITLE:

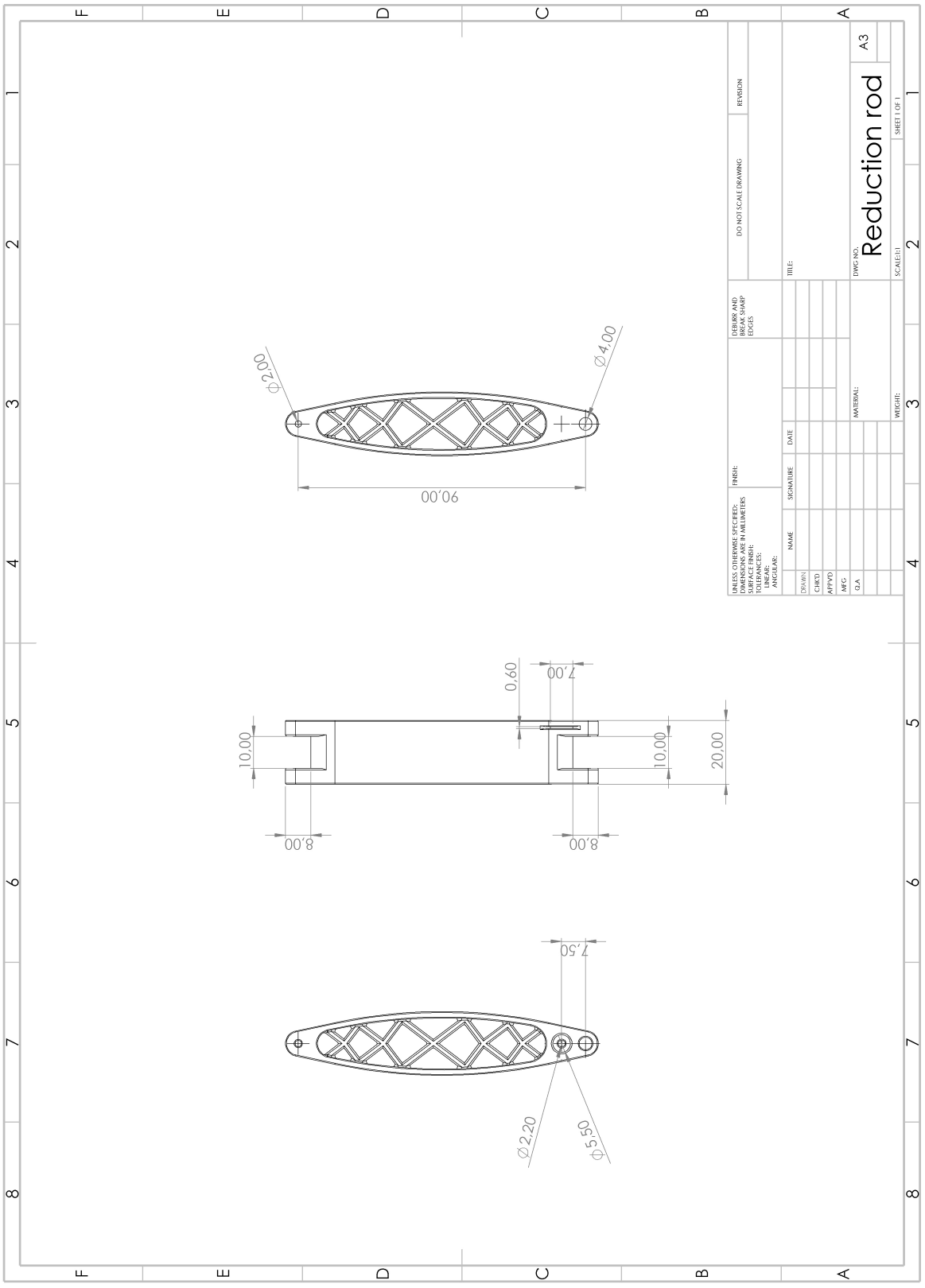
Reduction rod
A3
DWG NO.
SCALE:1:1
SHEET 1 OF 1
TITLE:
DO NOT SCALE DRAWING
REVISION
DEBURR AND BREAK ALL SHARP EDGES
FINISH:
MATERIAL:
WEIGHT:
NAME
SIGNATURE
DATE
DRAWN
CHK'D
APP'D
MFG
Q.A
UNLESS OTHERWISE SPECIFIED:
DIMENSIONS ARE IN MILLIMETERS
SURFACE FINISH:
TOLERANCES:
LINEAR:
ANGULAR:
Ø2,00
Ø4,00
90,00
0,60
7,00
10,00
10,00
20,00
8,00
8,00
7,50
Ø2,20
Ø5,50

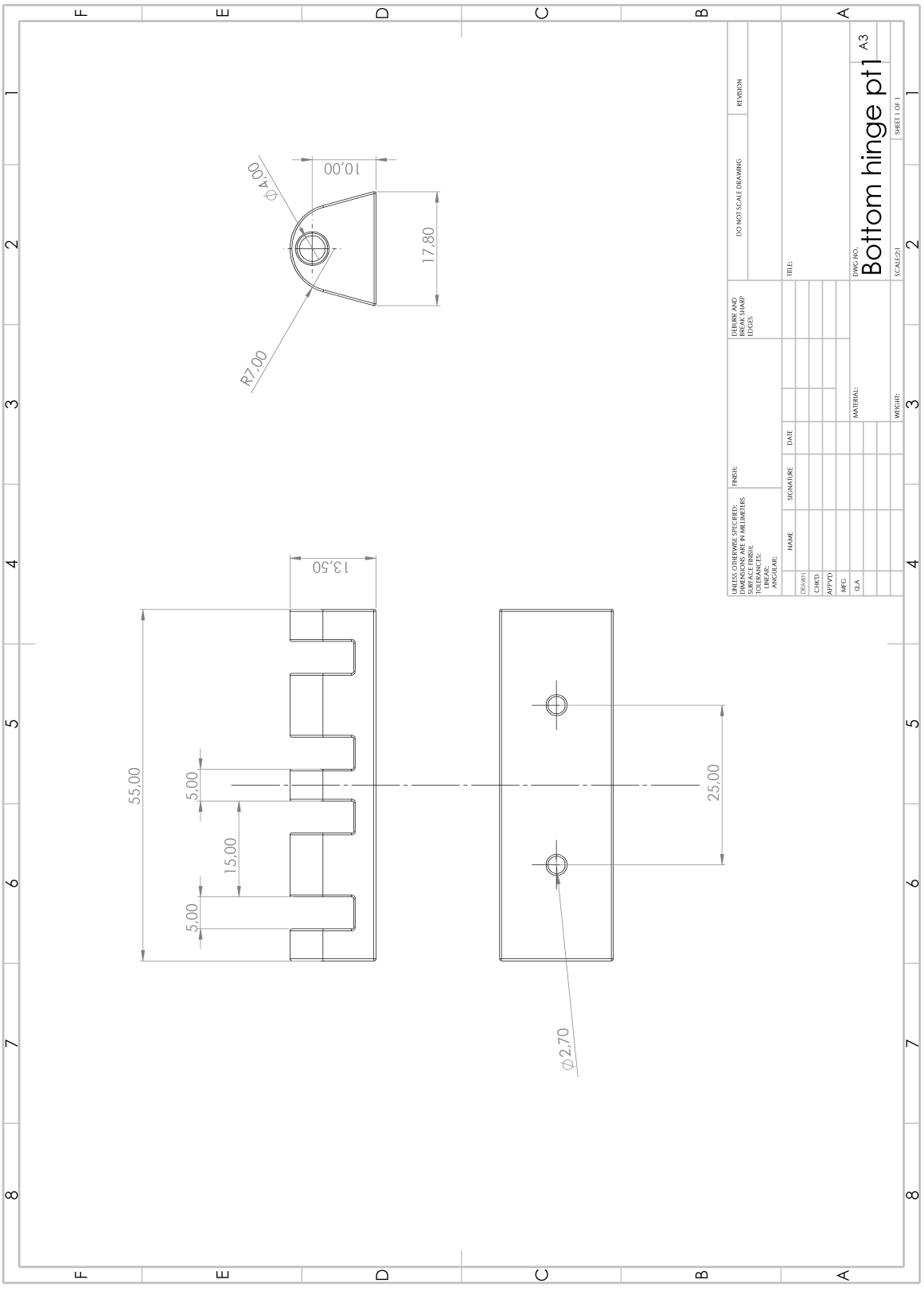
10,00
ϕ4,00
17,80
R7,00
13,50
55,00
5,00
15,00
5,00
25,00
ϕ2,70
DO NOT SCALE DRAWING
REVISION
DEBURR AND BREAK SHARP EDGES
FINISH:
UNLESS OTHERWISE SPECIFIED:
DIMENSIONS ARE IN MILLIMETERS
SURFACE FINISH:
TOLERANCES:
LINEAR:
ANGULAR:
NAME
SIGNATURE
DATE
DRAWN
CHK'D
APPV'D
MFG
Q.A
MATERIAL:
WEIGHT:
TITLE:
DWG. NO.
Bottom hinge pt1
A3
SCALE:2:1
SHEET 1 OF 1

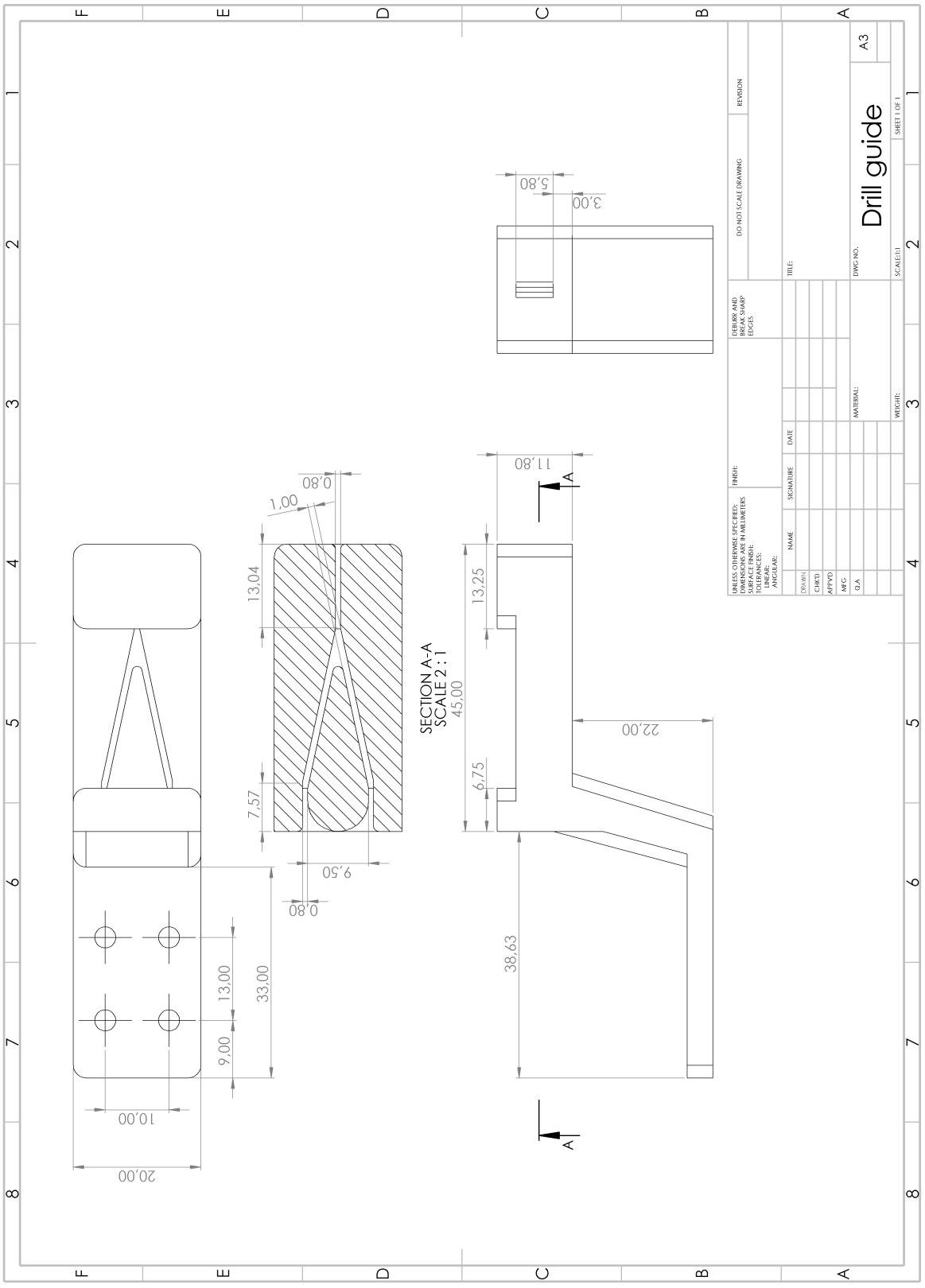
SECTION A-A
SCALE 2 : 1
45,00
13,04
13,25
7,57
6,75
38,63
22,00
11,80
5,80
3,00
1,00
0,80
9,50
13,00
33,00
9,00
10,00
20,00
A
A
DO NOT SCALE DRAWING
REVISION
DEBURR AND BREAK ALL SHARP EDGES
FINISH:
UNLESS OTHERWISE SPECIFIED:
DIMENSIONS ARE IN MILLIMETERS
SURFACE FINISH:
TOLERANCES:
LINEAR:
ANGULAR:
NAME
SIGNATURE
DATE
DRAWN
CHK'D
APPV'D
MFG
Q.A
MATERIAL:
WEIGHT:
TITLE:
DWG NO.
Drill guide
A3
SCALE:1:1
SHEET 1 OF 1

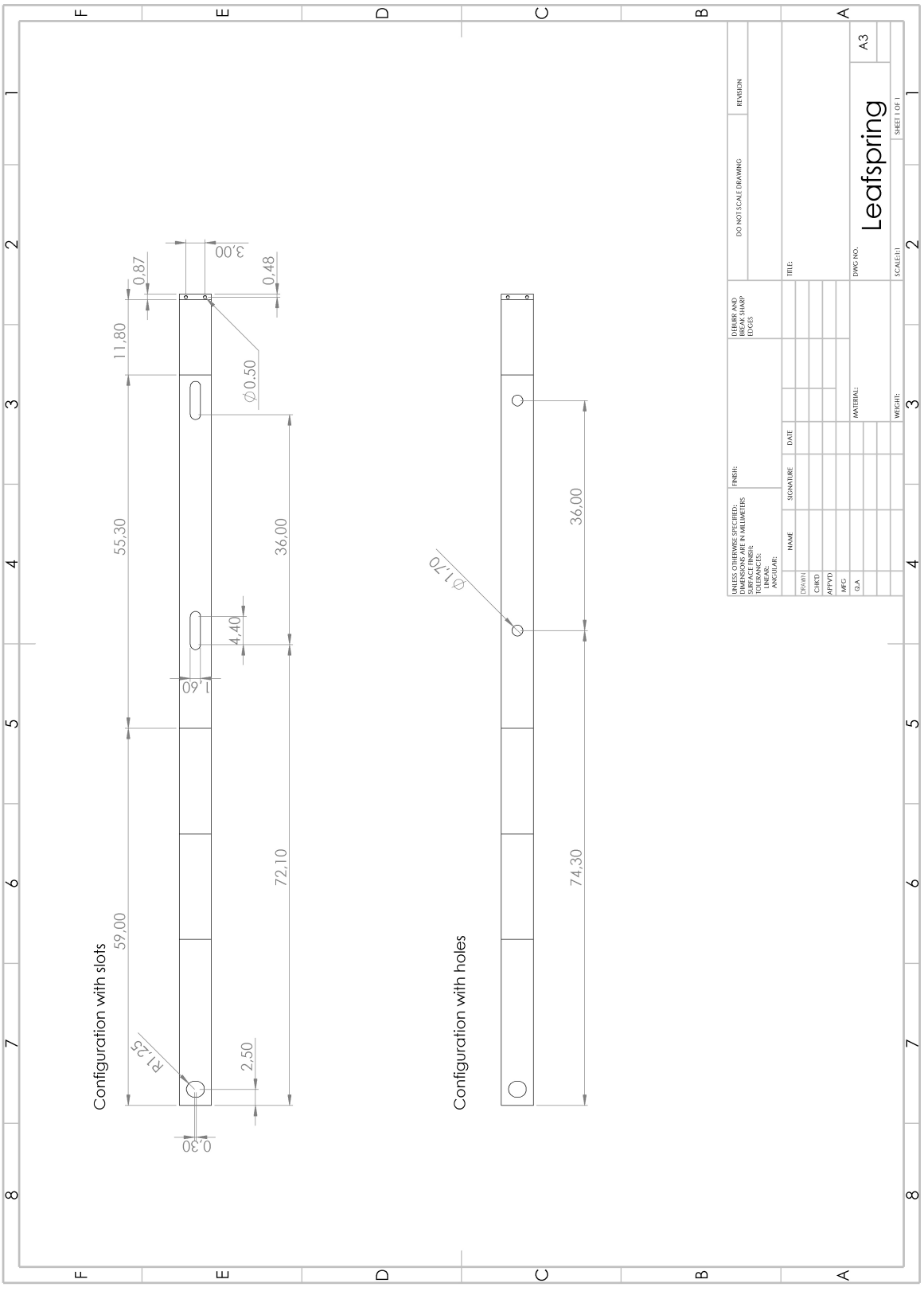
Configuration with slots
Configuration with holes
Leafspring
A3
DWG NO.
SCALE:1:1
SHEET 1 OF 1
DO NOT SCALE DRAWING
REVISION
TITLE:
DEBURR AND BREAK SHARP EDGES
FINISH:
UNLESS OTHERWISE SPECIFIED:
DIMENSIONS ARE IN MILLIMETERS
SURFACE FINISH:
TOLERANCES:
LINEAR:
ANGULAR:
NAME
SIGNATURE
DATE
DRAWN
CHKD
APPVD
MFG
Q.A
MATERIAL:
WEIGHT:
11,80
0,87
3,00
0,48
Ø0,50
55,30
36,00
4,40
1,60
59,00
72,10
R1,35
2,50
0,30
Ø1,70
36,00
74,30

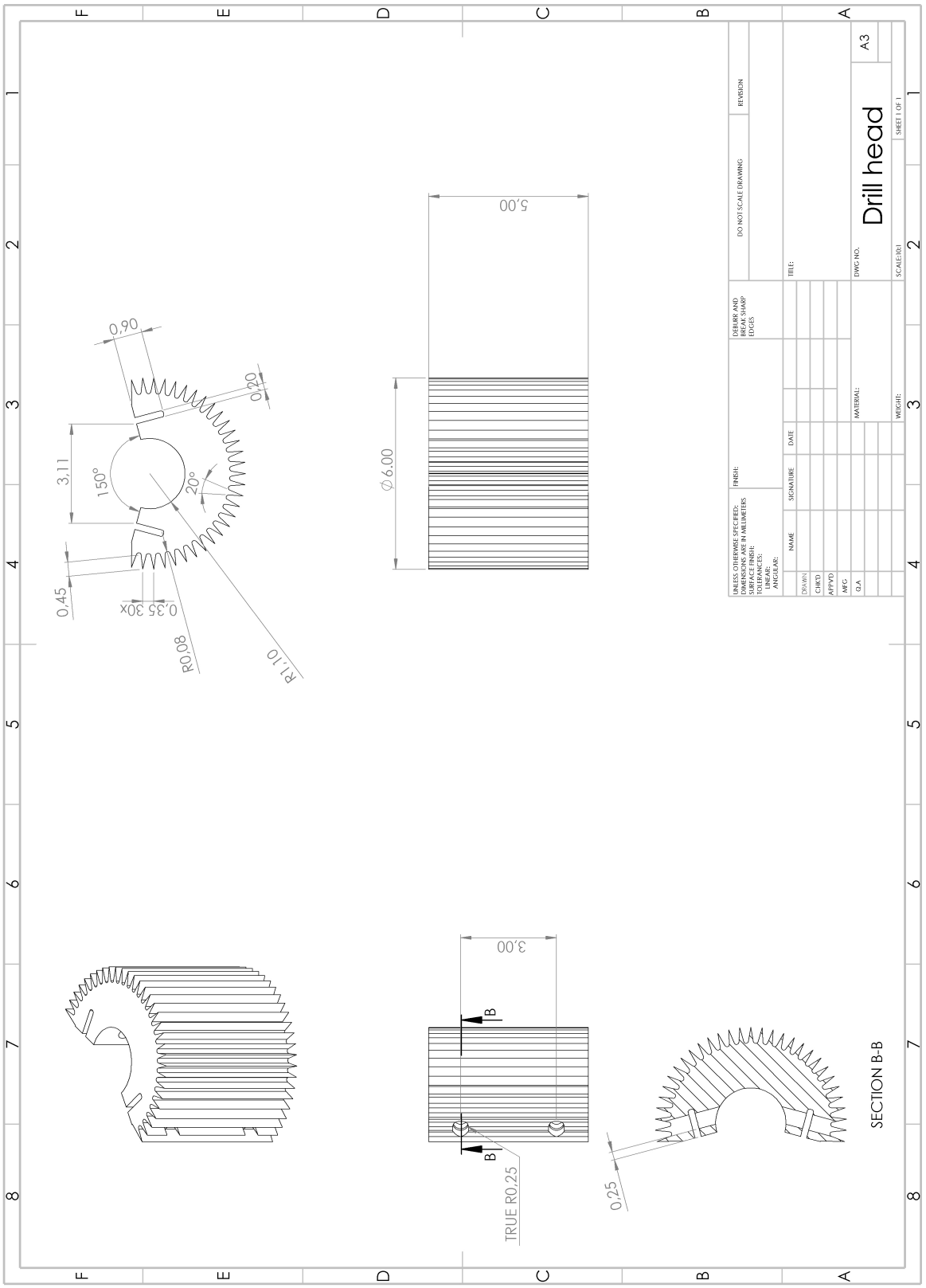
Drill head
A3
SCALE:10:1
SHEET 1 OF 1
DWG NO.
TITLE:
DO NOT SCALE DRAWING
REVISION
DEBURR AND BREAK ALL SHARP EDGES
FINISH:
MATERIAL:
WEIGHT:
UNLESS OTHERWISE SPECIFIED:
DIMENSIONS ARE IN MILLIMETERS
SURFACE FINISH:
TOLERANCES:
LINEAR:
ANGULAR:
NAME
SIGNATURE
DATE
DRAWN
CHK'D
APPV'D
MFG
Q.A
5,00
Ø6,00
0,90
0,20
3,11
150°
20°
0,45
0,35 30x
R0,08
R1,10
3,00
B
B
TRUE R0,25
0,25
SECTION B-B

D

Experiment data

Table D.1: List of theoretical drill positions and angles.

Test name	Date	crank angle	Amp left	Amp right	Phase diff	Position X	Position Y	Angle
		degrees	mm	mm	degrees	mm	mm	degrees
static, normal		0	0.75	0.75	180	0.00	0.00	0.00
static, normal		45	0.75	0.75	180	0.00	0.00	10.06
static, normal		90	0.75	0.75	180	0.00	0.00	14.14
static, normal		135	0.75	0.75	180	0.00	0.00	10.06
static, normal		180	0.75	0.75	180	0.00	0.00	0.00
static, normal		225	0.75	0.75	180	0.00	0.00	-10.06
static, normal		270	0.75	0.75	180	0.00	0.00	-14.14
static, normal		315	0.75	0.75	180	0.00	0.00	-10.06
static, normal		360	0.75	0.75	180	0.00	0.00	0.00
static, amp		0	0.75	0.25	180	0.01	0.18	6.74
static, amp		45	0.75	0.25	180	0.01	0.25	9.50
static, amp		90	0.75	0.25	180	0.01	0.18	6.74
static, amp		135	0.75	0.25	180	0.00	0.00	0.00
static, amp		180	0.75	0.25	180	0.01	-0.18	-6.74
static, amp		225	0.75	0.25	180	0.01	-0.25	-9.50
static, amp		270	0.75	0.25	180	0.01	-0.18	-6.74
static, amp		315	0.75	0.25	180	0.00	0.00	0.00
static, amp		360	0.75	0.25	180	0.00	0.00	0.00
static, phase		0	0.75	0.75	144	0.00	-0.22	4.21
static, phase		45	0.75	0.75	144	-0.01	-0.11	12.03
static, phase		90	0.75	0.75	144	0.00	0.07	12.82
static, phase		135	0.75	0.75	144	0.01	0.21	6.17
static, phase		180	0.75	0.75	144	0.00	0.22	-4.21
static, phase		225	0.75	0.75	144	-0.01	0.11	-12.03
static, phase		270	0.75	0.75	144	0.00	-0.07	-12.82
static, phase		315	0.75	0.75	144	0.01	-0.21	-6.17
static, phase		360	0.75	0.75	144	0.00	-0.22	4.21

Table D.2: List of the positions and angles for Drill 1.

Test name	Date	crank angle	Amp left	Amp right	Phase diff	Position X	Position Y	Angle
		degrees	mm	mm	degrees	mm	mm	degrees
Static, normal	28/06/2022	0	0.75	0.75	180	0.00	0.00	0.00
Static, normal	28/06/2022	90	0.75	0.75	180	1.18	0.16	9.80
Static, normal	28/06/2022	270	0.75	0.75	180	-0.71	0.07	7.00
Static, normal	28/06/2022	0	0.75	0.75	180	0.00	0.00	0.00
Static, normal	28/06/2022	90	0.75	0.75	180	0.87	0.05	7.50
Static, normal	28/06/2022	270	0.75	0.75	180	-0.78	-0.16	6.80
Static, amp	28/06/2022	0	0.75	0.25	180	0.00	0.00	0.00
Static, amp	28/06/2022	90	0.75	0.25	180	0.10	-0.21	0.00
Static, amp	28/06/2022	270	0.75	0.25	180	-0.22	-0.02	2.00
Static, amp	28/06/2022	450	0.75	0.25	180	0.00	-0.25	0.00
Static, amp	28/06/2022	540	0.75	0.25	180	0.00	0.00	0.00
Static, amp	28/06/2022	630	0.75	0.25	180	-0.25	-0.01	2.00
Static, amp	28/06/2022	0	0.75	0.25	180	0.00	-0.11	1.00
Static, amp	28/06/2022	90	0.75	0.25	180	0.56	-0.17	4.30
Static, amp	28/06/2022	270	0.75	0.25	180	-0.25	0.05	3.00
Static, amp	28/06/2022	360	0.75	0.25	180	-0.12	0.01	2.20
Static, amp	28/06/2022	450	0.75	0.25	180	0.56	-0.20	4.50
Static, amp	28/06/2022	360	0.75	0.25	180	0.00	-0.11	1.00
Static, phase	28/06/2022	0	0.75	0.75	144	0.00	0.00	0.00
Static, phase	28/06/2022	90	0.75	0.75	144	0.93	0.19	10.00
Static, phase	28/06/2022	180	0.75	0.75	144	0.00	0.25	0.50
Static, phase	28/06/2022	270	0.75	0.75	144	0.74	0.15	6.90
Static, phase	28/06/2022	360	0.75	0.75	144	0.00	0.00	0.00
Static, phase	28/06/2022	0	0.75	0.75	144	0.00	0.26	0.00
Static, phase	28/06/2022	90	0.75	0.75	144	0.74	0.22	7.00
Static, phase	28/06/2022	180	0.75	0.75	144	0.10	0.25	1.80
Static, phase	28/06/2022	270	0.75	0.75	144	-0.54	0.11	4.80
Static, phase	28/06/2022	360	0.75	0.75	144	-0.07	0.02	0.00
Static, phase	28/06/2022	450	0.75	0.75	144	0.62	0.12	6.60
Static, phase	28/06/2022	495	0.75	0.75	144	-0.49	0.20	5.70
Static, phase	28/06/2022	540	0.75	0.75	144	-0.02	0.26	0.00
Static, phase	28/06/2022	585	0.75	0.75	144	-0.56	0.15	4.50
Static, phase	28/06/2022	630	0.75	0.75	144	-0.71	0.16	5.76
Static, phase	28/06/2022	675	0.75	0.75	144	-0.32	0.12	2.00
Static, phase	28/06/2022	720	0.75	0.75	144	0.07	0.11	2.00

Table D.3: List of the positions and angles for Drill 2.

Test name	Date	crank angle	Amp left	Amp right	Phase diff	Position X	Position Y	Angle
		degrees	mm	mm	degrees	mm	mm	degrees
Static, normal	30/06/2022	0	0.75	0.75	180	0.00	0.00	0.00
Static, normal	30/06/2022	90	0.75	0.75	180	0.98	0.06	10.00
Static, normal	30/06/2022	180	0.75	0.75	180	0.00	-0.04	0.00
Static, normal	30/06/2022	270	0.75	0.75	180	-0.68	-0.04	7.00
Static, normal	30/06/2022	450	0.75	0.75	180	0.99	0.06	10.00
Static, normal	30/06/2022	630	0.75	0.75	180	-0.77	-0.05	7.20
Static, normal	30/06/2022	810	0.75	0.75	180	0.95	0.05	10.00
Static, normal	30/06/2022	990	0.75	0.75	180	-0.69	-0.01	7.00
Static, normal	30/06/2022	1080	0.75	0.75	180	0.00	0.00	0.00
Static, normal	30/06/2022	0	0.75	0.75	180	0.00	-0.06	1.50
Static, normal	30/06/2022	90	0.75	0.75	180	0.90	0.00	8.00
Static, normal	30/06/2022	180	0.75	0.75	180	0.20	-0.05	0.50
Static, normal	30/06/2022	270	0.75	0.75	180	-0.49	-0.11	7.00
Static, normal	30/06/2022	450	0.75	0.75	180	0.89	0.00	7.20
Static, normal	30/06/2022	630	0.75	0.75	180	-0.59	-0.14	7.20
Static, normal	30/06/2022	810	0.75	0.75	180	0.85	-0.01	7.20
Static, normal	30/06/2022	990	0.75	0.75	180	-0.58	-0.06	7.00
Static, normal	30/06/2022	1080	0.75	0.75	180	0.22	-0.06	0.80
Static, amp	30/06/2022	0	0.75	0.25	180	0.00	0.00	0.00
Static, amp	30/06/2022	90	0.75	0.25	180	0.52	-0.09	5.30
Static, amp	30/06/2022	180	0.75	0.25	180	0.05	-0.04	0.00
Static, amp	30/06/2022	270	0.75	0.25	180	-0.12	0.16	1.20
Static, amp	30/06/2022	360	0.75	0.25	180	0.00	0.06	0.00
Static, amp	30/06/2022	450	0.75	0.25	180	0.58	-0.05	5.50
Static, amp	30/06/2022	630	0.75	0.25	180	-0.12	0.19	1.50
Static, amp	30/06/2022	810	0.75	0.25	180	0.56	-0.05	5.00
Static, amp	30/06/2022	990	0.75	0.25	180	-0.12	0.16	1.00
Static, amp	30/06/2022	1080	0.75	0.25	180	0.00	0.11	0.00
Static, amp	30/06/2022	0	0.75	0.25	180	0.00	0.22	0.00
Static, amp	30/06/2022	90	0.75	0.25	180	0.15	-0.04	1.50
Static, amp	30/06/2022	180	0.75	0.25	180	0.00	0.22	0.00
Static, amp	30/06/2022	270	0.75	0.25	180	-0.06	0.17	1.20
Static, amp	30/06/2022	360	0.75	0.25	180	-0.04	0.20	0.50
Static, amp	30/06/2022	450	0.75	0.25	180	0.15	0.00	1.40
Static, amp	30/06/2022	630	0.75	0.25	180	-0.12	0.17	1.00
Static, amp	30/06/2022	810	0.75	0.25	180	0.16	0.05	1.50
Static, amp	30/06/2022	990	0.75	0.25	180	-0.06	0.15	1.00
Static, phase	30/06/2022	0	0.75	0.75	144	0.00	0.00	0.00
Static, phase	30/06/2022	90	0.75	0.75	144	0.67	0.02	7.00
Static, phase	30/06/2022	180	0.75	0.75	144	0.45	0.33	4.50
Static, phase	30/06/2022	270	0.75	0.75	144	-0.21	0.24	1.60
Static, phase	30/06/2022	360	0.75	0.75	144	0.00	0.00	0.00
Static, phase	30/06/2022	450	0.75	0.75	144	0.77	0.11	8.20
Static, phase	30/06/2022	540	0.75	0.75	144	0.27	0.36	3.50
Static, phase	30/06/2022	630	0.75	0.75	144	-0.42	0.16	4.50
Static, phase	30/06/2022	720	0.75	0.75	144	0.00	0.00	0.00
Static, phase	30/06/2022	810	0.75	0.75	144	0.62	0.06	6.60
Static, phase	30/06/2022	900	0.75	0.75	144	0.59	0.31	6.50
Static, phase	30/06/2022	990	0.75	0.75	144	-0.46	0.14	4.60
Static, phase	30/06/2022	1080	0.75	0.75	144	0.00	0.00	0.00
Static, phase	30/06/2022	1170	0.75	0.75	144	0.35	0.02	4.20
Static, phase	30/06/2022	1260	0.75	0.75	144	0.83	0.28	8.40
Static, phase	30/06/2022	1350	0.75	0.75	144	-0.16	0.25	2.20
Static, phase	30/06/2022	1440	0.75	0.75	144	0.00	0.00	0.00
Static, phase	30/06/2022	1530	0.75	0.75	144	0.75	0.10	8.20
Static, phase	30/06/2022	1620	0.75	0.75	144	0.51	0.31	6.20
Static, phase	30/06/2022	0	0.75	0.75	144	0.00	0.36	0.00
Static, phase	30/06/2022	90	0.75	0.75	144	0.38	0.16	3.90
Static, phase	30/06/2022	180	0.75	0.75	144	0.02	0.01	0.50

Table D.4: List of the positions and angles for Drill 3.

Test name	Date	crank angle	Amp left	Amp right	Phase diff	Position X	Position Y	Angle
		degrees	mm	mm	degrees	mm	mm	degrees
Static, amp	10/08/2022	0	0.75	0.25	180	0.00	0.00	0.00
Static, amp	10/08/2022	90	0.75	0.25	180	0.51	-0.11	6.50
Static, amp	10/08/2022	180	0.75	0.25	180	0.06	-0.07	2.50
Static, amp	10/08/2022	270	0.75	0.25	180	-0.25	0.14	3.20
Static, amp	10/08/2022	360	0.75	0.25	180	-0.06	0.07	1.20
Static, amp	10/08/2022	450	0.75	0.25	180	0.48	-0.10	5.30
Static, amp	10/08/2022	540	0.75	0.25	180	0.07	-0.06	2.00
Static, amp	10/08/2022	630	0.75	0.25	180	-0.25	0.17	3.00
Static, amp	10/08/2022	720	0.75	0.25	180	-0.21	0.17	2.50
Static, amp	10/08/2022	810	0.75	0.25	180	0.47	-0.11	5.50
Static, amp	10/08/2022	900	0.75	0.25	180	0.09	-0.06	1.50
Static, amp	10/08/2022	990	0.75	0.25	180	-0.27	0.15	3.20
Static, amp	10/08/2022	1080	0.75	0.25	180	-0.20	0.14	2.50
Static, amp	10/08/2022	0	0.75	0.25	180	0.00	0.00	0.00
Static, amp	10/08/2022	90	0.75	0.25	180	0.41	-0.04	5.30
Static, amp	10/08/2022	180	0.75	0.25	180	0.09	-0.04	1.00
Static, amp	10/08/2022	270	0.75	0.25	180	-0.15	0.10	2.00
Static, amp	10/08/2022	360	0.75	0.25	180	-0.05	0.11	0.50
Static, amp	10/08/2022	450	0.75	0.25	180	0.41	-0.04	5.50
Static, amp	10/08/2022	540	0.75	0.25	180	0.36	-0.09	4.50
Static, amp	10/08/2022	630	0.75	0.25	180	-0.17	0.11	2.00
Static, amp	10/08/2022	720	0.75	0.25	180	-0.05	0.15	0.50
Static, amp	10/08/2022	810	0.75	0.25	180	0.38	-0.05	5.00
Static, amp	10/08/2022	900	0.75	0.25	180	0.37	-0.07	5.00
Static, amp	10/08/2022	990	0.75	0.25	180	-0.22	0.11	2.70
Static, amp	10/08/2022	1080	0.75	0.25	180	-0.05	0.10	0.50
Static, phase	10/08/2022	0	0.75	0.75	144	0.00	0.00	0.00
Static, phase	10/08/2022	90	0.75	0.75	144	0.62	-0.12	7.00
Static, phase	10/08/2022	180	0.75	0.75	144	0.22	-0.22	2.50
Static, phase	10/08/2022	270	0.75	0.75	144	-0.49	-0.02	5.50
Static, phase	10/08/2022	360	0.75	0.75	144	0.06	0.05	0.80
Static, phase	10/08/2022	450	0.75	0.75	144	0.64	-0.11	8.20
Static, phase	10/08/2022	540	0.75	0.75	144	0.00	-0.22	0.80
Static, phase	10/08/2022	630	0.75	0.75	144	-0.46	0.02	5.20
Static, phase	10/08/2022	720	0.75	0.75	144	0.06	0.07	0.50
Static, phase	10/08/2022	810	0.75	0.75	144	0.71	-0.11	8.70
Static, phase	10/08/2022	900	0.75	0.75	144	0.10	-0.20	1.20
Static, phase	10/08/2022	990	0.75	0.75	144	-0.45	0.05	1.85
Static, phase	10/08/2022	1080	0.75	0.75	144	0.12	0.07	1.70
Static, phase	10/08/2022	0	0.75	0.75	144	0.00	0.00	0.00
Static, phase	10/08/2022	90	0.75	0.75	144	0.80	-0.17	9.80
Static, phase	10/08/2022	180	0.75	0.75	144	0.00	-0.27	1.10
Static, phase	10/08/2022	270	0.75	0.75	144	-0.45	-0.05	5.20
Static, phase	10/08/2022	360	0.75	0.75	144	0.15	-0.02	2.80
Static, phase	10/08/2022	450	0.75	0.75	144	0.94	-0.19	11.20
Static, phase	10/08/2022	540	0.75	0.75	144	0.12	-0.30	2.80
Static, phase	10/08/2022	630	0.75	0.75	144	-0.37	-0.17	4.20
Static, phase	10/08/2022	720	0.75	0.75	144	0.31	0.02	3.30
Static, phase	10/08/2022	810	0.75	0.75	144	0.87	-0.17	10.80
Static, phase	10/08/2022	900	0.75	0.75	144	0.06	-0.32	1.30
Static, phase	10/08/2022	990	0.75	0.75	144	-0.22	-0.17	3.20
Static, phase	10/08/2022	1080	0.75	0.75	144	0.49	-0.05	5.30